TURBULENT BOUNDARY LAYER OVER HEATED AND UNHEATED, PLANE, ROUGH SURFACES

by

Benoyendra Chanda

Department of Civil Engineering

Scientific Report No. 1

The research reported in this document has been sponsored by the Geophysics Research Directorate of the Air Force Cambridge Research Center, Air Research and Development Command, under Contract AF19(604) - 1706.

COLORADO STATE UNIVERSITY
Fort Collins, Colorado
May, 1958

CER 58BC 21

AFCRC
TN-58-428
ASTIA-AD 152599

TURBULENT BOUNDARY LAYER OVER HEATED AND UNHEATED, PLANE, ROUGH SURFACES

by

Benoyendra Chanda

Department of Civil Engineering

Scientific Report No. 1

The research reported in this document has been sponsored by the Geophysics Research Directorate of the Air Force Cambridge Research Center, Air Research and Development Command, under Contract AF19(604) - 1706.

COLORADO STATE UNIVERSITY
Fort Collins, Colorado
May, 1958

ABSTRACT

Turbulent boundary layers over plane, rough, heated and unheated surfaces were investigated. Crushed stone of sizes between 0.25 in. and 0.315 in. glued to open-mesh fiber-glass cloth and laid on the floor of the wind tunnel formed the rough surface. Two air speeds, U_o = 17 fps and 35 fps and one temperature difference for each velocity were used. The temperature differences were approximately 75^0F and 48^0F for U_o = 17 fps and 35 fps respectively. The heated surface was 10 ft long beginning 43 in. downstream from the leading edge of the rough surface. Constant-temperature type hot-wire anemometers and a resistance thermometer were used to obtain the experimental data.

Considering density as a function of temperature, the displacement thickness δ^*, momentum thickness δ^{**} for the momentum boundary layer and the convective thickness δ_T^{**} for the thermal boundary layer were used in forms similar to those used in the case of compressible fluids. The kinematic viscosity of air corresponding to the wall temperature (T_w) rather than free-stream temperature (T_o) was used as a reference viscosity.

Using an analysis similar to that presented by Townsend, Clauser, and Hama it is found that the velocity-defect law is universal for smooth, rough, heated and unheated surfaces. The logarithmic velocity-distribution curve (the wall law) is shifted by an amount $\Delta\overline{U}/U_*$ depending on the magnitude of the roughness effect. The skin-friction law obtained from the wall law for a rough surface and the velocity-defect law, agrees with the experimental data for heated and unheated surfaces. Townsend's equation for the distribution of shear stress in the boundary layer over a smooth surface derived from the hypothesis of self-preserving motion and a constant eddy viscosity represents fairly well the distribution of shear stress in the outer part of the boundary layer for the unheated surface. The eddy viscosity in the boundary layer $(y > 4K_r)$ over a rough unheated surface is found to be constant and proportional to the product of free-stream density and velocity, and displacement thickness. The constant of proportionality is approximately equal to 0.018 as given by Clauser.

Applying an analysis similar to that used for the distribution of the velocity and the law of skin-friction and introducing the concept of friction temperature, the wall law and temperature defect law are obtained. The wall law for temperature distribution

in the thermal boundary layer over a heated rough surface can be expressed by

$$\frac{T_\omega - \bar{T}}{T_*} = A_1 \log \frac{y U_*}{\nu_\omega} + B_1 - \Delta \frac{(T_\omega - \bar{T})}{T_*}$$

where $\bar{T}$ is the temperature at any point in the thermal layer, T_* is the friction temperature defined by $q_w/\rho_o g c_p U_*$. The quantity $\Delta(T_w - \bar{T})/T_*$ has the same significance for the temperature distribution as that of $\Delta\bar{U}/U_*$ for the velocity distribution. The temperature-defect law can be expressed by

$$\frac{\bar{T} - T_o}{T_*} = A_1 \log \frac{y}{\delta_T} + C_1$$

where δ_T is the thickness of the thermal boundary layer. The value of the constants A_1, B_1 and C_1 are 6.6, 1.0 and 0.3 respectively. The logarithmic temperature-defect law represents the major portion of the temperature distribution in the outer thermal boundary layer. From the above equations, the local coefficient of heat transfer is obtained in the following form

$$\frac{1}{S_t}\sqrt{\frac{c_f}{2}} = A_1 \log \frac{\delta_T U_*}{\nu_\omega} + (B_1 - C_1) - \Delta \frac{(T_\omega - \bar{T})}{T_*}$$

where S_t is the local Stanton number and c_f is the local coefficient of skin-friction.

Vertical distributions of the intensity of velocity fluctuations as well as the intensity of temperature fluctuations are also presented.

ACKNOWLEDGEMENTS

This report which formed part of the author's doctoral dissertation was made possible through the financial support of the Geophysics Research Directorate of the Air Force Cambridge Research Center, Air Research and Development Command, under Contract AF 19(604)-1706. Stimulating suggestions made during the planning stages of this work by Dr. Heinz Lettau, Contract Monitor, were especially helpful.

The writer is grateful to Professor Jack E. Cermak, under whose direction the project was carried out, for encouragement, for many stimulating discussions, and for experienced guidance which to a large extent has made the completion of this study possible.

Administrative support given by Dr. A. R. Chamberlain, Chief, Civil Engineering Section, Colorado State University Experiment Station, Professor T. H. Evans, Dean of Engineering, and Dr. M. L. Albertson, Director, Colorado State University Research Foundation was helpful to the progress of the work.

Acknowledgement is also made to Mr. Larry Fletcher for helping during the collection of data, to Mr. Ramesh C. Malhotra and to Mr. Ramachandra J. Garde for helping in the computation of data, to Mr. Y. G. Tsuei for drafting and to Mrs. June Simon for typing.

TABLE OF CONTENTS

TABLE OF CONTENTS -- Continued

LIST OF TABLES

LIST OF FIGURES

LIST OF FIGURES -- Continued

LIST OF FIGURES -- Continued

LIST OF FIGURES -- Continued

LIST OF SYMBOLS

		Dimension
A , A_1	Constant	
B , B_1	Constant	
C , C_1	Constant	
c_p	Specific heat of air at constant pressure	Btu/lb ^{0}F
D	Constant	
f	Function	
g	Gravitational acceleration	ft/sec^2
k	Thermal conductivity	Btu/sec ft ^{0}F
K	Constant	
K_r	Mean height of the roughness elements	in.
ℓ_o	Reference length	in.
L	Distance between the heated plate and the beginning of the rough surface	in.
n	Exponent	
P	Pressure	lb/ft^2
q	Heat flux per unit area	Btu/sec ft^2
R	Gas constant	
T	Instantaneous value of absolute temperature	^{0}F
T	Mean absolute temperature	^{0}F

LIST OF SYMBOLS -- Continued

		Dimension
T'	Temperature fluctuation about T	^0F
t'	Root-mean-square (rms) value of local temperature fluctuation	^0F
T_*	Friction temperature $\frac{q_w}{gc_p \rho_o U_*}$	^0F
t	Time	sec
U_i	Instantaneous value of velocity components in the direction of x_i	ft/sec
$\overline{U}_i$	Time-mean of the velocity component in the direction of x_i	ft/sec
U'_i	Instantaneous velocity fluctuation in the direction x_i	ft/sec
U, V, W	Instantaneous value of velocity components in the direction of x, y, z axes respectively	ft/sec
u_i	Root-mean square value of the fluctuating component of the local velocity in the direction of x_i	ft/sec
u_o	Reference velocity	ft/sec
$\overline{U'_i U'_j}$	Double velocity correlation	$(ft/sec)^2$
$\overline{P'U'_i U'_j}$	Triple correlation	lb ft^2/sec^2
$\overline{T'U'_i U'_j}$	Triple correlation	^0F ft^2/sec^2
U_*	Shear velocity $\sqrt{\frac{\tau_w}{\rho_w}} = U_o\sqrt{\frac{c_f}{2}}$	ft/sec
X_i	ith components of the body force	lb/ft^3

LIST OF SYMBOLS -- Continued

		Dimension
x_i	Coordinate axes	in.
x, y, z	Coordinate axes, x along the direction of flow, y vertically upward, z transverse to flow direction	in.
β	Coefficient of expansion	
δ	Velocity boundary layer thickness, value of y for $U = 0.99\, U_o$	in.
δ_T	Thermal boundary layer thickness, value of y for $y = 0.99\, (T_w - T_o)$	in.
δ^*	Displacement thickness $\int_o^\infty (1 - \frac{\bar{\rho}}{\rho_o} \frac{\bar{U}}{U_o})\, dy$	in.
δ^{**}	Momentum thickness $\int_o^\infty \frac{\bar{\rho}}{\rho_o} \frac{\bar{U}}{U_o} (1 - \frac{\bar{U}}{U_o})\, dy$	in.
δ_T^{**}	Convective thickness $\int_o^\infty \frac{\bar{\rho}}{\rho_o} \frac{\bar{U}}{U_o} \frac{\bar{T} - T_o}{T_w - T_o}\, dy$	in.
ΔT_o	Temperature difference $T_w - T_o$	^0F
ϵ	Eddy viscosity due to momentum	ft^2/sec
θ	Temperature difference $\bar{T} - T_o$	^0F
λ	Constant	
μ	Dynamic viscosity	lb/sec ft
ν	Kinematic viscosity	ft^2/sec
ρ	Density	$slug/ft^3$
ρ'	Density fluctuation	$slug/ft^3$

LIST OF SYMBOLS -- Continued

		Dimension
τ	shearing stress	lb/ft^2
Φ	Dissipation function	$1/sec^2$
φ	Function	

Subscripts

o	Free-stream or ambient condition
w	Wall condition
$\overline{(\ )}$	Time-mean $\lim_{(t_1-t_2)\to\infty} \frac{1}{t_1-t_2} \int_{t_1}^{t_2} (\ )(t)\, dt$
$(\ )'$	Instantaneous value
i	ith component, i = 1 , 2 , 3 referred to components in the x , y , z direction respectively

Dimensionless Groups

c_f	Drag coefficient	$\tau_w / \frac{1}{2} \rho_o U_o^2$
Ec	Eckert number	$\frac{U_o^2}{g c_p (T_w - T_o)}$
Gr	Grashof number	$\frac{g L_o^3 \beta \theta}{\nu}$
H	Form parameter	δ^* / δ^{**}
Pr	Prandtl number	$\frac{\mu g c_p}{k}$

LIST OF SYMBOLS -- Continued

Dimensionless Groups

Re	Reynolds number	$\frac{U\ell_o}{\nu}$
Re_*	=	$\frac{U_* y}{\nu}$
Re_δ	=	$\frac{U_o \delta}{\nu}$
Re_{δ^*}	=	$\frac{U_o \delta^*}{\nu}$
Re_{δ_T}	=	$\frac{U_o \delta_T}{\nu}$
S_t	Stanton number	$\frac{q_w}{g c_p \rho_o U_o (T_w - T_o)}$

LIST OF SYMBOLS FOR PLOTTING DATA

Symbol	$x + L$ in.	U_o fps	ΔT_o ^0F
○	55	17.0	0
◁	67	17.2	0
◇	86	16.9	0
▽	114	17.0	0
▷	154	17.1	0
◉	55	17.2	77
◀	67	17.0	77
◆	86	17.5	77
▼	114	17.0	75
▶	154	17.5	75
●	55	35.3	0
◀	67	35.0	0
◆	86	35.2	0
▼	114	34.5	0
▶	154	35.0	0
◑	55	35.0	53
◀	67	34.5	50
◆	86	34.5	50
▼	114	36.0	48
▶	154	35.5	48

Chapter I

INTRODUCTION

The turbulent boundary layer over heated and unheated, plane, rough surfaces are special cases of the general phenomena of turbulent fluid flow and heat transfer. Specifically, the turbulent boundary layer is a particular case of turbulent shear flow. Turbulent shear flows comprise turbulent boundary layers formed over flat plates, jets, wakes, and pipe and channel flow.

The turbulent boundary layer is extremely important in the fields of aerodynamics, hydraulics, meteorology, and many other branches of applied science. In the field of meteorology, flow over a heated rough surface is particularly important for an understanding of the problem of turbulence and diffusion in the atmospheric boundary layer.

The theory of turbulent flow over heated rough surfaces is extremely complex. At the present time no theoretical analysis is available which completely describes the turbulent boundary layer over plane rough surfaces, heated or unheated, although great progress towards an understanding of the phenomena has been made in recent years. For a moderate air speed

and relatively low surface temperature, analyses have been made which neglect compressibility, buoyancy, and the interaction of heat with the flow. In these analyses the temperature distribution and the mechanism of heat transfer are assumed to be similar to those of the velocity distribution and the mechanism of momentum transfer respectively. The experimental data for flow over a smooth boundary do not fully justify these assumptions. This may be in part due to the unknown effect of heat upon the flow field. The information about the mean-velocity distribution, skin friction, and the turbulence parameters for flow over a plane, unheated rough boundary in which the roughness elements are not geometrically similar is limited. The available experimental data are mostly for the case of geometrically similar roughness elements. Furthermore, they are mainly limited to mean velocity distributions and skin-friction coefficients. The reasons for the scarcity of experimental data of this type are (i) earlier investigations have assumed that the flow over plane, rough surfaces was similar to flow through rough pipes, and (ii) earlier analyses of the turbulent mechanism involved quantities which are derivable from mean-velocity measurements. Experimental data on the boundary layer characteristics have not been previously obtained for the rough, heated boundary.

It has been established that the turbulent boundary layers over flat plates are not similar to those in pipes except for the region close to the solid boundary ($y/\delta \leq 0.15$). Moreover, recent studies of flow over smooth plates show that the mean-velocity distribution does not give correct information about the structure of turbulence. Consequently, more experimental data on flow over plane, rough surfaces both heated and unheated are essential for a complete understanding of the complex flow problem.

The objective of this experimental investigation is to provide additional data necessary for an analysis of the turbulent boundary layer over heated and unheated rough surfaces. In particular, information is sought regarding distribution of mean-velocity, turbulent-shear stress, intensities of turbulence, and skin friction for flow over an unheated surface with dissimilar roughness elements. Parallel information, and in addition the distribution of mean temperature and intensity of temperature fluctuations, are sought for the case of rough surfaces which are moderately heated.

The investigation is limited to one type of rough surface. Crushed stone of sizes between 0.25 in. and 0.315 in. were used to form the roughness elements. The heated surface

was 10 ft long and began 43 in. downstream from the beginning of the roughness. Studies were made using two ambient air velocities, 17 fps and 35 fps, for both the heated and unheated surfaces. For the heated surface, only one value of the temperature difference between the heated surface and the ambient air was investigated for each air speed. The temperature differences corresponding to an air speed of 17 fps and 35 fps were 75^{0}F and 48^{0}F respectively.

Chapter II

REVIEW OF LITERATURE

Turbulent Boundary Layer Over an Unheated Smooth Plate

Townsend (22)[1] recently presented a theoretical analysis of the turbulent boundary layer over flat plates. He used experimental data and the equations governing the flow as a basis of analysis. A two-layer model for the turbulent boundary layer was suggested. According to this concept the entire boundary layer is arbitrarily divided into (i) an inner layer, and (ii) an outer layer. Within the inner layer most of the turbulent energy is produced by interaction of the Reynolds stress and the mean velocity gradient. Since the layer is thin and close to the solid boundary, the shear stress may be considered as constant over this layer. The motion in this layer is determined only by the wall stress and the fluid viscosity. This layer is also called a constant-stress layer. The outer layer, which comprises the major part of the boundary layer, receives its greatest portion

---

[1] Number in the parenthesis refers to entries in the bibliography.

of turbulent energy by diffusion from the constant-stress layer, and the flow is retarded by the Reynolds stress. The local shear stress at the wall depends on the local structure of the outer layer which in turn depends on the distribution of wall stress for some distance upstream from the point of observation. On the other hand, turbulent motion in the outer layer resembles that observed in wakes. Townsend applied the hypothesis of self-preservation to analyze the flow in the outer layer. His analysis is approximately valid when the variation of wall shear is negligible. The hypothesis of self-preservation requires that the variation of any time-mean flow characteristic over a plane, x = constant, should be expressible by a non-dimensional parameter. The scales of length and velocity used to form dimensional parameters are functions of x only. By the application of the self-preserving hypothesis equations for mean-velocity distribution and Reynolds-stress distribution are obtained. By assuming that the eddy viscosity is constant in the outer layer, Townsend was able to eliminate the discrepancies between observed and derived distributions of velocity

Clauser (3) also presented an analysis (based on published experimental data) of the turbulent boundary layer with

and without pressure gradients. This analysis was carried out by dividing the turbulent boundary layer into three parts (i) a laminar sublayer next to the wall, about 0.1 to 1.0 percent of the total thickness, (ii) turbulent portion near the wall, about 10 to 20 percent of the layer, and (iii) fully-turbulent outer region, about 80 to 90 percent of the thickness. He concluded that it is not possible to have complete similarity of velocity profiles for turbulent boundary layers at different sections in the direction of flow. However, velocity profiles exhibit near similarity for turbulent boundary layers without pressure gradients and under equilibrium conditions. The scales of velocity and length for such a universal plot are (i) shear velocity, $U_* = \sqrt{\tau_w/\rho}$, and (ii) boundary-layer thickness, δ. Clauser assumed that the eddy viscosity ϵ is constant for the outer region of the turbulent layer. The eddy viscosity of the outer layer is proportional to $U_o\delta^*$ and appears not to be affected by the pressure gradient, Reynolds number, or roughness.

Turbulent Boundary Layers Over Unheated, Plane, Rough Surfaces

Perhaps the earliest paper on the study of boundary layers over rough horizontal surfaces is due to Prandtl and Schlichting (12). They used Nikuradse's data on flow through

rough pipes to calculate the drag on a rough plate. Rotta (13) presented an analysis of the turbulent boundary layer over rough and smooth plates. He assumed that the kinematic viscosity and the wall roughness were effective only in a thin layer near the wall. Outside this layer, the velocity distribution could be represented by the universal profile using the parameters (yU_*/δ^*U_o) and $(\overline{U} - U_o)/U_*$. He used the data published by Schultz-Grunow and Tillman for his analysis.

Moore (11) studied the development of turbulent layers over a rough surface. He used bars placed normal to the direction of flow on a plane surface as the roughness elements. To obtain a better agreement for the plot of $(U_o - \overline{U})/U_*$ vs y/δ, he added $\frac{2}{3}$ of the height of the bar to y. He also measured $\overline{U'V'}$ to obtain the distribution of shear stress in the boundary layer and remarked ". . .the hot-wire results were too erratic to be of value." Therefore, he determined the distribution of shear stress by evaluating the momentum integral, starting at successive points in the boundary layer and integrating outward to the free stream. Hama (8) published comprehensive data from his own experiments and from the experiments of others. His roughness elements consisted of a wire mesh. He employed the same parameter for the velocity profile as used by Rotta (13),

Hama showed that the effect of roughness is to shift the intercept of the logarithmic plot of velocity. For various roughnesses all of the logarithmic velocity plots shifted parallel to each other with the magnitude of the displacement expressed by $(\Delta\overline{U}/U_*)$ being equal to the difference between $\sqrt{2/c_f}$ for the smooth and for the rough boundaries. Both Townsend (22) and Clauser (3) (in their analyses of turbulent boundary layers over rough plates) concluded that in the neighborhood of the roughness elements the flow is affected by their presence. If the variation of the wall stress is comparatively small, however, the characteristics of the self-preserving or equilibrium outer layer is similar to that for the smooth plates. Therefore, it is possible to employ an analysis of the turbulent layer over rough surfaces identical to that for a smooth plate, and the motion can be determined by the wall stress τ_w and the boundary-layer thickness δ .

Turbulent Boundary Layers Over Smooth-Heated Plates

The earliest measurements of mean velocity and temperatures in the turbulent boundary layer over heated, smooth plates were made by Elias (6). Elias's results are discussed by Squire (17) in the light of the theory of momentum transport. The mean

velocity and temperature profiles were observed to be similar. Johnson (10) made measurements of temperature, velocity, turbulent shear and other turbulent quantities for U_o = 25 fps and ΔT_o = 15°C. He found that the mean velocity and temperature distributions are dissimilar. The wall-shear stress obtained by the extrapolation of Reynolds stress was found to be higher than those obtained by the momentum integral or other standard empirical equations. Batchelor (1) presented some experimental data obtained by Nicholl for U_o = 7.9 fps and ΔT_o = 175°F. Since the temperature was high compared to the velocity, buoyancy effects were considered. The other experimental data are those of Spengos (18) and Spengos and Cermak (19), also Cermak and Spengos (4), and Reynolds, Kays and Kline (14). The present research is a continuation of the work of Cermak and Spengos (4) in which measurements of velocity, temperature, intensities of turbulence and turbulent shear stress were made for combinations of U_o and ΔT_o of 6, 10, 17 and 35 fps; and 100, 110, 85, and 60°F respectively.

Turbulent Boundary Layers Over Plane, Heated, Rough Plates

The writer is not aware of any published data on flow over plane, rough surfaces with heat transfer to the air. There are

some experimental data, however, for flow through rough pipes. These will not be discussed here because they do not relate directly to this investigation.

Chapter III

THEORETICAL ANALYSIS

The basic equations governing the flow of fluid with heat transfer are first presented for instantaneous values of the dependent variables. The instantaneous quantities are then expressed as the sum of a time-mean value and a fluctuation about this mean value. The resulting equations are used to obtain the equations of motion (known as Reynolds equations) and the equation of energy for heat. Applying an approximation of the boundary-layer type, the equations of motion and energy are simplified and integrated over the boundary layer to obtain the momentum integral and the energy integral equations.

Dimensionless parameters are obtained by expressing in dimensionless form the equations of motion, energy, and the integral forms of these equations. The hypothesis of self-preservation is used in the equation of motion to obtain the conditions of self-preserving motion as given by Townsend (22). These conditions together with the equation of motion yield quasi-empirical equations for the distribution of velocity, the law of skin-friction, and the distribution of turbulent shear stress (commonly called Reynolds stress).

Following an approach similar to the development of the relationship for the velocity distribution and the law of skin-friction, a relationship for the mean temperature distribution and the law of local coefficient of heat transfer are obtained.

The following references were used as sources for the various theoretical equations which were modified for use in this study: (3), (8), (16), (17), (22), and (23).

Basic Equations

Equations for a complete description of the motion of a compressible fluid are:

(i) Navier-Stokes equations :

$$\rho \frac{DU_i}{Dt} = X_i - \frac{\partial P}{\partial x_i} + \frac{\partial}{\partial x_i}\left(\mu \frac{\partial U_i}{\partial x_j}\right) + \frac{\partial}{\partial x_j}\left(\mu \frac{\partial U_j}{\partial x_i}\right) - \frac{2}{3}\frac{\partial}{\partial x_i}\left(\mu \frac{\partial U_j}{\partial x_j}\right) \quad (1)$$

in which $\frac{D}{Dt} = \frac{\partial}{\partial t} + U_j \frac{\partial}{\partial x_j}$; $i, j = 1, 2, 3$

and a repeated index indicates summation.

(ii) Equation of continuity :

$$\frac{\partial \rho}{\partial t} + \frac{\partial}{\partial x_i}(\rho U_i) = 0 \quad (2)$$

(iii) Energy equation[1] for heat (considered c_p and k as being independent of temperature) :

$$g\rho c_p \frac{DT}{Dt} = \frac{DP}{Dt} + k\frac{\partial}{\partial x_i}\left(\frac{\partial T}{\partial x_i}\right) + \mu\Phi \qquad (3)$$

in which the dissipation function

$$\Phi = \frac{\partial U_i}{\partial x_j}\left(\frac{\partial U_i}{\partial x_j} + \frac{\partial U_j}{\partial x_i}\right) \qquad (4)$$

(iv) Equation of state (for perfect gas) :

$$P = \rho g R T \qquad (5)$$

(v) Empirical viscosity law :

$$\mu = \mu(T) \qquad (6)$$

If the body force X_i is considered to be given, then there are seven simultaneous equations and seven unknowns - U_i , P , ρ , T and μ .

Any fluid motion (fluid considered as a continuum) must satisfy the equations of motion and the equation of continuity.

---

[1] In the energy equation the terms involving thermal energy are implicitly converted to units of mechanical energy.

The equation of state, gives a relationship between P, ρ, and T under the assumption that the perfect gas law holds. The energy equation expresses a balance between heat and mechanical energy. Finally, interdependence of viscosity and temperature is given by an empirical viscosity law.

For the steady state condition, assuming viscosity to be constant (which is justifiable if $\Delta T_o < 90^0 F$), and replacing the body force X_i by buoyancy per unit volume ($\rho g_i \beta \theta$) caused by the density difference, the above sets of equations reduce to the following form.

The Navier-Stokes equations are:

$$\rho U_j \frac{\partial U_i}{\partial x_j} = - \frac{\partial P}{\partial x_i} + \rho g_i \beta \theta$$

$$+\mu \left[\frac{\partial^2 U_i}{\partial x_j \partial x_j} + \frac{1}{3} \frac{\partial}{\partial x_i} \left(\frac{\partial U_j}{\partial x_j} \right) \right] \qquad (7)$$

The equation of continuity is:

$$\frac{\partial}{\partial x_i} (\rho U_i) = 0 \qquad (8)$$

The energy equation is :

$$c_p \rho g \left(U_i \frac{\partial T}{\partial x_i} \right) = k \frac{\partial^2 T}{\partial x_i \partial x_i} + U_i \frac{\partial P}{\partial x_i} + \mu \Phi \, . \qquad (9)$$

The equation of state is :

$$P = \rho g R T \quad . \qquad (5)$$

In these equations U_i , ρ , P , and T represent instantaneous values. Following Reynolds hypothesis that the instantaneous value of each fluid properly can be considered as the sum of two parts: (i) a mean value which varies slowly with time if at all, and (ii) a fluctuating component which is a function of time, one can write,

$$\begin{aligned} U_i(t) &= \overline{U}_i + U_i'(t) \, , \\ \rho(t) &= \overline{\rho} + \rho'(t) \, , \\ P(t) &= \overline{P} + P'(t), \end{aligned} \qquad (10.a)$$

and

$$\rho U_i(t) = \overline{\rho U_i} + (\rho U_i)' .$$

The mean of a quantity (Q) is defined by

$$\overline{(Q)} = \lim_{(t_1 - t_2) \to \infty} \frac{1}{t_1 - t_2} \int_{t_1}^{t_2} Q(t)\, dt$$

The following rules of averaging were introduced by Reynolds :

$$\overline{(Q)'} = 0$$

$$\overline{(\overline{Q})(Q)} = (\overline{Q})(\overline{Q}) \qquad (10.b)$$

and

$$\overline{\frac{\partial}{\partial x_i}(Q)} = \frac{\partial}{\partial x_i}(\overline{Q})$$

The second rule leads to the result,

$$\overline{U_i'(t)} = \overline{P'(t)} = \overline{\rho'(t)} = \overline{(\rho U_i)'} = 0 \qquad (10.c)$$

Replacing the instantaneous values by the sum of their mean and fluctuating quantities in Eq 8, upon taking a time-average, the equation of continuity for mean and fluctuating quantities become

$$\frac{\partial}{\partial x_i}(\overline{\rho U_i}) = 0 \qquad (11.a)$$

and $$\frac{\partial}{\partial x_i}(\rho U_i)' = 0 \quad . \tag{11.b}$$

Reynolds equations: -- Replacing the instantaneous values by their mean and fluctuation values in the equation of motion, taking the time average, and making use of Eq 11.b, Eq 7 reduces to

$$\overline{\rho U_j}\frac{\partial}{\partial x_j}\overline{U_i} = -\frac{\partial \bar{P}}{\partial x_i} + \bar{\rho} g_i \beta \bar{\theta} + g_i \beta \overline{\rho' T'}$$

$$+\mu\left[\frac{\partial^2 U_i}{\partial x_j \partial x_j} + \frac{1}{3}\frac{\partial}{\partial x_i}\left(\frac{\partial \bar{U}_j}{\partial x_j}\right)\right] + \frac{\partial}{\partial x_j}\left[-\overline{(\rho U_j)' U_i'}\right] . \tag{12}$$

The term $-\overline{(\rho U_j)' U_i'}$ is the generalized Reynolds stress (or apparent stress) for compressible flow.

Energy equation: -- Multiplying Eq 7 by U_i, adding the resulting equation to Eq 9 and using the Eq 8, an energy equation in the following form is obtained:

$$g c_p \frac{\partial}{\partial x_i}(\rho U_i T) + \frac{1}{2}\frac{\partial}{\partial x_i}(\rho U_i U_j U_j)$$

$$= \left[k\frac{\partial^2 T}{\partial x_i \partial x_i} + U_i \frac{\partial P}{\partial x_i} + \mu \Phi\right] + \left[-U_i \frac{\partial P}{\partial x_i}\right.$$

$$\left. + \rho g_i \beta \theta U_i\right] + \mu\left[U_i \frac{\partial^2 U_i}{\partial x_j \partial x_j} + \frac{1}{3} U_i \frac{\partial}{\partial x_i}\left(\frac{\partial U_j}{\partial x_j}\right)\right] . \tag{13}$$

An energy equation useful for turbulent flow analysis can be obtained by replacing the instantaneous values in Eq 13 by the sum of their mean and fluctuation values and taking a time mean. Various terms from the left hand and right hand side of Eq 13 can be eliminated by the use of the equation obtained by multiplying Eq 12 by $\overline{U}_i$. An energy equation in the following form is obtained:

$$g c_p \overline{\rho U_i} \frac{\partial \overline{T}}{\partial x_i} + g c_p \frac{\partial}{\partial x_i} \overline{T'(\rho U_i)'} + \frac{1}{2} \overline{\rho U_j} \frac{\partial}{\partial x_j} \overline{U_i' U_i'}$$

$$+ \overline{U'(\rho U_j)'} \frac{\partial}{\partial x_j} \overline{U}_i + \frac{1}{2} \frac{\partial}{\partial x_j} \overline{(\rho U_j)' U_i' U_i'}$$

$$= k \frac{\partial^2 \overline{T}}{\partial x_i \partial x_i} + \overline{U}_i \frac{\partial \overline{P}}{\partial x_i} + \overline{U_i' \rho'} g_i \beta \overline{\theta} + \overline{U_i' T'} \overline{\rho} g_i \beta \overline{\theta} + \overline{U_i' \frac{\partial P'}{\partial x_i}}$$

$$+ \mu \overline{\Phi} + \mu \Phi' + \mu \overline{U_i' \frac{\partial^2 U_i'}{\partial x_j \partial x_j}} + \frac{1}{3} \mu \overline{U_i' \frac{\partial}{\partial x_i} \left(\frac{\partial U_j'}{\partial x_j} \right)}, \qquad (14)$$

in which

$$\Phi' = \overline{\left(\frac{\partial U_i'}{\partial x_j} \right) \left(\frac{\partial U_i'}{\partial x_j} \right)} + \overline{\left(\frac{\partial U_j'}{\partial x_i} \right) \left(\frac{\partial U_i'}{\partial x_j} \right)} .$$

By analogy with $-\overline{(\rho U_j)' U_i'}$ the term $\overline{(\rho U_i)' T'}$ may be called a generalized apparent heat-flux.

For the two-dimensional case Eqs 11.a, 11.b and 12 become

$$\frac{\partial}{\partial x_1}(\overline{\rho U_1}) + \frac{\partial}{\partial x_2}(\overline{\rho U_2}) = 0 , \tag{16.a}$$

$$\frac{\partial}{\partial x_1}(\rho U_1)' + \frac{\partial}{\partial x_2}(\rho U_2)' = 0 , \tag{16.b}$$

$$\begin{aligned}\overline{\rho U_1}\frac{\partial}{\partial x_1}\overline{U}_1 + \overline{\rho U_2}\frac{\partial}{\partial x_2}\overline{U}_1 = & -\frac{\partial \bar{P}}{\partial x_1} + g_1\beta\bar{\rho}\bar{\theta} + g_1\beta\overline{\rho'T'} \\ & + \mu\left[\frac{\partial^2 \bar{U}_1}{\partial x_1^2} + \frac{\partial^2 \bar{U}_1}{\partial x_2^2} + \frac{1}{3}\frac{\partial}{\partial x_1}\left(\frac{\partial \bar{U}_1}{\partial x_1} + \frac{\partial \bar{U}_2}{\partial x_2}\right)\right] \\ & + \frac{\partial}{\partial x_1}\left[-\overline{(\rho U_1)'U_1'}\right] + \frac{\partial}{\partial x_2}\left[-\overline{(\rho U_2)'U_1'}\right] ,\end{aligned} \tag{17.a}$$

$$\begin{aligned}\overline{\rho U_1}\frac{\partial}{\partial x_1}\overline{U}_2 + \overline{\rho U_2}\frac{\partial \bar{U}_2}{\partial x_2} = & -\frac{\partial \bar{P}}{\partial x_2} + \bar{\rho} g_2\beta\theta + g_2\beta\,\overline{\rho'T'} \\ & + \mu\left[\frac{\partial^2 \bar{U}_2}{\partial x_1^2} + \frac{\partial^2 \bar{U}_2}{\partial x_2^2} + \frac{1}{3}\frac{\partial}{\partial x_2}\left(\frac{\partial \bar{U}_1}{\partial x_1} + \frac{\partial \bar{U}_2}{\partial x_2}\right)\right] \\ & + \frac{\partial}{\partial x_1}\left[-\overline{(\rho U_1)'U_2'}\right] + \frac{\partial}{\partial x_2}\left[-\overline{(\rho U_2)'U_2'}\right] ,\end{aligned} \tag{17.b}$$

and

$$\begin{aligned}0 = & \frac{\partial}{\partial x_1}\left[-\overline{(\rho U_1)'U_3'}\right] + \frac{\partial}{\partial x_2}\left[-\overline{(\rho U_2)'U_3'}\right] \\ & + \bar{\rho} g_3\beta\bar{\theta} + g_3\beta\,\overline{\rho'T'} .\end{aligned} \tag{17.c}$$

Applying boundary-layer approximations, taking $g_1 = 0$ and neglecting Eq 17.c, Eqs 17.a and 17.b reduce to

$$\overline{\rho U_1}\,\frac{\partial \bar{U}_1}{\partial x_1} + \overline{\rho U_2}\,\frac{\partial \bar{U}_1}{\partial x_2} = -\frac{\partial \bar{P}}{\partial x_1} + \mu\frac{\partial^2 \bar{U}_1}{\partial x_2^2} + \frac{\partial}{\partial x_1}\left[-\overline{(\rho U_1)'U_1'}\right] + \frac{\partial}{\partial x_2}\left[-\overline{(\rho U_2)'U_1'}\right], \quad (18.a)$$

and $$0 = -\frac{\partial \bar{P}}{\partial x_2} + g_2\beta\bar{\rho}\theta + g_2\beta\overline{\rho'T'} + \frac{\partial}{\partial x_2}\left[-\overline{(\rho U_2)'U_2'}\right]. \quad (18.b)$$

On integration between any point in the boundary layer to a point outside the boundary layer and assuming that $\overline{(\rho U_2)'U_2'} = 0$ for $x_2 > \delta$ and $\overline{\rho'T'}$ is small compared to the other terms, Eq 18.b yields on integration

$$P_o - \bar{P} = \int_{x_2}^{h} g_2\beta\bar{\rho}\bar{\theta}\,dx_2 + \overline{(\rho U_2)'U_2'}, \quad (19)$$

in which P_o is the pressure outside the boundary layer and $h > \delta$. Differentiating with respect to x_1 and rearranging, Eq 19 becomes

$$-\frac{\partial \bar{P}}{\partial x_1} = -\frac{\partial P_o}{\partial x_1} + \frac{\partial}{\partial x_1}\overline{(\rho U_2)'U_2'} + \frac{\partial}{\partial x_1}\int_{x_2}^{h} g_2\beta\bar{\rho}\,\bar{\theta}\,dx_2, \quad (20)$$

Substituting this value of $\frac{\partial \bar{P}}{\partial x_1}$ in Eq 18.a and assuming that $\frac{\partial P_o}{\partial x_1} \neq 0$, Eq 18.a becomes

$$\overline{\rho U_1}\,\frac{\partial \bar{U}_1}{\partial x_1} + \overline{\rho U_2}\,\frac{\partial \bar{U}_1}{\partial x_2} + \frac{\partial}{\partial x_1}\left[-\overline{(\rho U_1)' U_1'} - \overline{(\rho U_2)' U_2'}\right]$$

$$= \mu \frac{\partial}{\partial x_2}\left(\frac{\partial \bar{U}_1}{\partial x_2}\right) + \frac{\partial}{\partial x_1}\int_{x_2}^{h} g_2 \beta \bar{\rho}\,\theta\, dx_2 + \frac{\partial}{\partial x_2}\left[-\overline{(\rho U_2)' U_1'}\right] . \qquad (21)$$

For the two-dimensional case, using boundary-layer approximations, neglecting the 3rd, 4th, 6th and 7th terms on the right hand side of Eq 14, using the value of $\frac{\partial \bar{P}}{\partial x_1}$ from Eq 20 and assuming $\frac{\partial P_0}{\partial x_1} = 0$, Eq 14 can be reduced to

$$g c_p\left(\overline{\rho U_1}\,\frac{\partial \bar{T}}{\partial x_1} + \overline{\rho U_2}\,\frac{\partial T}{\partial x_2}\right) + \tfrac{1}{2}\left(\overline{\rho U_1}\,\frac{\partial}{\partial x_1}\overline{U_1' U_1'} + \overline{\rho U_2}\,\frac{\partial}{\partial x_2}\overline{U_1' U_1'}\right.$$

$$\left. + \overline{\rho U_1}\,\frac{\partial}{\partial x_1}\overline{U_2' U_2'} + \overline{\rho U_2}\,\frac{\partial}{\partial x_2}\overline{U_2' U_2'}\right)$$

$$= - g c_p \frac{\partial}{\partial x_2}\left[\overline{T'(\rho U_2)'}\right] + k\frac{\partial^2 \bar{T}}{\partial x_2^2} + \overline{U_2' \rho'}\, g_2 \beta \bar{\theta} + \overline{U_2' T'} \bar{\rho} g_2 \beta \bar{\theta}$$

$$+ \mu\left(\frac{\partial \bar{U}_1}{\partial x_2}\right)^2 - \overline{U_1'(\rho U_2)'}\,\frac{\partial \bar{U}_1}{\partial x_1} + \frac{\partial}{\partial x_1}\left[\overline{(\rho U_2)' U_2'}\right]$$

$$+ \frac{\partial}{\partial x_1}\int_{x_2}^{h} g_2 \beta \bar{\theta} \bar{\rho}\, dx_2 . \qquad (22)$$

The various quantities in Eqs 16.a, 21, and 22 can be expanded as follows:

$$\begin{aligned}
\overline{\rho U_1} &= \bar{\rho}\,\bar{U}_1 + \overline{\rho' U_1'} \\
\overline{(\rho U_1)' U_1'} &= \bar{\rho}\,\overline{U_1' U_1'} + \bar{U}_1 \overline{\rho' U_1'} + \overline{\rho' U_1' U_1'} \qquad (23) \\
\overline{T'(\rho U_1)'} &= \bar{\rho}\,\overline{U_1' T'} + \bar{U}_1 \overline{T' \rho'} + \overline{U_1' T' \rho'}
\end{aligned}$$

Similar expressions for $\overline{\rho U_2}$, $\overline{(\rho U_1)' U_2'}$, $\overline{(\rho U_2)' U_1'}$ and $\overline{T'(\rho U_2)'}$ can be obtained.

Substituting Eq 23 in Eq 16.a, the following equation is obtained,

$$\frac{\partial}{\partial x_1}\bar{\rho}\,\bar{U}_1 + \frac{\partial}{\partial x_2}\bar{\rho}\,\bar{U}_2 + \frac{\partial}{\partial x_1}\overline{\rho' U_1'} + \frac{\partial}{\partial x_2}\overline{\rho' U_2'} = 0 \,. \tag{24}$$

If the last two terms are neglected, Eq 25.a becomes

$$\frac{\partial}{\partial x_1}\bar{\rho}\,\bar{U}_1 + \frac{\partial}{\partial x_2}\bar{\rho}\,\bar{U}_2 = 0 \,. \tag{25}$$

Substituting Eq 23 in Eq 21 and 22 neglecting $\overline{\rho' U_1'}$, $\overline{\rho' U_2'}$, $\overline{\rho' T'}$ and the triple correlation terms, Eq 21 and 22 become

$$\bar{\rho}\,\bar{U}_1 \frac{\partial}{\partial x_1}\bar{U}_1 + \bar{\rho}\,\bar{U}_2 \frac{\partial \bar{U}_1}{\partial x_2} + \frac{\partial}{\partial x_1}\left[\bar{\rho}\,\overline{(U_1')^2} - \bar{\rho}\,\overline{(U_2')^2}\right]$$
$$= \mu \frac{\partial}{\partial x_2}\left(\frac{\partial \bar{U}_1}{\partial x_2}\right) - \frac{\partial}{\partial x_2}\bar{\rho}\,\overline{U_1' U_2'} - \frac{\partial}{\partial x_1}\int_{x_2}^{h} \bar{\rho}\, g_2 \beta \bar{\theta}\, dx_2 \,, \tag{26}$$

$$g c_p (\bar{\rho}\,\bar{U}_1)\frac{\partial \bar{T}}{\partial x_1} + g c_p (\bar{\rho}\,\bar{U}_2)\frac{\partial \bar{T}}{\partial x_2} + \frac{1}{2}\left[\bar{\rho}\,\bar{U}_1 \frac{\partial}{\partial x_1}\overline{U_1' U_1'} + \bar{\rho}\,\bar{U}_2 \frac{\partial}{\partial x_2}\overline{U_1' U_1'}\right.$$
$$\left. \bar{\rho}\,\bar{U}_2 \frac{\partial}{\partial x_2}\overline{U_1' U_1'} + \bar{\rho}\,\bar{U}_1 \frac{\partial}{\partial x_1}\overline{U_2' U_2'} + \bar{\rho}\,\bar{U}_2 \frac{\partial}{\partial x_2}\overline{U_2' U_2'}\right]$$
$$= k \frac{\partial}{\partial x_2}\left(\frac{\partial \bar{T}}{\partial x_2}\right) + \mu \left(\frac{\partial \bar{U}_1}{\partial x_2}\right)^2 - g c_p \frac{\partial}{\partial x_2}\left(\bar{\rho}\,\overline{U' T'}\right) + \bar{\rho}\,\overline{U_2' U_1'}\,\frac{\partial \bar{U}_1}{\partial x_2}$$
$$+ \frac{\partial}{\partial x_1}\left(\bar{\rho}\,\overline{U_2' U_1'}\right) + \frac{\partial}{\partial x_1}\int_{x_2}^{h} g_2 \beta \bar{\rho}\,\bar{\theta}\, dx_2 \,. \tag{27}$$

Momentum Integral

Since the pressure within the boundary layer is essentially established by the free-stream pressure, the pressure gradient can be eliminated by Bernoulli's equation written for a streamline at the outer edge of the boundary layer. Therefore, from the Bernoulli equation one obtains

$$\frac{\partial P_o}{\partial x_1} = - \bar{\rho}_o U_o \frac{\partial U_o}{\partial x_1} \quad . \tag{28}$$

From Eq 25 the following relationship is obtained,

$$\bar{\rho}\,\bar{U}_2 = - \int_o^{x_2} \frac{\partial}{\partial x_1}(\bar{\rho}\,\bar{U}_1)\, dx_2 \tag{29}$$

Substitution of Eqs 28 and 29 in Eq 26 and integration over the entire boundary layer yields the momentum integral equation for the momentum boundary-layer in the following form:

$$\frac{d\delta^{**}}{dx_1} + \frac{\delta^{**}}{U_o}\frac{dU_o}{dx_1}\left(2 + \frac{\delta^*}{\delta^{**}}\right) + \left[\frac{U_o}{\rho_o}\frac{d\rho_o}{dx_1}\frac{\delta^{**}}{U_o}\right]$$

$$= \frac{\tau_w}{\rho_o U_o^2} + \frac{1}{\rho_o U_o^2}\int_o^h \frac{\partial}{\partial x_1}\left[\bar{\rho}\,\overline{(U_1')^2} - \bar{\rho}\,\overline{(U_2')^2}\right] dx_2$$

$$+ \int_o^h \frac{\partial}{\partial x_1}\int_{x_2}^h g_2\,\bar{\rho}\,\beta\,\bar{\theta}\, dx_2\, dx_2 \tag{30}$$

The displacement thickness (δ^*) and the momentum thickness (δ^{**}) are defined as

$$\delta^* = \int_0^\infty \left(1 - \frac{\bar{\rho}}{\rho_0}\frac{\bar{U}_1}{U_0}\right) dx_2 \qquad (31.a)$$

and

$$\delta^{**} = \int_0^\infty \frac{\bar{\rho}}{\rho_0}\frac{\bar{u}}{U_0}\left(1 - \frac{\bar{u}}{U_0}\right) dx_2 \,. \qquad (31.b)$$

If the variation of $\bar{p}$ in the boundary layer is assumed to be negligible, from Eq 5 the following approximate relationship is obtained,

$$\frac{\bar{\rho}}{\rho_0} = \frac{T_0}{\bar{T}} \qquad (31.c)$$

Assuming that the pressure gradient outside the boundary layer to be zero and the fluid outside the boundary layer to be incompressible, Eq 30 reduces to

$$\frac{d\delta^{**}}{dx_1} = \frac{\tau_\omega}{\rho_0 U_0^2} + \frac{1}{\rho_0 U_0^2}\int_0^h \frac{\partial}{\partial x_1}\left[\bar{\rho}\,\overline{(u_1')^2} - \bar{\rho}\,\overline{(u_2')^2}\right] + \int_0^h \frac{\partial}{\partial x_1}\int_{x_2}^h \bar{\rho} g_2 \beta \bar{\theta}\, dx_2\, dx_2 \qquad (32)$$

The second term on the right hand side of Eq 31 is due to anisotropy of the normal apparent stresses and the last term is due

to buoyancy. If these two terms are neglected, Eq 32 takes the familiar form of the von Kármán momentum integral equation for incompressible fluids with a zero pressure gradient:

$$2\frac{d\delta^{**}}{dx_1} = \frac{\tau_\omega}{\frac{1}{2}\rho_0 U_0^2} \tag{33.a}$$

or

$$\frac{d\delta^{**}}{dx_1} = \frac{c_f}{2} \quad . \tag{33.b}$$

It should be noted that in Eq 33.a, δ^{**} is evaluated by Eq 31.b.

Energy Integral

By a similar simplification and use of the continuity equation, Eq 27 can be integrated over the thermal boundary layer to yield

$$g c_p \frac{d}{dx_1}\int_0^\infty \bar{\rho}\,\bar{U}_1\,(\bar{T}-T_0)\,dx_2 = k\left(\frac{\partial \bar{T}}{\partial x_2}\right)_{x_2=0} \tag{34}$$

or

$$g c_p \bar{\rho}\,\bar{U}_0\,(T_\omega - T_0)\frac{d\delta_T^{**}}{dx_1} = q_\omega \quad , \tag{35}$$

in which the convective thickness δ_T^{**} is defined by

$$\delta_T^{**} = \int_0^\infty \frac{\bar{\rho}}{\rho_0}\frac{\bar{U}_1}{U_0}\frac{\bar{T}-T_0}{T_\omega - T_0}\,dx_2 \quad ,$$

$$\delta_T^{**} = \int_0^\infty \frac{\bar{\rho}}{\rho_0} \frac{\bar{U}}{U_0} \left(1 - \frac{T_w - \bar{T}}{T_w - T_0}\right) dx_2$$

An equation for the local heat-transfer coefficient analogous to that for c_f is

$$S_t = \frac{d\delta_T^{**}}{dx_1} \tag{37}$$

in which S_t is the Stanton heat-transfer coefficient. [1]

Dimensional Consideration

By use of U_o, l_o, ΔT_o as inference velocity, length and temperature respectively, Eqs 7 and 9 can be written in dimensionless form as :

$$U_j \cdot \frac{\partial U_i}{\partial x_j} = -\frac{\partial P}{\partial x_i} + \frac{Gr}{Re^2}$$

$$+ \frac{1}{Re}\left[\frac{\partial^2 U_i}{\partial x_j \partial x_j} + \frac{1}{3}\frac{\partial}{\partial x_i}\left(\frac{\partial U_j}{\partial x_j}\right)\right] \tag{38}$$

---

[1] Jakob, M. Heat Transfer, Vol. I, 1949. p. 519 and Ref (16) pp. 763 and 828.

and

$$U_i \frac{\partial T}{\partial x_i} = \frac{1}{Pr \cdot Re} \left(\frac{\partial^2 T}{\partial x_i \partial x_i} \right) + Ec \left(U_i \frac{\partial P}{\partial x_i} \right)$$

$$+ \frac{Ec}{R} \Phi \qquad (39)$$

The dimensionless parameters [1] are defined as

Re	Reynolds number	$\frac{U_o l_o}{\nu}$
Pr	Prandtl number	$\frac{\mu g c_p}{k}$
Gr	Grashof number	$\frac{g \beta \Delta T_o l_o^3}{\nu}$
Ec	Eckert number [1]	$\frac{U_o}{g c_p \Delta T_o}$

Since integration of Eqs 21 and 22, which are derivable from Eqs 7 and 9, yield the wall shear and the heat flux at the wall $\left[q_w = k \left(\frac{\partial \bar{T}}{\partial x_2} \right)_{x_2} = 0 \right]$, they will involve the same dimensionless parameter as Eqs 38 and 39; therefore, the velocity field, the temperature field, the local coefficient of wall shear c_f, and the local coefficient of heat transfer, Stanton number S_t

---

[1] Schlichting (14) p. 250

depend upon the dimensionless groups:

$$\begin{aligned} \frac{\bar{U}}{U_o} &= f_1(x_i', Re, Pr, Gr, Ec), \\ \frac{T_\omega - T}{T_\omega - T_o} &= f_2(x_i', Re, Pr, Gr, Ec), \\ c_f &= f_3(x_i', Re, Pr, Gr, Ec), \\ \text{and} \quad St &= f_4(x_i', Re, Pr, Gr, Ec), \end{aligned} \tag{40}$$

in which x_i' is dimensionless space coordinates. For a constant **Pr** and for forced convection with moderate temperature difference between the heated surface and the free stream temperature, the effect of Gr and Ec will be negligible.

Mean Velocity Distribution

For the unheated case, simultaneous solution of the equation of motion, Eq 26; the equation of continuity, Eq 25.b; together with the equation of the turbulent energy, Eq 22 will give the description of turbulent flow. However, this is not possible, because the number of variables are more than the number of equations. Therefore, further hypothesis based on the experimental data and physical reasoning are required. Turbulent boundary layers may be divided into (i) an inner layer,

and (ii) an outer layer. The inner layer can further be subdivided into (a) a laminar sublayer, and (b) a transition layer. If the variation of wall stress is small, it is assumed that the shear stress over the inner layer is constant. The flow in the outer layer which comprises about 80-90 percent of the boundary layer is assumed to be nearly similar. Then the hypothesis of self-preservation as presented by Townsend (22) can be applied to this layer. According to this assumption, it should be possible to express the variation of mean quantities at any plane x = constant, by some suitable scale of length ℓ_o and velocity u_o as universal functions of (x_2/ℓ_o). The scale of velocity and length are functions of distance in the flow direction.

For a zero pressure gradient, and assuming that the variation of density is very small as well as neglecting buoyancy, Eq 26 reduces to

$$\bar{U}\frac{\partial \bar{U}}{\partial x} + \bar{V}\frac{\partial \bar{U}}{\partial y} + \frac{\partial}{\partial x}\left(\overline{u'^2} - \overline{v'^2}\right) = \nu\frac{\partial^2 \bar{U}}{\partial y^2} + \frac{\partial}{\partial y}\overline{u'v'} \qquad (41)$$

The conditions of self-preservation (22) can be written as

$$\bar{U} = U_o + U_o f_5 (y/\ell_o)$$
$$\overline{U'V'} = U_o^2 \Phi_{12} (y/\ell_o)$$
$$\overline{U'^2} = U_o^2 \Phi_1 (y/\ell_o) \qquad (42.a, b, c, d)$$
$$\overline{V'^2} = U_o^2 \Phi_2 (y/\ell_o)$$

It is further assumed that this hypothesis can be extended to a part of the inner layer which is in turbulent motion. Since the variation of wall stress is assumed to be small, the scales of velocity and length for the two layers are taken as the same.

Laminar layer: -- The wall shear stress is given by the equation,

$$\tau_\omega = \mu \left(\frac{\partial \bar{U}}{\partial y}\right)_{y=0} \qquad (43)$$

If it is assumed that within this layer τ is constant and equal to τ_ω, Eq 43 can be written as

$$\tau_\omega = \mu \left(\frac{\partial \bar{U}}{\partial y}\right),$$

and by definition

$$\tau_\omega = \bar{\rho} U_*^2 ,$$

therefore,

$$\bar{\rho} U_*^2 = \mu \left(\frac{\partial \bar{U}}{\partial y}\right) \qquad (44)$$

with the boundary condition $y = 0$; $U = 0$, the solution of the above equation is

$$\bar{U}/U_* = \frac{U_* y}{\nu},$$

or
$$\frac{\bar{U}}{U_*} = f_6(Re_*) . \tag{45}$$

Transition region: -- Using the assumption that the shear stress is constant over this region and equal to that at the wall, the velocity distribution can be described by only the wall stress and the viscosity. Therefore,

$$\bar{U} = f_7(\tau_\omega, \mu, \rho, y) \tag{46}$$

The above variables can be combined to yield the following dimensionless equation

$$\frac{\bar{U}}{U_*} = f_8\left(\frac{U_* y}{\nu}\right),$$

or
$$\frac{\bar{U}}{U_*} = f_8(Re_*) . \tag{47}$$

Outerlayer: -- From the hypothesis of self-preservation of the mean motion, velocity distribution can be expressed as

$$\bar{U} = U_o + u_o f_5(y/l_o) . \tag{42.a}$$

Using U_* and δ which depend on x, as the scale of velocity and length respectively, Eq 42.a can be written as

$$\frac{\bar{U}}{U_*} = \frac{U_o}{U_*} + f_5 (y/\delta) , \tag{48.a}$$

or

$$\frac{\bar{U} - U_o}{U_*} = f_5 (y/\delta) . \tag{48.b}$$

Since the division of the boundary layer into inner and outer layers is arbitrary, there must be a region in which both Eq 47 and 48 are valid. This has been established experimentally. Therefore, in the overlapping region,

$$\frac{\bar{U}}{U_*} = f_8 \left(\frac{U_* y}{\nu}\right) = \frac{U_o}{U_*} + f_5 (y/\delta),$$

or

$$f_9 \left[(y/\delta)\left(\frac{U_* \delta}{\nu}\right) \right] = \frac{U_o}{U_*} + f_5 (y/\delta) . \tag{49}$$

To satisfy the above equality, functions f_5 and f_9 must be logarithmic. Therefore, for the overlapping region the velocity distribution can be expressed as

$$\frac{\bar{U}}{U_*} = A \log \left(\frac{U_* y}{\nu}\right) + B \tag{50.a}$$

and

$$\frac{U_o - \bar{U}}{U_*} = -(A \log y/\delta + C) . \tag{50.b}$$

Since δ is not well defined by the experimental data, it is assumed by Hama (8) that δ can be expressed as

$$\delta = \frac{1}{m} \frac{\delta^* U_o}{U_*} \tag{51}$$

Eq 50.b can be written as

$$\frac{U_o - \bar{U}}{U_*} = A \log \left(\frac{y U_*}{\delta^* U_o} \right) + D \quad , \tag{52}$$

in which

$$D = A \log m + C \quad . \tag{50.a}$$

The parameter $(\frac{y}{\delta^*} \frac{U_*}{U_o})$ was originally suggested by Rotta (13). For the outer layer Eq 48.b will take the form

$$\frac{U_o - \bar{U}}{U_*} = f_{10} \left(\frac{y U_*}{\delta^* U_o} \right) \tag{53}$$

If the roughness elements are larger than the thickness of the laminar sub-layer, it seems reasonable from physical reasoning that the wall shear stress will be larger than for a smooth boundary. The increase of wall stress is due to distortion of the streamlines and drag on the roughness elements.

The effect of velocity distortion is assumed to be limited to the neighborhood of the roughness element. The outer layer then can be analyzed on the hypothesis of the self-preserving flow. Furthermore, since the wall shear and boundary layer thickness express the effect of roughness and can still be taken as scales of velocity and length, the velocity distribution in the outer layer can be expressed by Eqs 48.b and 53

$$\frac{\bar{U}-U_0}{U_*} = f_5(y/\delta) \tag{48.b}$$

$$\frac{\bar{U}-U_0}{U_*} = f_{10}\left(\frac{y U_*}{\delta^* U_0}\right) . \tag{53}$$

Since in the overlapping region the logarithmic velocity distribution holds, it must have the same slope as A because Eq 48.b is valid for both the rough and the smooth surfaces. However, when the velocity distribution near the wall is expressed by Eq 50.a, the increased wall shear must shift the intercept B . Eq 50.a takes the following form for a rough surface

$$\frac{\bar{U}}{U_*} = A \log\left(\frac{y U_*}{\nu}\right) + B - \frac{\Delta \bar{U}}{U_*} . \tag{54}$$

If the roughness elements are large enough so that there is no laminar sublayer, Eq 54 must be independent of viscosity μ. This requires that $\frac{\Delta \bar{U}}{U_*}$ be of the form:

$$\frac{\Delta \bar{U}}{U_*} = A \log \frac{U_* K_r}{\nu} + E , \qquad (55)$$

that is, $\frac{\Delta \bar{U}}{U_*}$ is a function of roughness Reynolds number Re_{K_r}. Therefore,

$$\frac{\Delta \bar{U}}{U_*} = f_{11} (Re_{K_r}) \qquad (55)$$

Skin-friction Law

A skin-friction law can be derived from Eqs 52 and 54,

$$(U_o - \bar{U})/U_* = A \log(yU_*/\delta^* U_o) + D \qquad (52)$$

and

$$\bar{U}/U_* = A \log(U_* y/\nu) + B - \frac{\Delta \bar{U}}{U_*} . \qquad (54)$$

Subtracting Eq 52 from Eq 54, the following equation is obtained

$$\frac{U_o}{U_*} = A \log \left(\frac{\delta^* U_o}{\nu} \right) + (B - D) - \frac{\Delta \bar{U}}{U_*} ,$$

or

$$\sqrt{\frac{2}{c_f}} = A \log R_{\delta^*} + (B - D) - \frac{\Delta \bar{U}}{U_*} . \qquad (56.a)$$

This is the skin-friction law for a rough boundary. It differs from the skin-friction law for the smooth boundary,

$$\sqrt{\frac{2}{c_f}} = A \log R_{\delta^*} + (D - B) \tag{56.b}$$

by the term $\frac{\Delta \bar{U}}{U_*}$. The quantity $\frac{\Delta \bar{U}}{U_*}$ can be obtained from Eq 54. Substracting Eq 56.a from Eq 56.b one obtains

$$\frac{\Delta \bar{U}}{U_*} = \left(\sqrt{\frac{2}{c_f}}\right)_{smooth} - \left(\sqrt{\frac{2}{c_f}}\right)_{rough} \tag{57}$$

Distribution of Reynolds Stress

The distribution of shear stress can be obtained by the use of a self-preserving function for mean velocity and Reynolds stress, Eqs 42.a and 42.b; the equation of motion, Eq 41; and by assuming constant eddy viscosity ϵ . The self-preserving function $\varphi_{12}(y/\delta)$ is related to the mean velocity distribution [Eq 10, 11.1 Ref. (22)] by

$$-\frac{\kappa}{I_1}\eta f' + \varphi_{12}' = 0 \tag{58}$$

in which

$$\kappa = \frac{1}{A} \quad ; \quad I_1 = -\int_0^\infty f(\eta)\, d\eta \quad ; \quad \eta = (y/\delta)$$

For high Reynolds number these yield the Reynolds stress distribution [Eq 10, 11.2 Ref (22)] as

$$\varphi_{12} = -K^2 + \frac{K^2}{I}\eta \quad , \qquad \eta < \eta_0$$

$$= -\frac{K^2 \alpha}{I_1 R} e^{-\frac{1}{2}R^2\eta^2} \quad , \qquad \eta > \eta_0 \qquad (59)$$

in which, $R = \dfrac{\tau_\omega^{1/2}\delta}{K\epsilon}$

and α is obtained from

$$f(\eta) = -R\int_\eta^\infty e^{-R^2x^2}\,dx .$$

Temperature Distribution

Eq 27 may be further simplified assuming that $\bar{U}_2\frac{\partial}{\partial x_2}\overline{U_1'U_1'}$, $\bar{\rho}\bar{U}\frac{\partial}{\partial x}\overline{U_2'U_2'}$, $\frac{\partial}{\partial x_1}\int_{x_2}^{h}\bar{\rho}\,g_2\beta\bar{\theta}\,dx_2$, $\mu\left(\frac{\partial \bar{U}_1}{\partial x_2}\right)^2$ and $\overline{U_2'U_1'}\frac{\partial \bar{U}_1}{\partial x_2}$ are small compared to the other terms in the equation. With this simplification Eq 27 reduces to

$$\bar{U}_1\frac{\partial \bar{T}}{\partial x_1} + \bar{U}_2\frac{\partial \bar{T}}{\partial x_2} + \frac{1}{2}\frac{\bar{\rho}\bar{U}}{\bar{\rho}c_p g}\left\{\frac{\partial}{\partial x_1}\overline{U_1'U_1'} + \frac{\partial}{\partial x_1}\overline{U_2'U_2'}\right\}$$

$$= \frac{K}{\rho c_p g}\frac{\partial}{\partial x_2}\left(\frac{\partial \bar{T}}{\partial x_2}\right) - \frac{1}{\bar{\rho}g c_p}\frac{\partial}{\partial x_2}\bar{\rho}\,\overline{U_2'T'} \quad . \qquad (60)$$

This equation is similar to the equation of motion (Eq 41). A simultaneous solution of this equation together with the equations of motion (Eq 41) will give the temperature field. However, this

is not possible, because the number of unknowns exceeds the number of equations. The form of this equation suggests that at least as a first approximation the temperature profile can be expressed in a form similar to Eqs 45, 47, and 48.b provided the parameters involved are computed in a corresponding manner. This requires that analogous to the friction velocity $\sqrt{\tau_\omega/\rho_\omega}$ there must be defined a friction temperature T_*. The friction temperature[1] T_* is defined by

$$T_* = \frac{q_\omega}{g\rho_o c_p U_*} \tag{61}$$

The temperature distribution may be expressed by dividing the thermal boundary layer into an inner and outer layer by analogy with the momentum boundary layer. The temperature distribution in the inner layer and the outer layer may be expressed in the following way,

$$\frac{T_\omega - \bar{T}}{T_*} = f_{12}\left(\frac{y U_*}{\nu}\right) \tag{62}$$

also $$[(T_\omega - T_o) - (T_\omega - T)]/T_* = f_{13}(y/\delta_T)$$

or, $$\frac{\bar{T} - T_o}{T_*} = f(y/\delta_T) \tag{63}$$

[1] p. 823, Ref. 17.

Eq 62 gives the temperature distribution in the inner layer whereas Eq 63 gives the temperature distribution in the outer part of the thermal boundary layer. Accordingly, similar to the velocity profile there will be an overlapping zone in which both Eqs 62 and 63 will express the temperature distribution. This leads to a logarithmic distribution of temperature for the overlapping zone expressed by the following equations:

$$\frac{T_\omega - \bar{T}}{T_*} = A_1 \log \frac{y U_*}{\nu} + B_1 \tag{64}$$

and

$$\frac{\bar{T} - T_0}{T_*} = A_1 \log y/\delta_T + C_1 \quad . \tag{65}$$

Eqs 64 and 65 are analogous to the wall law and velocity defect law for smooth surface. For a rough surface, following the similar reasoning used to derive Eq 54 from Eq 50.a for the velocity profile, one will obtain Eq 64 in the following form

$$\frac{T_\omega - \bar{T}}{T_*} = A_1 \log \frac{y U_*}{\nu} + B_1 - \frac{\Delta(T_\omega - \bar{T})}{T_*} \tag{66}$$

in which $\frac{\Delta(T_W - \bar{T})}{T_*}$ represents the profile shift similar to $\frac{\Delta \bar{U}}{U_*}$.

Law of the Local Transfer Coefficient

Eqs 64 and 65 can be used to obtain a coefficient of heat transfer in a manner similar to the way in which the skin-friction law (Eq 56.b) was derived. The law of the local coefficient of heat transfer becomes

$$\frac{T_\omega - T_o}{T_*} = A_1 \log \frac{\delta_T U_*}{\nu} + (B_1 - C_1)$$

or $$(T_\omega - T_o) \frac{g \rho_o c_p U_*}{q_\omega} = A_1 \log \frac{\delta_T U_*}{\nu} + (B_1 - C_1)$$

or $$\frac{1}{S_t} \sqrt{\frac{c_f}{2}} = A_1 \log \frac{\delta_T U_*}{\nu} + (B_1 - C_1) \qquad (67)$$

in which the Stanton number S_t, defined by

$$S_t = \frac{q_\omega}{(T_\omega - T_o) \rho g c_p U_o}$$

or $$\frac{1}{S_t} \sqrt{\frac{c_f}{2}} = A_1 \log \left\{ R\delta_T \sqrt{\frac{c_f}{2}} \right\} + (B_1 - C_1) \qquad (68)$$

in which $R_{\delta_T} = \frac{\delta_T U_o}{\nu}$. Eq 67 or Eq 68 gives the local coefficient of heat transfer for smooth surface. It can be argued that the roughness will increase the local coefficient of heat transfer similar to the way it increases the local skin-friction. Then the

counterpart of Eq 67 for a rough surface will be

$$\frac{1}{St}\sqrt{\frac{C_f}{2}} = A_1 \log \frac{\delta_T U_*}{\nu} + (B_1 - C_1) - \frac{\Delta(T_\omega - \bar{T})}{T_*}. \quad (69)$$

This isthe law of local heat transfer coefficient for a rough surface.

Chapter IV

EXPERIMENTAL EQUIPMENT AND PROCEDURE

The experimental equipment consisted of (i) a wind tunnel, (ii) a rough boundary, (iii) a traversing mechanism, (iv) hot-wire anemometers, (v) thermocouples, and (vi) a resistance thermometer. This equipment, with the exception of the rough boundary, was the same as described by Spengos and Cermak (19).

Wind Tunnel

The wind tunnel (Fig. 2) in which the experiments were performed is located in the Industrial Research Building at the Colorado State University. The tunnel is of the closed-circuit type with a test section six feet square and thirty feet long. Air flow is produced in the tunnel by a propeller driven by a 150 hp diesel engine. The air speed in the test section can be varied from approximately 20 to 50 fps. To reduce the air speed to 17 fps it was necessary to use a cloth extending over the entire flow area and fastened to the guide vanes located at the downstream end of the test section. The pressure distribution (Fig. 3) along the center line of the test section was measured with a pitot tube and Whalen gage. Kerosene and alcohol were used in the Whalen

gage and the gage had a sensitivity of 0.0001 feet of alcohol. The pressure distribution was everywhere within 3 percent of the mean values. The level of turbulence of the free air stream in the test section was about 1.0 percent at 17 fps.

Rough Boundary

The floor of the test section formed the rough boundary for both the heated and unheated cases. A schemetic diagram of the test section without roughness elements is shown in Fig. 4. In order to utilize the existing heating surface for the rough boundary, roughness elements were cemented onto a fiber-glass cloth which was placed on the floor. The rough surface was 14 feet long and six feet wide extending to the beginning of the test section. Crushed stone passing through a standard sieve with $\frac{5}{16}$ - in. openings and retained on a sieve with $\frac{1}{4}$ - in. openings was used as roughness elements. They were cemented to the cloth with heat-resisting cement.[1] The stones were placed approximately at a mean distance of $1\frac{1}{2}$ ins. along the width of the tunnel. The interval between the rows was also about $1\frac{1}{4}$ in., but the roughness elements were placed approximately at the center of

[1] Sauereisen Insa-lute adhesive cement No. 1
Sauereisen Cements Company, Pittsburgh 15, Penn.

the two elements of adjacent rows. The test section floor which constituted the heating surface was 6 ft wide and 9 ft $11\frac{1}{2}$ ins. long. The surface was heated electrically by 23 separate heating elements of various widths cemented to the top surface of a $\frac{1}{2}$ - in. aluminum plate. The details of the heating arrangement are shown in Fig. 5. The heating elements were made by placing a thin layer of carbon on varnish-covered fiber glass which was cemented to aluminum plates of $\frac{1}{16}$ - in. thickness. The top of the carbon layer was electrically insulated by several layers of silicon varnish. The heating elements were placed on the top of the main aluminum plate of $\frac{1}{2}$ - in. thickness under which a 4 - in. layer of glass wool provided thermal insulation. The bus bars connected to the main powerstat, as well as the electrical circuit for the No. 1 heater strip are shown in Fig. 6. The electrical connections for other heater strips were identical. The total input of electrical power to the heated boundary was adjusted by the powerstat. A rheostat connected in series with each heater provided further control of the power to each strip. The physical dimensions and electrical characteristics of the strips are shown in Table I.

Traversing Mechanism

The Pitot tube and the sensing elements of the hot-wire anemometers and thermocouple were mounted on a carriage located 3 ft above the floor of the test section. The carriage was supported by the rails fastened to the tunnel walls. Two small D.C. motors with controls located outside the tunnel, were used to produce lateral and vertical motions. The error in the vertical coordinate values was within 0.005 in. The probe assembly for the sensing elements is shown in Fig. 8.

Hot-Wire Anemometers

Hot-wire anemometers of the constant-temperature type were used. The sensing element of the hot-wire anemometer used for measuring mean velocity was platinum wire, 0.001 in. in diameter and 0.4 in. in length, which was operated at about $1000^{0}F$. The electrical circuit for this anemometer is shown in Fig. 10. Compensation of the mean-velocity hot-wire for variations of mean air temperature in the boundary layer was originally accomplished by mounting a resistance element consisting of a tungsten wire, 0.00031 in. in diameter and 12.0 ins. long, on the same probe with the hot-wire but in the adjacent arm of the bridge. This arrangement was found to be

unsatisfactory because of the difficulty in keeping the many turns of the compensating wire electrically separated. Therefore, a variable resistance was installed in the wheatstone bridge which was controlled manually to compensate for the variation of mean temperature. The hot-wire anemometer for the mean velocity was calibrated by fastening the anemometer to a whirling arm, 2.92 ft long, rotating in a cylindrical chamber. The correction for the induced velocity in the chamber was made by the method of Cowdrey described by Hromas and Kentzer (9).

The intensities of turbulence and shearing stress in the boundary layer were measured with a pair of crossed hot-wires of the constant-temperature type. This hot-wire anemometer consisted of (i) a current control device for each wire, (ii) an adding and subtracting arrangement for the signals from the two individual wires, and (iii) a turbulence amplifier and root-mean-square indicator. The sensing element of each of the crossed hot-wires were inclined 45^0 with the direction of flow, and was made of tungsten wire 0.00031 in. diameter and 0.1 in. in length. The mean operating temperature was approximately 450^0F. An extra length of 0.05 in. on each side of the central part of the tungsten wire was copper plated for soft soldering

onto the probe. Thus, the total length of the wires was 0.2 in. Compensation for the variations in mean temperature was obtained by mounting a similar tungsten wire, 2 ins. long, on the same probe in the opposite arm of the bridge. Figs. 8 and 9 show the probe assembly and a photographic view of the instruments. Each separate hot-wire anemometer with the associated circuit for controlling the current is shown in Figs. 10 and 11. The signals from the two wires were passed through the adding and subtracting circuit (Fig. 13) to the turbulence amplifier and RMS indicator (Fig. 14). By the use of a selector switch the two signals could be added, subtracted, or passed unamplified through the adding and subtracting circuit. The frequency response of the crossed hot-wire and associated electronic circuits was about 5000 cps. The mathematical equations associated with operation of the hot-wire anemometer of the constant-temperature type were derived by Baines (2). The equations used for computing turbulent shear stress and intensities of turbulence are,

$$\frac{\overline{U'V'}}{U_o^2} = \frac{A^2}{4n^2I^2} \cdot \frac{G^2}{G_t^2}\left[(I_t)_1^2 - (I_t)_2^2\right] \quad , \tag{70}$$

$$\frac{u}{U_o} = \frac{A}{2nI} \cdot \frac{G}{G_t} (I_t)_{add} \quad , \tag{71}$$

$$\frac{v}{U_o} = \frac{A}{2nI} \cdot \frac{G}{G_t} (I_t)_{sub} \quad , \tag{72}$$

in which A , G , G_t and n are calibration constants. $(I_t)_1$ and $(I_t)_2$ are the readings of the RMS meter corresponding to the signals from the No. 1 or No. 2 hot-wire anemometers respectively. $(I_t)_{add}$ and $(I_t)_{sub}$ are the readings of the RMS meter when the two signals were added or subtracted respectively.

The calibration constant A is the ratio of the grid voltage to the cathode voltage of the 6L6 electronic tubes of the current-control circuit, (Figs. 11 and 12). G is the transconductance for the current-control circuits of the No. 1 and No. 2 hot-wire anemometers. The RMS circuit transconductance is given by G_t . The calibration constant n is the exponent of the empirical equation relating the bridge reading (Figs. 11 and 12) to the local mean velocity, U ,

$$I = bU^n \quad . \tag{73}$$

The Eqs 70, 71 and 72 had been obtained on the assumption that the two crossed hot-wires were identical and that they were operated at the same temperatures. This implied A , G , G_t and n for each of the hot-wires were the same.

Thermocouples

The mean-temperature of the air was measured with a copper-constantan thermocouple 0.010 in. in diameter. The thermocouple was connected to a Minneapolis-Honeywell potentiometer of the recording type.

Resistance Thermometer

The resistance thermometer for the measurement of the intensity of the temperature fluctuations was similar to that of the hot-wire anemometers for measurement of turbulence intensities. The main difference is that the operating temperature for the thermometer is only slightly greater than the temperature of the air whereas that of the hot-wire anemometer is 450°F . The resistance thermometer of the constant-temperature type and the associated current control circuit is shown in Fig. 15. The circuit for the signal amplifier for temperature fluctuations for the RMS indicator is identical to that of the hot-wire anemometer, Fig. 14. The sensing elements made of tungsten wire were

similar in dimension to those of the turbulence anemometer. The equation used for the computation of the intensity of temperature fluctuations is,

$$\frac{T'}{T} = \frac{A}{nI} \cdot \frac{G}{G_t} \cdot I_t \quad , \tag{74}$$

in which A, G, G_t are the calibration constants similar to the hot-wire anemometer, and n is the exponent of the equation,

$$I = bT^n \tag{75}$$

Experimental Procedure

At the beginning of the experimental work the pressure distribution along the center line of the wind tunnel was measured. A piezometer opening on the tunnel wall at the upstream end of the section was used as reference pressure. The difference of pressure between this piezometer and the static-pressure opening of a Pitot tube, moving along the center line of the test section was measured by a Whalen gage.

The calibration constants A, G, and G_t for the crossed hot-wire and the resistance thermometer were obtained by the method described by Spengos and Cermak (19). The

calibration constants were checked after approximately 50 hours of operation.

The diesel engine supplying power to the wind-tunnel fan was run for about an hour before the collection of data began. This procedure helped to reduce the fluctuation of speed of the diesel engine due to initial warming as well as to stabilize the tunnel temperature. The electronic instruments were also warmed for about an hour to avoid transient effects.

The mean-velocity hot-wire was calibrated each day before making any measurements. The value of n used in Eqs 70, 71 and 72 was obtained by direct calibration of the crossed wire in the tunnel.

For the heated boundary, the uniform temperature on the surface was obtained by adjusting the power input to the individual heater strips by trial and error. The surface temperature as well as the temperature in the boundary layer were obtained by the thermocouple placed on the probe assembly. Approximately three hours of tunnel operation were required to establish the steady state condition for the heated surface. The value of n used in Eq 74 was obtained by measurement of the mean temperature at various points in the boundary layer

with a thermocouple and the resistance thermometer for the corresponding level.

To obtain experimental data, each station along the center line of the test section was selected in the central part of the area defined by four roughness elements. Mean velocity, mean temperature and data for turbulence parameters were measured at a point above the boundary layer ($y > \delta$). The probe assembly was then lowered to a height approximately 0.05 ± 0.005 in. from the surface. Because of the vibration of the tunnel it was not possible to lower the probe further without breaking the wire. The mean-velocity probe was first placed on the center line and was moved vertically upward to obtain mean-velocity measurements at various levels in the boundary layer. The probe assembly was then moved laterally to place the crossed-wire probe over the station. It was then lowered to the same elevation at which the mean-velocity measurements began and moved upward for measurements at various levels in the boundary layer.

For the heated boundary the same procedure was repeated to obtain the mean-velocity and turbulent data at different stations. Data for the temperature and for the intensities of temperature fluctuation were obtained in a similar manner. The power input to the heater strips was measured by a voltmeter and ammeter.

Chapter V

PRESENTATION AND DISCUSSION OF DATA

The boundary layer thickness, the displacement thickness, the momentum thickness and the skin-friction coefficient for unheated and heated surfaces are compared in an effort to find the effect of heating the surface. The mean velocity distributions are discussed in the light of the universal velocity distribution using the modified definition of displacement thickness for the heated surface. The skin-friction law derived from the logarithmic velocity distribution law for the region in which both the inner law and the velocity defect law hold is compared for heated and unheated surfaces. The distribution of shear stress in the boundary layer for the unheated surface is compared with the equation given by Townsend derived from the hypothesis of self-preserving motion. The shear stress distribution, the eddy viscosity and the intensities of turbulence in the boundary layer over an unheated surface is compared with the corresponding distributions obtained over a heated surface in an effort to determine the effect of heating the surface.

Methods of obtaining the thermal boundary layer thickness, the convective thickness and local coefficient of heat transfer are discussed. The universal law of temperature distribution and local heat-transfer coefficient are discussed by analogy with the universal velocity profile and the law of skin-friction. The intensity of temperature fluctuations is compared with the intensity of velocity fluctuations in the vertical direction.

Boundary Layer Thickness

The thickness δ of the boundary layer due to velocity was obtained from the plot of y vs $\frac{\overline{U}}{U_o}$. Since the roughness elements were about 1.25 to 1.75 in. apart, it was decided to take the origin of y-axis at the floor of the tunnel. The values of δ for the heated boundary are always greater than those of the unheated boundary at every station as can be seen from the values tabulated in Table II. The ratio of δ for the heated to that of the unheated boundary is between 1.08 and 1.22 . Since it is difficult to obtain an accurate value of δ from the measured velocity profile, the ratio is only approximate.

Displacement and Momentum Thickness

The displacement thickness δ^* and the momentum thickness δ^{**} were obtained by graphical integration. The

ratio of $\bar{\rho}/\rho_o$ appearing in the definition for the above thicknesses is unity for the unheated boundary. For the heated boundary it was assumed that the perfect gas law holds and the variation of pressure within the boundary layer is very small. Then the following relationship is approximately true $\bar{\rho}/\rho_o = T_o/\bar{T}$, and $\bar{\rho}/\rho_o$ was replaced by $T_o/\bar{T}$. The values of δ^* and δ^{**} tabulated in Table II for the heated case are greater than those for the unheated case. The ratio of δ^* for heated to δ^* unheated surfaces varies from 1.06 to 1.215. The mean difference of the momentum thickness due to heated and unheated surfaces is approximately 0.057 in. and 0.0476 in. for U_o = 17 and 35 fps[1] respectively.

Skin-friction

The local skin-friction coefficient c_f for the heated and unheated boundary were obtained from the graphical differentiation of the momentum integral equation (Eq 33.b). The graphical differentiation was performed by passing a smooth curve through the set of points corresponding to a given free stream velocity

---

[1] The mean velocity was not the same at every station because of the variation of speed of the diesel and the difficulties of setting the diesel engine to the same speed on different dates. Therefore, U_o = 17 fps refers to all velocities approximately equal to 17 fps. Exact values of mean velocities at different stations are given in Table II. A similar explanation also applies to U_o = 35 fps.

(Fig. 16). For a smooth boundary it is also possible to obtain the skin-friction coefficient by extrapolating the Reynolds stress $-\overline{\rho u'v'}$. The results obtained by the extrapolation of the Reynolds stress and by the graphical differentiation of Eq 33.b are in fair agreement. But for the case of a rough boundary such extrapolation of Reynolds stress is very difficult. This is because the roughness elements distort the stream lines. Therefore, the signals obtained from the crossed hot-wire anemometers used for measuring the Reynolds stress do not represent the true value near the surface. Furthermore, the terms due to anisotropy of the normal stress in Eq 32 is of appreciable magnitude near the rough boundary. It is very difficult to obtain the gradient of the normal stresses near the roughness elements. Therefore, Eq 33.b was used to obtain the skin-friction coefficient for both heated and unheated surfaces. The momentum thickness δ^{**} used in this equation was evaluated by Eq 31.b. In deriving Eq 33.b from Eq 32, the terms due to anistropy of the normal stress as well as the buoyancy effect in case of a heated boundary are neglected. The effect of anisotropy of the normal stress is predominant near the boundary but their effect when integrated over the entire boundary layer is probably small; however, the validity

of this assumption has not yet been conclusively proved for a rough boundary. Townsend (22) estimated that the value of this term to be approximately 3% for smooth boundary. For the case of separation on a smooth boundary, Ross (15) gave a value of 10% for the term due to anisotropy of normal stress.

The momentum thickness δ^{**} is the thickness of the free-stream that carries the same momentum flux that is destroyed by the total wall stresses between the beginning of the boundary layer and the section at which the momentum thickness is determined. For a boundary layer with heat transfer the momentum thickness has been generally evaluated by the equation,

$$\delta^{**} = \int_0^\infty \frac{\bar{u}}{u_0}\left(1 - \frac{\bar{u}}{u_0}\right) dy$$

assuming that the flow is incompressible. This does not represent the true loss of momentum for boundary layers with heat transfer. This is evident from physical reasoning as well as from the momentum integral equation (Eq 30). Therefore, the momentum thickness defined by Eq 31.b was used for all computations. For a heated surface the momentum thickness was greater than for the unheated surface under corresponding conditions of mean velocity and roughness. Yet the value of the

term $d\delta^{**}/dx$ for the heated and unheated surfaces is approximately the same. This implies that a very rapid rate of increase in δ^{**} occurs near $x = 0$.

Since the experiment was performed at an elevation of 5000 ft above sea level and at different temperatures, the values of various properties of the fluid were corrected for elevation as well as temperature.

The density of air was obtained by the relationship [1]

$$\rho = \frac{P}{g_s R T}$$

in which P is the pressure (lb/ft^2)

g_s is the standard gravitational aceleration (32.2 fps^2)

R is the gas constant (53.3 $ft/^0F$)

T is the absolute temperature in ^0F.

The dynamic viscosity at different temperatures was obtained from the graph given by Rouse. [2]

Mean Velocity Distribution

Vertical distributions of mean velocity for the unheated surface at different values of $(x + L)$ are shown in Figs. 18

---

[1] Rouse, H. (Ed.) Engineering Hydraulics, New York, John Wiley, 1950, p. 1005.

[2] ibid. p. 1006

and 19 using the parameter $\frac{U_o - \bar{U}}{U_*}$ as a function of y/δ and $yU_*/\delta^* U_o$ respectively. Since the roughness elements were large, there was no laminar sublayer. The straight-line portion of the logarithmic plot of the velocity-defect law can be well represented by Eqs 50.b and 52 with the values of the constants A , C , and D as 5.6, 2.5, and 0.6 respectively. These values of the constants were given by Clauser (3) and Hama (8) after analysis of a large amount of experimental data for both smooth and rough surfaces. Substituting these values of the constant in Eqs 50.b and 52 one obtains:

$$\frac{U_o - \bar{U}}{U_*} = 5.6 \log (y/\delta) + 2.5 \tag{76}$$

and

$$\frac{U_o - \bar{U}}{U_*} = 5.6 \log \frac{yU_*}{\delta^* U_o} + 0.6 \, . \tag{77}$$

Although the roughness element used in this investigation is dissimilar in shape, Eqs 76 and 77 are a good approximation to the experimental data for the logarithmic portion of the velocity profile. The scatter of the experimental data is partly due to the distortion of the flow caused by the roughness elements and partly due to the difficulty in reading the meter of mean velocity hot-wire anemometer when the sensing wire was close to the

surface. The velocity profiles in Figs. 18 and 19 show deviation from the straight line portion at about $y/\delta = 0.15$ or $\frac{yU}{\delta^* U_o} = 0.05$. For the outer portion of the velocity profile in turbulent boundary layers Hama suggested the following empirical equation,

$$\frac{U_o - \bar{U}}{U_*} = 9.6 \left(1 - 3.33 \frac{y\, U_*}{\delta^* U_o}\right)^2 \qquad (78.a)$$

or

$$\frac{U_o - \bar{U}}{U_*} = 9.6 \left(1 - y/\delta\right)^2 \qquad (78.b)$$

in which $\delta = m \frac{\delta^* U_o}{U_*}$, with $m = 0.30$. Eq 78.a represents the experimental data (Fig. 19) fairly well, however, Eq 78.b is not in good agreement with the experimental data near the outer edge of the boundary layer $(y/\delta > 0.5)$. A solution of Eq 52.a using the values of A, C and D from Eqs 76 and 77 yields $m = 0.279$. Use of $m = 0.279$ instead of 0.30 will yield the following relationship from Eq 78.a,

$$\frac{U_o - \bar{U}}{U_*} = 9.6 \left(1 - 0.925 \frac{y}{\delta}\right)^2 \qquad (78.c)$$

This equation is in error because at $y/\delta = 1$, it will give a value of 0.054 rather than zero. The value of U_* is small compared

to U_o , therefore, this anamoly will not be observed in the experimental data. Thus, for U_o = 35 fps, U_* is approximately 2.24 fps at $(x + L)$ = 67 in. and for $\frac{U_o - \overline{U}}{U_*}$ = 0.054 , U_o = 34.878 fps . One alternative is to accept this anamoly and the other alternative is to modify the values of the constants A , C and D to yield Eq 78.b from Eq 78.a for m = 0.279 . In Fig. 18, Eq 78.c is shown by broken lines. It will be seen Eq 78.c gives a slightly higher value. For the second alternative there is a wide choice for the values of A , C , and D because different values of these constants have been proposed by different investigators. The values that are accepted here are the ones giving the best fit for a wide range of data. From the result shown in Figs. 18 and 19 it appears that a modification of the value of C may be the most reasonable. For m = 0.279, and taking Eq 78.a as a basis, the value of C in Eq 50.b should be 2.3 instead of 2.5 as suggested to satisfy both Eqs 78.a and 78.b . Substitution of this value of C in Eq 50.b then yields

$$\frac{U_o - \overline{U}}{U_*} = 5.6 \log (y/\delta) + 2.3 \qquad (79)$$

This equation is plotted in Fig. 18 by the broken lines. For $0.07 < y/\delta < 0.15$ the agreement of Eq 79 with experimental data is fair.

For the heated surface Eqs 77 and 78.a with δ^* defined by Eq 31.b , are in good agreement with the experimental data (Fig. 21). However, Eq 78.a gives values lower than the experimental data for $yU_*/\delta^*U_o > 0.17$. In Fig. 20 the experimental data are generally lower than values given by Eq 76. Eq 78.b gives values higher than the experimental data for $0.15 < y/\delta < 0.35$ and values lower than the experimental data for $y/\delta > 0.35$. Figs. 21, 22 and 23 show velocity profiles for both heated and unheated surfaces. Observation of these figures indicates that Eqs 77 and 78.a represent the experimental data for both the heated and unheated surfaces fairly well. This may be due to the fact that the effect of temperature is partly taken care of by δ^* defined by Eq 31.a .

The effect of surface roughness is expressed by Eq 54. The values of the constant A and B (3) are 5.6 and 4.9 respectively. Therefore, Eq 54 becomes

$$\frac{\bar{U}}{U_*} = 5.6 \log \frac{yU_*}{\nu_\omega} + 4.9 - \frac{\Delta \bar{U}}{U_*} \qquad (80)$$

The downward shift of the straight line portion of the logarithmic plot in Fig. 25, is given by $\frac{\Delta \bar{U}}{U_*}$. Eq 63 without the last term

is the wall law for the turbulent boundary layer over a smooth surface. Since the viscosity of the air near the wall is one of the boundary conditions for Eq 54, it is reasonable to use the viscosity of the air ν_w corresponding to the temperature at the wall rather than the viscosity of air corresponding to the temperature of the free-stream. Figs. 25, 26 and 27 show the effect of roughness for the unheated and heated surfaces. Eq 55 indicates that $\frac{\Delta \bar{U}}{U_*}$ is a function of the Reynolds number formed by using a representative roughness height as the length dimension.

Using $A = 5.6$, Eq 55 can be written as

$$\frac{\Delta \bar{U}}{U_*} = 5.6 \frac{K_r U_*}{\nu_w} + E \qquad (81)$$

Since the roughness elements used have no particular geometrical shape, a value of 0.28 in. is used as the mean size for K_r. The selection of 0.28 in. as mean value for K_r is purely arbitrary. Although Fig. 28 shows that in general $\frac{\Delta \bar{U}}{U_*}$ is a function of $K_r U_* / \nu_w$ with a slope of 5.6, the variation of $\frac{\Delta \bar{U}}{U_*}$ for any particular velocity along the direction of flow does not follow any definite trend. This is true for both heated and unheated surfaces.

Skin-friction Law

The local skin-friction as a function of $R_{\delta^*} = \frac{\delta^* U_o}{\nu_w}$ is plotted in Fig. 29. Here also as before ν_w instead of ν_o is used to evaluate R_{δ^*}. Substituting the values of the constants A , B and D in Eq 56.a the law of the skin-friction is obtained in the following form:

$$\sqrt{\frac{2}{c_f}} = 5.6 \log \frac{U_o \delta^*}{\nu_w} + 4.3 - \frac{\Delta \bar{U}}{U^*} \qquad (82)$$

The term $\frac{\Delta \bar{U}}{U_*}$ is the same as obtained from Eq 80. The skin-friction law is derived from the velocity-defect law, Eq 77, and the wall law, Eq 80. These equations are true for both the heated and unheated surface as shown by Figs. 24, 25, 26 and 27. Therefore, Eq 82 must holds for both the heated and unheated case. This is true within the experimental accuracy as can be seen by comparing Fig. 29 with Figs. 25, 26 and 27. A careful observation will indicate that the value of $\frac{\Delta \bar{U}}{U_*}$ obtained from Eq 80 (Figs. 25, 26 and 27) when subtracted from the skin-friction law for the smooth surface do not give the correct values of $\sqrt{\frac{2}{c_f}}$ (x = const.). The variation, however, is about $\pm$ 5 % which is within the experimental accuracy. The variation of

$\frac{\Delta\overline{U}}{U_*}$ obtained from Eq 80 (Figs. 25, 26 and 27) and from the plot of $\sqrt{\frac{2}{c_f}}$ vs R_{δ_*} are tabulated in Table III. It shows that in general the value of $\frac{\Delta\overline{U}}{U_*}$ obtained from the plot of the wall law is smaller than those obtained from the plot of the skin-friction law, but the variation is small.

Form Parameter

The form parameter H defined as a ratio of the displacement thickness to the momentum thickness of the boundary layer is shown in Fig. 30. As pointed out by Clauser (3), H is a function of streamwise pressure gradient as well as skin-friction. For a smooth boundary H can reach a value as high as 2.6 when separation of the boundary layer occurs. High values of H having a similar magnitude was obtained for a rough surface without separation as mentioned by Clauser. In the case of a boundary layer on a plane surface without pressure gradient, H is a function of skin-friction only. Hama (8) has given the following equation for H when $dP/dx = 0$,

$$H = \left(1 - G\sqrt{\frac{c_f}{2}}\right)^{-1} \qquad (83)$$

in which

$$G = \int_0^\infty \left(\frac{U_o - \bar{U}}{U_*} \right) d \left(\frac{y U_*}{\delta^* U_o} \right) \qquad (84)$$

For $dp/dx = 0$, the value of G (8) is approximately equal to 6.10. Eq 83 for the case of zero pressure gradient and the values of H obtained from the experimental data of this study and from the data presented by Hama are shown in Fig. 30.

The experimental data are in fair agreement with the Eq 83 except for $(x + L) = 114$ and 154 in. In these cases, the values of H obtained from the experimental results are 10 % higher than those given by Eq 83.

Reynolds Stress Distribution

A typical distribution of the Reynolds stress in the boundary layer for heated and unheated surfaces at $(x + L) = 154$ in. is shown in Fig. 31. The value of $\overline{u'v'}$ gradually increases from near the surface to its maximum value between $0.15 < y/\delta < 0.3$, then decreases. For a smooth surface the value of the Reynolds stress is constant near the boundary [1] $(y/\delta < 0.1)$ and equal to the wall shear stress. For this

---

[1] Klebanoff, P. S. Characteristics of turbulence in a boundary layer with zero pressure gradient. NACA TN 3178, July 1954. p. 35.

reason it is possible to extrapolate the Reynolds stress to obtain the wall stress. For a rough surface the Reynolds stress obtained from the crossed-wire measurement near the surface is smaller than the wall stress obtained by $d\delta^{**}/dx$, therefore, the extrapolation is not possible. One reason for this low value is that of anisotropy of the normal stress as discussed earlier. It was pointed out in Chapter III that neglect of anisotropy on the normal stress may not introduce appreciable errors while evaluating the momentum integral, but may give lower values of total stress near a rough boundary. The total resistance in this layer is due to the drag on the roughness elements and the turbulence shear stress. Therefore, measurement of $-\overline{u'v'}$ will not give the total stress near the surface. Another source of error is in the measurement of $\overline{u'v'}$ itself due to the orientation of the crossed-wire with respect to the streamlines near the rough surface. However, away from the boundary where the influence on the individual roughness element on the mean flow is negligible (approximately four times the roughness heights) the distribution of Reynolds stress can be expected to be similar to that for the smooth surface. In Fig. 32 the distribution of the Reynolds stress over a smooth boundary (Eq 59) given by Townsend is compared with those for the rough unheated surface. The

value of δ_o used in Fig. 32 is the value of y at which $U_o - \overline{U} = U_*$. For $y/\delta_o > 0.5$ the agreement of the experimental data with Eq 59 is fairly good.

For the heated surface (Fig. 33) the maximum value of $\overline{u'v'}$ is about 160 % of the unheated surface value. This maximum value of Reynolds stress is much higher than the wall stress, but drops at a faster rate with increasing y than in the case of the unheated surface for $y/\delta > 0.50$. It is difficult to determine whether this higher value of $\overline{u'v'}$ for the heated boundary is due to actual increase of shear stress or due to the superposition of temperature fluctuation signals upon the velocity fluctuation signals. One way to reduce the temperature fluctuation effect is to operate the crossed wire at a higher temperature (above 1000°F). It was observed that when the tungsten wire was heated above 475°F, the characteristics of the wire changed rapidly. The operating temperature of the tungsten wire was limited to about 450°F. Therefore, the accuracy of the results for the heated surface is still open to question and requires further study.

Eddy Viscosity

Eddy viscosity as defined by $\epsilon = -\bar{\rho}\overline{u'v'}/\frac{d\bar{U}}{dy}$, is shown in Fig. 34. The velocity gradient $\partial \bar{U}/\partial y$ was obtained by graphical differentiation. Clauser (3) showed that ϵ is proportional to $\rho U_o \delta^*$. Furthermore, the constant of proportionality ($\lambda = \frac{\epsilon}{\rho U_o \delta^*}$) is a constant which is not affected by the pressure gradient, Reynolds number or roughness. The value of this constant (3) is approximately equal to 0.018. The value of for an unheated rough surface obtained from the present investigation agrees very well with the value given by Clauser, for $y/\delta^* > 1.50$. In the derivation of Eq 59 Townsend (22) also assumed constant eddy viscosity.

The eddy viscosity ϵ for the heated surface is not constant for the outer layer. However, as mentioned before, the turbulent shear stress measurement for the heated surface is open to question. Therefore, it is not justifiable to draw any conclusion for ϵ obtained for the heated plate.

Intensitites of Turbulence

The intensities of turbulence u and v for the heated and unheated surfaces are shown in Fig. 35, 36 and 37. In all cases the values for heated surface is larger than the corresponding values for the unheated surface. As before results for

the heated surface is questionable. However, in the case of v, values for the heated case may be more reliable than the values of u because the effect of superimposed temperature fluctuation may have cancelled when the two signals from the crossed-wire were subtracted instantaneously (Eq 72). Whereas for u the effect of temperature may be increased due to addition of the two signals (Eq 71). However, the plot for the unheated case follows the general trend. Fig. 38 shows comparison of u data for unheated surface with those of Tillman for rough and smooth surfaces and of Klebanoff for a smooth surface.

The maximum value of v/U_o over a smooth surface as given by Klebanoff is 0.40. The maximum value of v/U_o from Fig. 35 for the unheated surface is 0.049. The maximum value of v/U_o obtained by Spengos (18) is also approximately 0.05.

Thermal Boundary Layer Thickness

The thickness δ_T of the thermal boundary layer was obtained by plotting $\frac{\bar{T} - T_o}{T_w - T_o}$ against y and drawing a smooth curve through these points. The thermal boundary layer thickness is the height above the floor at which $\frac{\bar{T} - T_o}{T_w - T_o} = 0.01$

For a laminar thermal boundary layer $\delta_T/\delta \propto 1/\sqrt{Pr}$, but for a turbulent boundary no such relationship is known. Table II shows that δ_T was less than δ for all values of x .

Convective Thickness

The convective thickness δ_T^{**} was obtained by the graphical integration of $\int_0^\infty \frac{\bar{\rho}}{\rho_o} \frac{\bar{U}}{U_o} \frac{\bar{T} - T_o}{T_w - T_o} dy$. Its value as shown in Table II closely corresponds to the value of momentum thickness, but is smaller than the displacement thickness.

Stanton Number

The Stanton number S_t was obtained by graphical differentiation of the smooth curve obtained by plotting δ_T^{**} as a function of distance along the direction of flow. S_t was also computed from the heat input. The values obtained by the two methods are in close agreement.

Mean Temperature

Since the heated surface began at a distance of 43 in. from the leading edge of the rough boundary, the thickness of the thermal boundary layer was smaller than the momentum boundary layer within the test length. The temperature and velocity distribution in the boundary layer are shown in Figs.

39 and 40 for $(x + L) = 114$ and 154 in. In Fig. 41 the universal temperature profile (temperature defect law) is plotted as a function of y/δ_T. The constants A_1 and C_1 of the Eq 65 are found to be 6.6 and 0.30 respectively. Substituting the values of the constants A_1 and C_1 in Eq 65, the following equation for the temperature defect law can be obtained.

$$\frac{\bar{T}-T_0}{T_*} = 6.6 \log \frac{y}{\delta_T} + 0.3 \qquad (85)$$

The wall law for the temperature distribution for a smooth surface is given by Eq 64. The value of the constant B_1 is obtained by drawing a best fit line with slope 6.6 through the points plotted by Reynolds, Kays and Kline [1] (14). They used yU_*/ν_0 instead of yU_*/ν_w. Since a low temperature difference of 29°F was used, the difference between the values of yU_*/ν, evaluated using ν_0 or ν_w will be small. The value of the constant B_1 is found to be 1.0. Substituting the values of the constants in Eq 64 one obtains for the smooth surface, the wall temperature law in the following form,

$$\frac{T_\omega-\bar{T}}{T_*} = 6.6 \log \frac{yU_*}{\nu_\omega} + 1.0 \qquad (86)$$

---

[1] Fig. 1.12, p. 48

The corresponding equation for the rough surface, Eq 66 becomes,

$$\frac{T_\omega - \bar{T}}{T_*} = 6.6 \log \frac{y U_*}{\nu_\omega} + 1.0 - \frac{\Delta (T_\omega - \bar{T})}{T_*} \qquad (87)$$

Eqs 86 and 87 are plotted in Fig. 42. The above discussion and the Figs. 41 and 42 indicates that temperature profiles can be expressed by the wall law for temperature and temperature defect law using the concept of friction temperature analogous to the wall law for velocity and the velocity defect law respectively. The slope of the straight line portion of the logarithmic portion of the temperature and velocity profile is not the same. The slope for the temperature profile is 6.6 where as for velocity it is 5.6 . Furthermore, the straight line portion of the temperature defect law represents the larger portion of the outer temperature profile than the corresponding velocity defect law represents of the outer portion of the velocity profile, (Figs. 18, 20 and 41).

Local Coefficient of Heat Transfer

The law of local heat transfer coefficient for a smooth surface can be obtained by substituting the value of the constants

in Eq 68. This law is

$$\frac{1}{S_t}\sqrt{\frac{c_f}{2}} = 6.6 \log \frac{\delta_T U_*}{\nu_\omega} + 0.7 \qquad (88)$$

For a rough surface the local heat transfer coefficient law is obtained from Eq 69. With the substitution of the value of the constants, Eq 69 reduces to

$$\frac{1}{S_t}\sqrt{\frac{c_f}{2}} = 6.6 \log \frac{\delta_T U_*}{\nu_\omega} + 0.7 - \frac{\Delta(T_\omega - \bar{T})}{T_*} \qquad (89)$$

The numerical value of the term $\frac{\Delta(T_w - \bar{T})}{T_*}$ is obtained from Eq 87. In Fig. 43, Eq 89 is compared with the experimental results. The discrepancy is mostly due to the inaccuracy of obtaining the numerical value of the term $\frac{\Delta(T_w - \bar{T})}{T_*}$. The Stanton number S_t used in Fig. 43 is computed from the heat input.

Intensities of Temperature Fluctuation

Fig. 44 shows the intensities of temperature fluctuation at $x + L = 114$ and 154 in. The comparison of t'/T with ν/U_o (Fig. 37) shows similar trend but the values of t'/T

is smaller than the values of v/U_o for the same value of y/δ_T or y/δ. This is because T is the absolute temperature rather than $(T_w - T_o)$.

Chapter VI

CONCLUSIONS

The following conclusions are reached for a turbulent boundary layer over plane, rough, heated and unheated surfaces. These conclusions are applicable for a range of free-stream air velocities of 17 fps to 35 fps, with moderate temperature differences of $75^{0}F$ to $48^{0}F$ for the heated surface. The heated plate was 10 ft long beginning 43 in. downstream from the leading edge of the roughened surface. Crushed stone of sizes between 0.25 in. and 0.312 in. placed approximately at a distance of 1.75 in. along the direction of flow and 1.25 in. at right angles to the direction of flow formed the rough surface. The pressure gradient along the center line of the wind tunnel was approximately zero.

1. The velocity-defect law for the outer part of the boundary layer is universal for smooth, rough, unheated, and moderately heated surfaces, provided the displacement and momentum thickness are modified in the following manner to account for the change of density when heating occurs

$$\delta^* = \int_0^\infty \left(1 - \frac{\bar{\rho}}{\rho_0}\frac{\bar{U}}{U_0}\right) dy$$

$$\delta^{**} = \int_0^\infty \frac{\bar{\rho}}{\rho_0}\frac{\bar{U}}{U_0}\left(1 - \frac{\bar{U}}{U_0}\right) dy .$$

The experimental data can be correlated by the parameters $(U_0 - \bar{U})/U_*$ and $(yU_*)/(\delta^* U_0)$. These parameters are related by the equation

$$\frac{U_0 - \bar{U}}{U_*} = 5.6 \log \frac{yU_*}{\delta^* U_0} + 0.6$$

$$\frac{U_0 - \bar{U}}{U_*} = 9.6 \left(1 - 3.33 \frac{yU_*}{\delta^* U_0}\right)^2$$

2. The wall law for the velocity distribution for rough, heated and unheated surfaces can be expressed by an equation of the form given by Hama and Clauser,

$$\frac{\bar{U}}{U_*} = 5.6 \log \frac{yU_*}{\nu_w} + 2.5 - \frac{\Delta \bar{U}}{U_*}$$

where ν_w is the kinematic viscosity of air corresponding to the wall temperature. The shift of the intercept represented by $\Delta \bar{U}/U_*$ depends on the magnitude of the roughness effect.

3. The downward shift of the straight line section of the logarithmic law of the wall for the velocity distribution

(expressed by the quantity, $\frac{\Delta \overline{U}}{U_*}$) is a function of the roughness parameter $K_R U^*/\nu_w$ formed by roughness height K_R, shear velocity U_*, and kinematic viscosity ν_w corresponding to the temperature of the wall.

4. The local skin-friction coefficient is a function of Reynolds number formed by the displacement thickness δ^*, the free-stream velocity U_o, and the kinematic viscosity ν_w corresponding to the wall temperature. The quantity $\frac{\Delta \overline{U}}{U_*}$ obtained from the logarithmic velocity plot for rough surfaces represents the difference in the skin-friction coefficient for rough and smooth surfaces; i.e., $-\frac{\Delta \overline{U}}{U_*} = \left(\sqrt{\frac{2}{c_f}}\right)_{rough} - \left(\sqrt{\frac{2}{c_f}}\right)_{smooth}$ for both moderately heated and unheated rough surfaces.

5. The turbulent shear-stress distribution for the outer part of the turbulent boundary layer over a rough unheated surface can be represented by the equation obtained by Townsend for smooth surfaces. This equation does not represent the turbulent shear stress in the boundary layer over a rough unheated surface for y less than approximately four times the height of the roughness elements.

6. The eddy viscosity in the outer part of the turbulent boundary layer $(y > 4K_R)$ for an unheated rough surface is constant and is proportional to $\rho_o U_o \delta^*$. The average value of the

constant of proportionality was found to be equal to 0.018 as given by Clauser.

7. The temperature distribution in the thermal boundary layer can be represented by a wall law and a temperature-defect law analogous to the velocity-distribution law using the friction temperature defined by $T_* = q_w/(\rho_o c_p g U_*)$. The logarithmic wall law and temperature defect law for rough surfaces can be expressed as

$$\frac{T_\omega - \bar{T}}{T_*} = 6.6 \log \frac{y U_*}{\nu_\omega} + 1 - \frac{\Delta (T_\omega - T)}{T_*}$$

and

$$\frac{\bar{T} - T_o}{T_*} = 6.6 \log y/\delta_T - 0.30$$

respectively.

8. The quantity $\frac{\Delta (T_W - \bar{T})}{T_*}$ has the same significance for the temperature distribution as the quantity $\Delta \bar{U}/U_*$ for the velocity distribution. This represents the parallel shift of the temperature-distribution curve and depends on the magnitude of the roughness effect.

9. The local coefficient of heat transfer (the Stanton number) for rough surfaces is analogous to the local skin-friction coefficient and is given by the equation

$$\frac{1}{S_t}\sqrt{\frac{c_f}{2}} = 6.6 \log \frac{\delta_T U_*}{\nu_\omega} + 0.7 - \frac{\Delta(T_\omega - \bar{T})}{T_*}$$

This equation is restricted in its generality to fluids having a Prandtl number equal to that of air or 0.7 .

BIBLIOGRAPHY

1. Batchelor, G. K. Heat convection and buoyancy effects in fluids. Royal Meteor. Soc., London, Quart. Jour., 80:339 - 58, July 1954.

2. Baines, W. D. Equations for use with the constant temperature hot wire anemometer. State University of Iowa, Iowa Institute of Hyd. Research, 1949.

3. Clauser, F. H. The turbulent boundary layer. in Advances in Applied Mechanics, Vol. IV. New York, Academic Press, 1956. pp. 1-51.

4. Cermak, J. E. and Spengos, A. C. Turbulent diffusion of momentum and heat from a smooth, plane boundary with zero pressure gradient. Final report, Part II - Presentation of data and analysis. Cambridge, Massachusetts, U. S. Air Force Cambridge Research Center, AFCRC-TN-56-273, Contract AF19 (604)-421, December 1956. 77 pp.

5. Corrsin, S. Extended applications of the hot-wire anemometer. NACA TN 1864, April 1949.

6. Elias, F. The transfer of heat from a hot plate to an air stream. NACA TN 614, 1931.

7. Eckert, E. R. G. Introduction to the Transfer of Heat and Mass. New York, McGraw-Hill, 1950. pp. 86-140.

8. Hama, F. R. Boundary layer characteristics for smooth and rough surfaces. Soc. Naval Architects and Marine Engineers, Trans. 62:333 - 358, 1954.

9. Hromas, L. A. and Kentzer, C. P. Calibration of a hot-wire anemometer for low velocities in steady flow with temperature gradients. Proc. Fourth Midwestern Conf. on Fluid Mechanics, September 8 and 9, 1955. pp. 23 - 44. (Purdue University Engineering Experiment Station, Research Bulletin No. 128, 1956).

BIBLIOGRAPHY -- Continued

10. Johnson, D. S. Velocity, temperature, and heat-transfer measurement in a turbulent boundary layer downstream of a step wise discontinuity in wall temperature. Jour. Appl. Mechanics 24(1): 2-8, March 1957.

11. Moore, W. L. An experimental investigation of the boundary-layer development along a rough surface. Ph.D. Dissertation, State University of Iowa, 1951. 58 pp.

12. Prandtl, L. and Schlichting, H. The resistance law of rough plates (Das widerstandsgesetz rauher platten werft, Reederei, Haven 15(1):1-4, January 1934). Translated by NACA.

13. Rotta, J. On the theory of turbulent boundary layer (Uber die theorie der turbulenten grenzschichten, Mitteilungen aus dem Max-Plank-Institut fur stromungsforschung, Gottingen, No. 1, 1950). NACA TM 1344, 1953. 50 pp.

14. Reynolds, W. C., Kays, W. M. and Kline, S. J. Heat transfer in the turbulent in compressible boundary layer with constant wall temperature. Final report - Part I, Prepared under Contract NAw-6494, The Natl. Adv. Com. Aero., Department of Mechanical Engineering, Stanford University, July 1958. 51 pp.

15. Ross, Donald. Integration of the Reynolds equation for incompressible boundary layers. State College, Pennsylvania State College, Ordinance Research Laboratory, Serial No. NOrd 7958-268, May 1953.

16. Schlichting, H. Boundary Layer Theory. New York, McGraw-Hill, 1955. 535 pp.

17. Squire, H. B. Heat Transfer in Modern Developments in Fluid Dynamics: High Speed Flow, Vol. II. L. Howarth (Edi.), Oxford University Press, 1953. pp. 815-832.

BIBLIOGRAPHY -- Continued

18. Spengos, A. C. Turbulent diffusion of momentum and heat from a smooth, plane boundary with zero pressure gradient. Scientific report I. Cambridge, Massachusetts, U. S. Air Force Cambridge Research Center, AFCRC-TN-56-259, Contract AF 19(604)-421, February 1956. 50 pp.

19. Spengos, A. C. and Cermak, J. E. Turbulent diffusion of momentum and heat from a smooth, plane boundary with zero pressure gradient. Final report, Part I-Experimental equipment. Cambridge, Massachusetts, U. S. Air Force Cambridge Research Center, AFCRC-TN-56-273, Contract AF 19(604)-421, December 1956, 36 pp.

20. Spengos, A. C. and Cermak, J. E. Heat transfer by forced convection from a horizontal flat plate into a turbulent boundary layer. Stanford University, Heat Transfer and Fluid Mechanics Institute, Preprints of Papers, June 21 - 23, 1956. pp. 89-104.

21. Shapiro, A. H. The Dynamics and Thermodynamics of Compressible Fluid Flow, Vol. II. New York, Ronald Press, 1954. pp. 1080-1117.

22. Townsend, A. A. The Structure of Turbulent Shear Flow, Cambridge University Press, 1956. 315 pp.

23. Van Driest, E. R. Turbulent boundary layer in compressible fluids. Jour. Aeronaut. Science, 18(3):145-160, March 1951.

24. Von Karman, Th. The analogy between fluid friction and heat transfer. Trans. ASME, 61(8):705-10, November 1939.

Table I

HEATER STRIP CHARACTERISTICS

Strip No.	Strip Width in.	Strip Length in.	Strip Res. ohms	Fuse amps	Rheostat ohms
1	0.5	70.5	225	1.5	25.0
2	1.0	"	185	1.5	15.0
3	1.0	"	225	1.5	25.0
4	1.0	"	210	1.5	35.0
5	2.0	"	130	3.0	22.0
6	2.0	"	130	3.0	25.0
7	2.0	"	128	3.0	25.0
8	2.0	"	136	3.0	22.0
9	4.0	"	68	4.0	10.0
10	4.0	"	77	4.0	15.0
11	4.0	"	68	3.0	15.0
12	8.0	"	48	6.0	7.5
13	8.0	"	43	6.0	7.5
14	8.0	"	47	6.0	7.5
15	8.0	"	57	5.0	7.5
16	8.0	"	48	5.0	7.5
17	8.0	"	51	5.0	7.5
18	8.0	"	48	5.0	7.5
19	8.0	"	44	5.0	7.5
20	8.0	"	56	5.0	7.5
21	8.0	"	64	5.0	7.5
22	8.0	"	50	5.0	7.5
23	8.0	"	54	5.0	7.5

Table II

BASIC DATA

$x + L$ in.	U_o ft/sec	T_o ^0F	ΔT_o ^0F	ρ_o slug/ft^3 10^{-3}	ν_o ft^2/sec 10^{-4}	ρ_w slug/ft^3 10^{-3}	ν_w ft^2/sec 10^{-4}	δ in.	δ^* in.	δ^{**} in.	δ_T in.	δ_T^{**} in.
55	17.0	93.0	0.0	1.880	2.09			3.0	0.700	0.411		
67	17.2	97.5	0.0	1.875	2.11			3.4	0.788	0.469		
86	16.9	90.0	0.0	1.875	2.07			4.5	0.942	0.551		
114	17.0	97.5	0.0	1.875	2.10			5.3	1.204	0.678		
154	17.1	89.0	0.0	1.885	2.67			6.5	1.388	0.815		
55	35.3	85.0	0.0	1.905	2.04			2.7	0.630	0.377		
67	35.0	86.0	0.0	1.910	2.04			3.2	0.691	0.422		
86	35.2	86.0	0.0	1.905	2.05			4.0	0.898	0.520		
114	34.5	70.0	0.0	1.950	1.96			5.0	1.080	0.612		
154	35.0	73.0	0.0	1.935	1.98			6.1	1.240	0.764		
55	17.2	62.0	77.0	1.950	1.93	1.705	2.45	3.5	0.793	0.472	1.75	.080
67	17.0	64.0	77.0	1.980	1.91	1.73	2.41	4.2	0.880	0.516	2.75	.156
86	17.5	64.5	77.0	1.940	1.95	1.695	2.47	5.0	1.074	0.627	4.0	.275
114	17.0	69.0	75.0	1.960	1.94	1.72	2.44	5.9	1.312	0.735	5.0	.344
154	17.5	69.0	75.0	1.960	1.94	1.72	2.44	7.1	1.470	0.862	6.0	.486
55	35.0	106.0	53.0	1.835	2.19	1.675	2.55	3.2	0.701	0.401	1.5	.101
67	34.5	82.0	50.0	1.895	2.04	1.735	2.38	3.8	0.840	0.466	2.5	.151
86	34.5	82.0	50.0	1.895	2.04	1.735	2.32	4.7	1.000	0.575	3.5	.201
114	36.0	80.0	48.0	1.920	2.01	1.765	2.32	5.4	1.140	0.663	4.5	.321
154	35.5	80.0	48.0	1.920	2.01	1.765	2.32	6.7	1.384	0.826	5.8	.420

Table II -- Continued

BASIC DATA

$x + L$ in.	ft/sec	$c_f = 2\frac{d\delta^{**}}{dx}$	U_* ft/sec	$R_{\delta^*} = \frac{U_o \delta^*}{\nu_w}$	$S_t = \frac{d\delta_T^{**}}{dx}$	$T_* = \frac{q_w}{g \rho_o c_p U_*}$
		10^{-3}		10^3		
55	17.0	9.60	1.178	4.75		
67	17.2	9.00	1.153	5.36		
86	16.9	8.56	1.100	6.41		
114	17.0	7.98	1.073	8.105		
154	17.1	7.24	1.029	9.57		
55	35.3	9.12	2.380	9.06		
67	35.0	8.46	2.274	9.90		
86	35.2	8.08	2.360	12.87		
114	34.5	7.44	2.105	15.9		
154	35.0	6.66	2.005	18.24		
55	17.2	9.60	1.190	5.57	.00520	
67	17.0	9.06	1.142	6.28	.00460	5.04
86	17.5	8.64	1.150	7.64	.00420	4.65
114	17.0	7.96	1.071	9.17	.00385	4.28
154	17.5	7.24	1.053	10.50	.00335	4.205
55	35.0	9.40	2.400	9.6	.00500	
67	34.5	8.70	2.270	12.2	.00399	2.66
86	34.5	8.16	2.205	14.5	.00339	2.49
114	36.0	7.64	2.225	17.7	.00300	2.08
154	35.5	6.96	2.095	21.2	.00270	2.16

Table III

Comparison of Values of $\frac{\Delta\overline{U}}{U_*}$ Obtained from the Plot of the Mean Velocity and from the Plot of $\sqrt{\frac{2}{c_f}}$ vs $R_{\delta*}$

x + L in.	U_o ft/sec	ΔT_o °F	$(\frac{\Delta\overline{U}}{U_*})_v$ (from velocity plot Figs. 25, 26, 27)	$(\frac{\Delta\overline{U}}{U_*})_s$ (from the plot of skin-friction law Fig. 29)	$(\frac{\Delta\overline{U}}{U_*})_s - (\frac{\Delta\overline{U}}{U_*})_v$	Deviation %
55	17.0	0	10.00	10.50	0.50	5.0
67	17.2	0	9.80	10.35	0.55	5.6
86	16.9	0	10.30	10.35	0.05	0.5
114	17.0	0	10.50	10.35	-0.15	-1.4
154	17.1	0	10.40	9.90	-0.50	-4.8
55	17.2	77	9.85	10.86	1.01	10.3
67	17.0	77	9.90	10.67	0.77	7.8
86	17.5	77	10.20	10.86	0.66	6.5
114	17.0	75	10.40	10.67	0.27	2.6
154	17.5	75	9.40	10.18	0.78	8.3
55	35.3	0	10.90	11.68	0.78	7.2
67	35.0	0	10.70	11.35	0.65	6.1
86	35.2	0	11.50	11.60	0.10	0.9
114	34.5	0	11.40	11.45	0.05	0.4
154	35.0	0	10.75	10.87	0.12	1.1
55	35.0	53	11.45	12.00	0.55	4.8
67	34.5	50	11.70	12.00	0.30	2.6
86	34.5	50	11.60	11.95	0.35	3.0
114	36.0	48	11.35	11.95	0.60	5.3
154	35.5	48	11.10	11.60	0.50	4.5

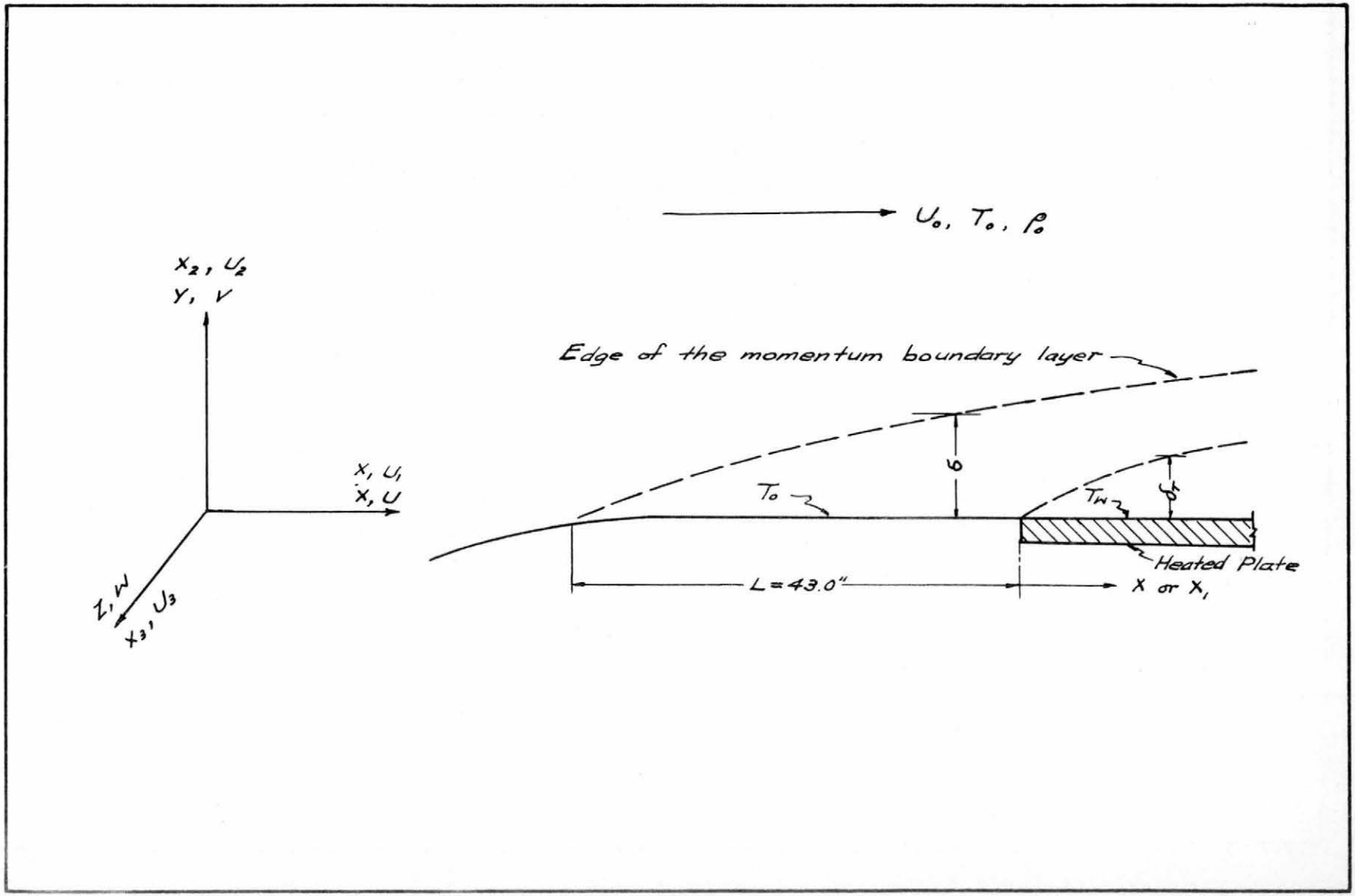

Fig 1 Definition sketch for momentum and thermal boundary layers

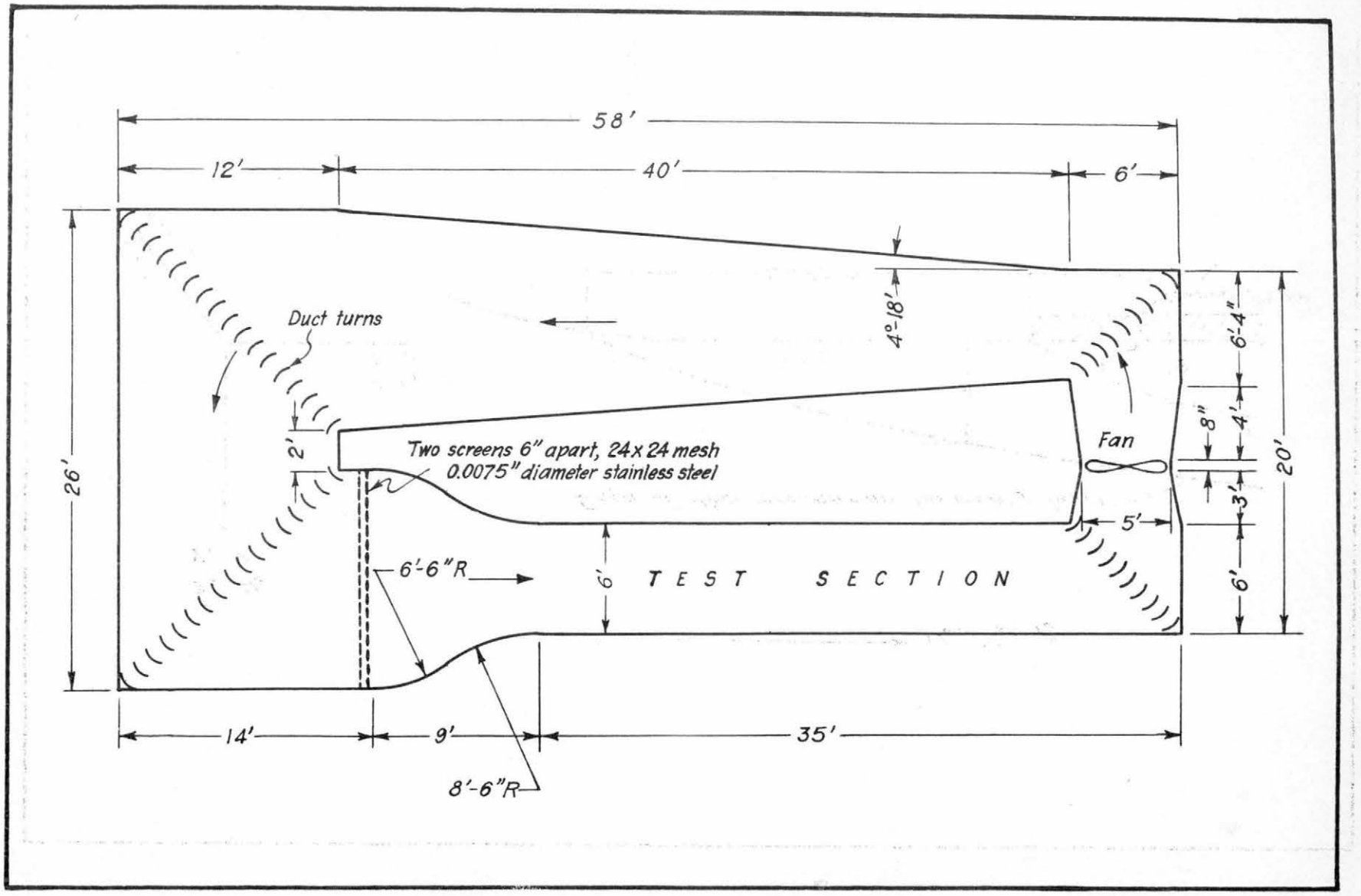

Fig. 2 Plan of wind tunnel

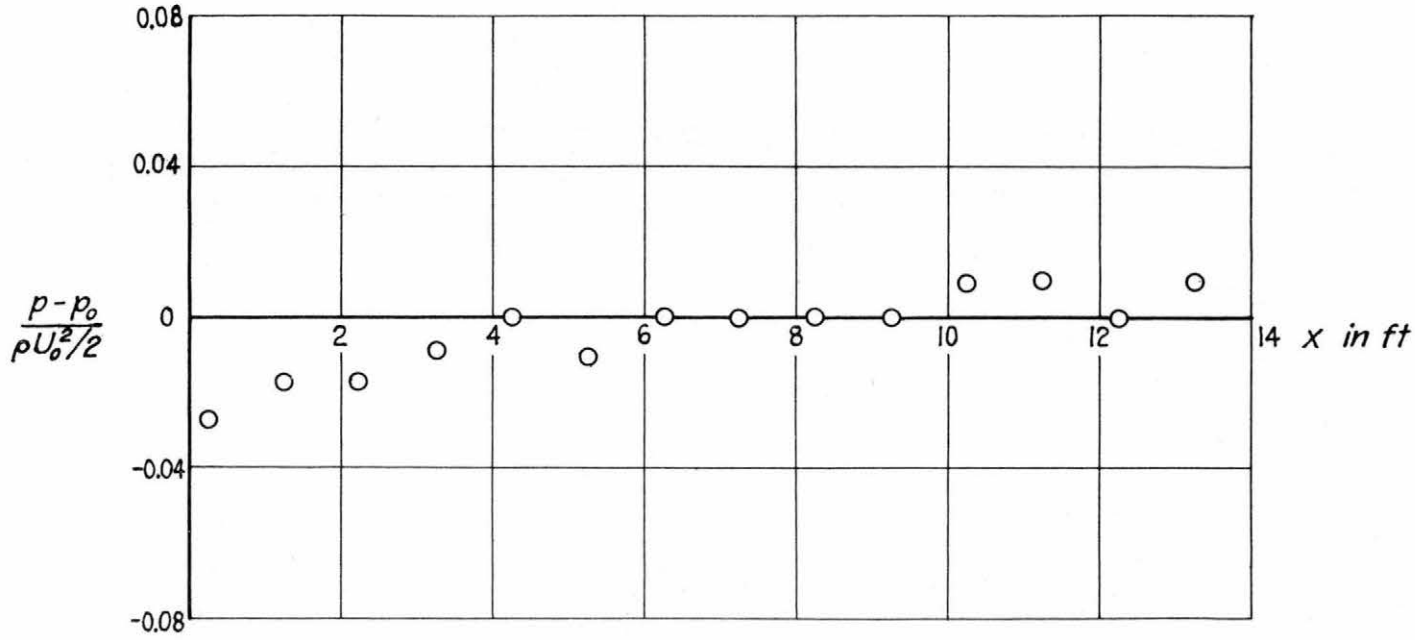

p_o Upstream reference wall pressure

U_o Upstream reference uniform velocity

Fig. 3 Pressure distribution along the centerline of test section

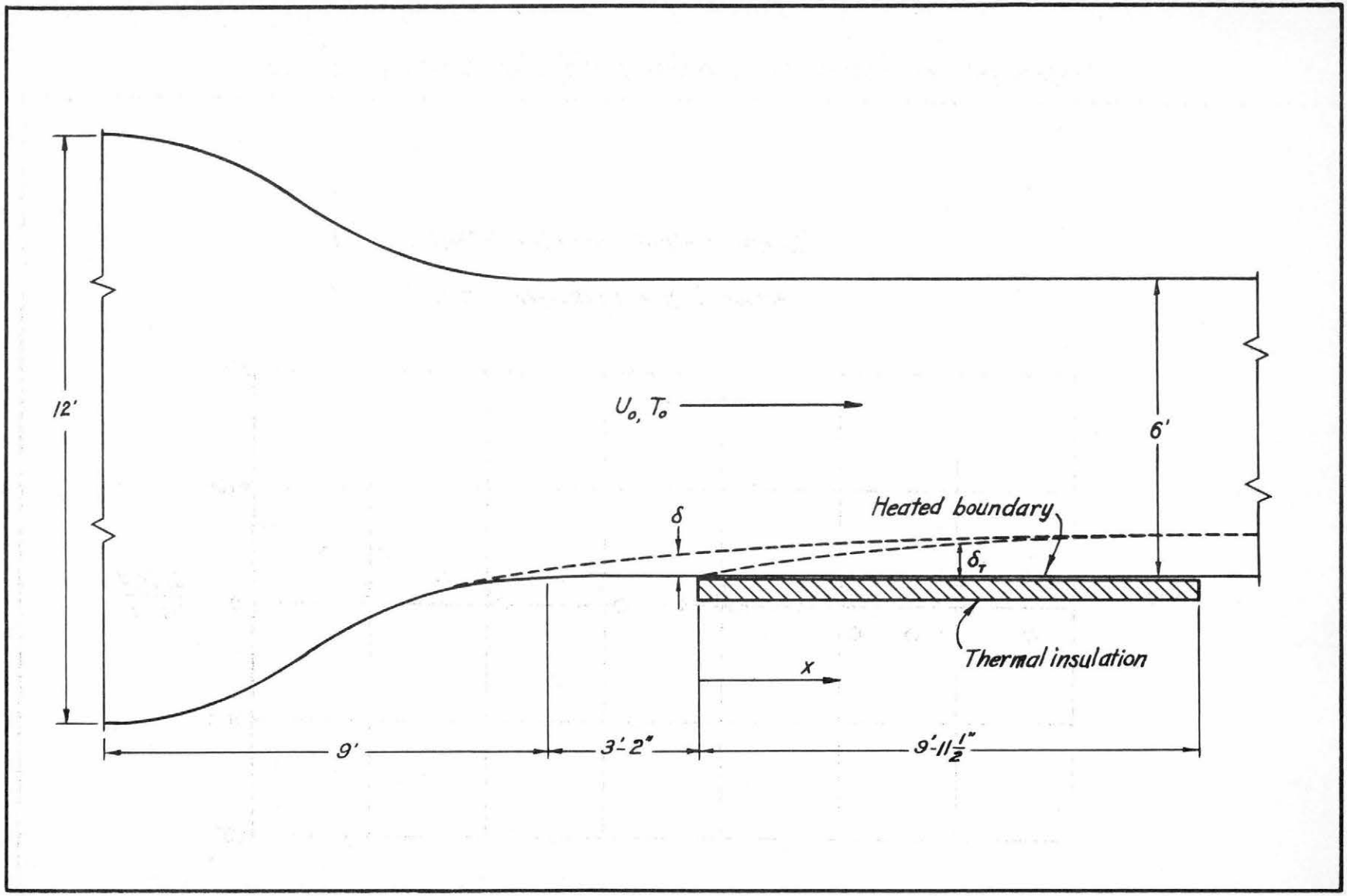

Fig. 4 Schematic diagram of test section

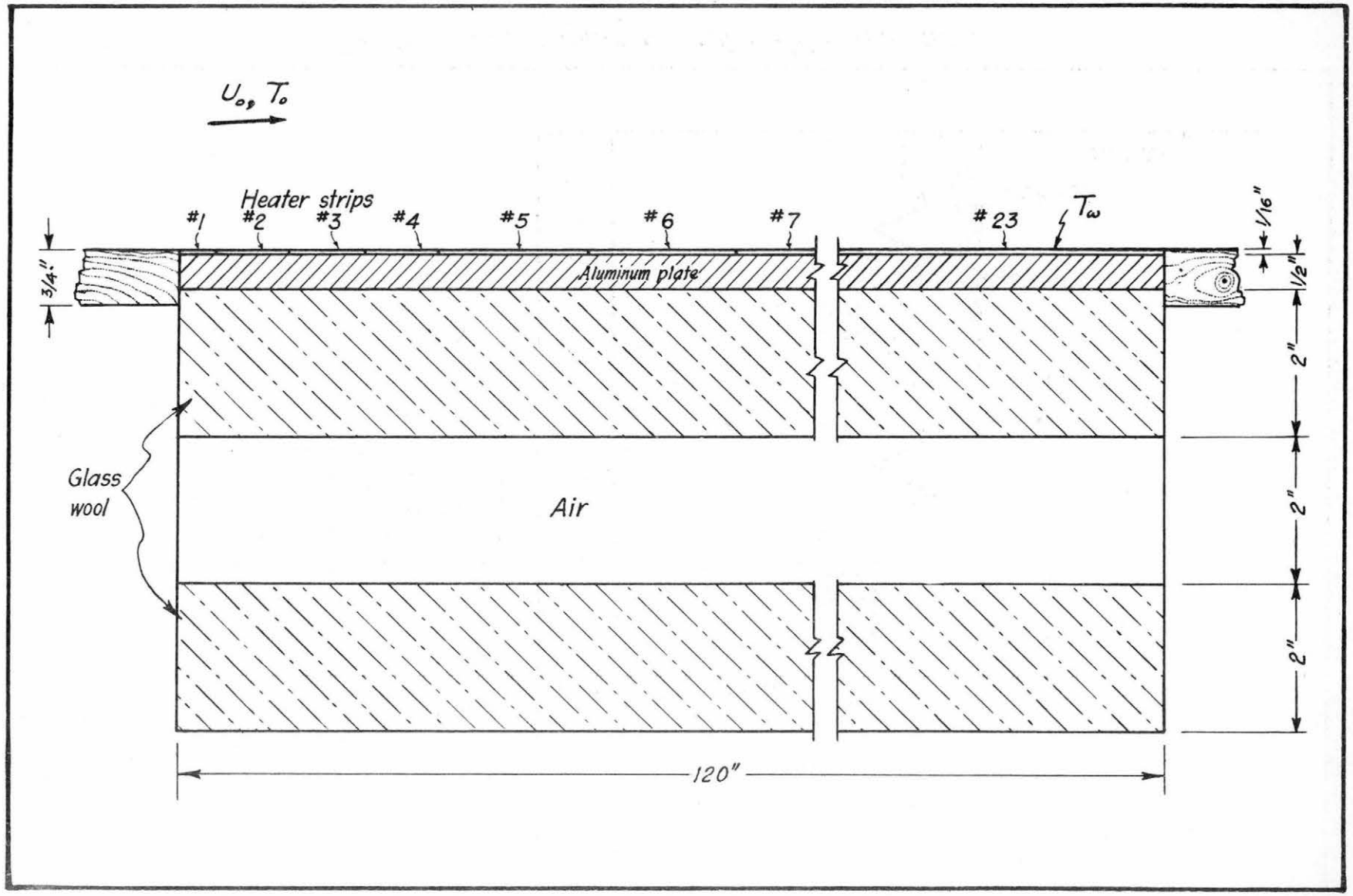

Fig. 5 Heated boundary

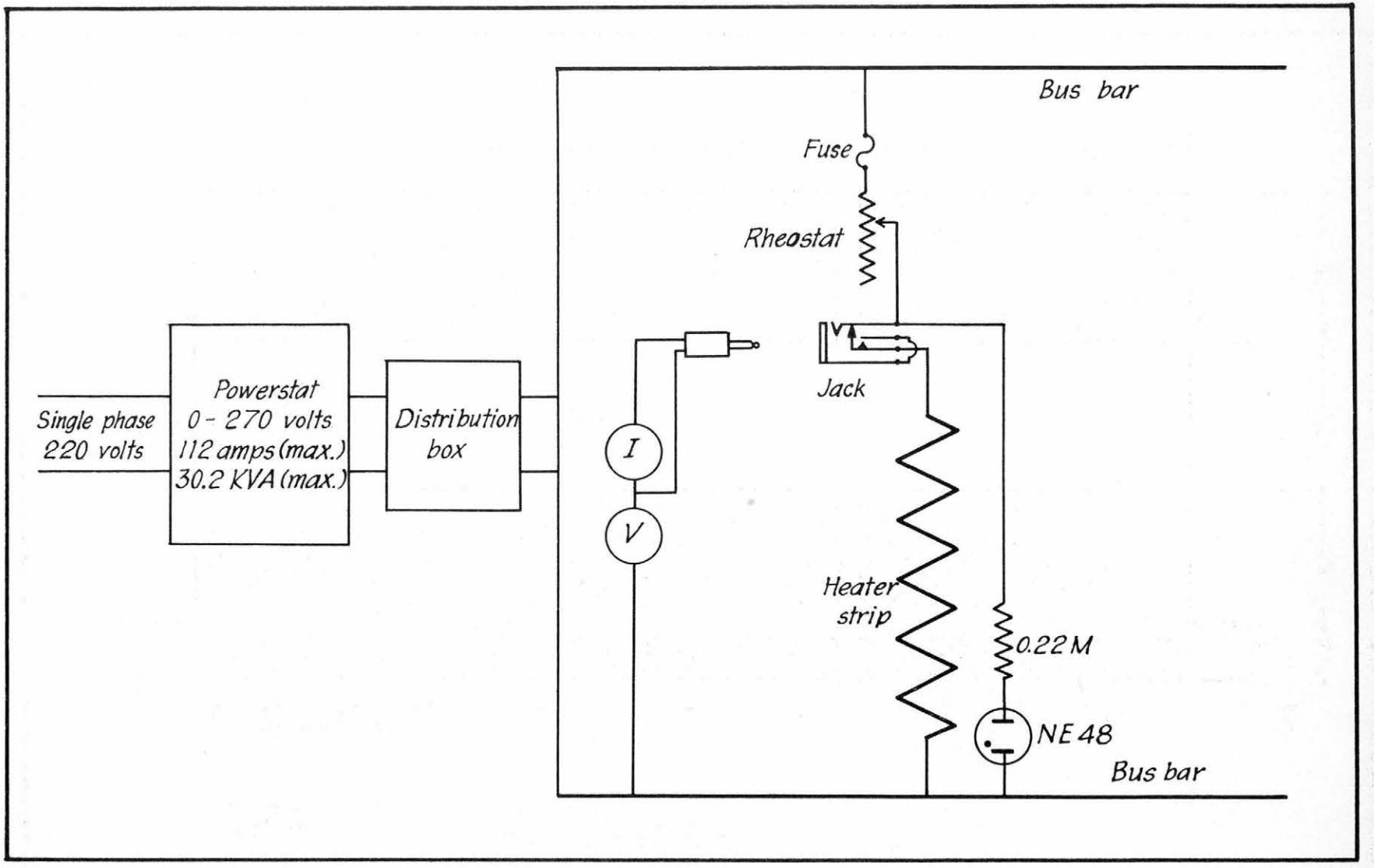

Fig. 6 Circuit diagram of heater strip connections

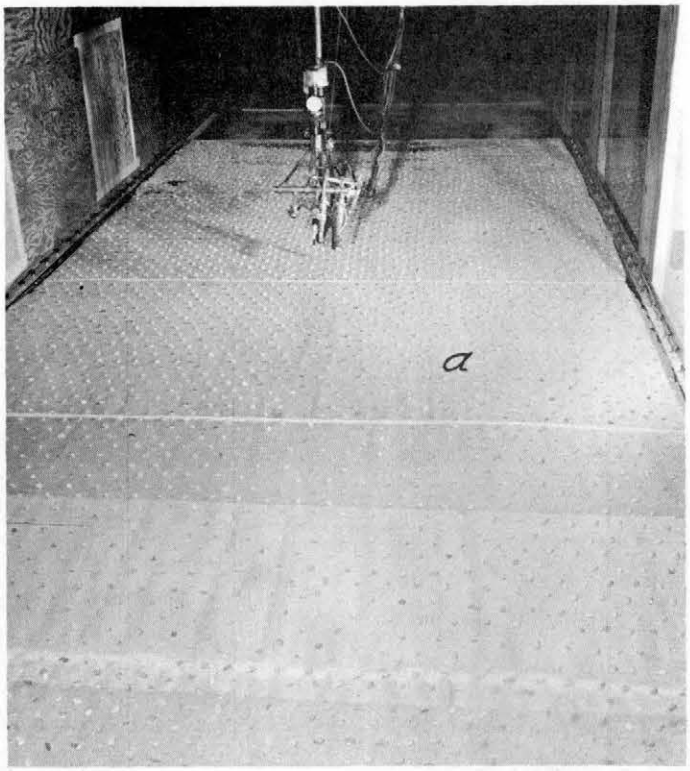

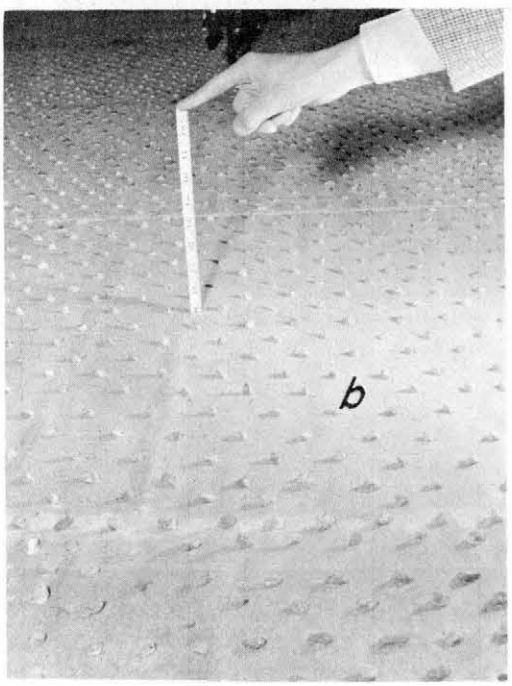

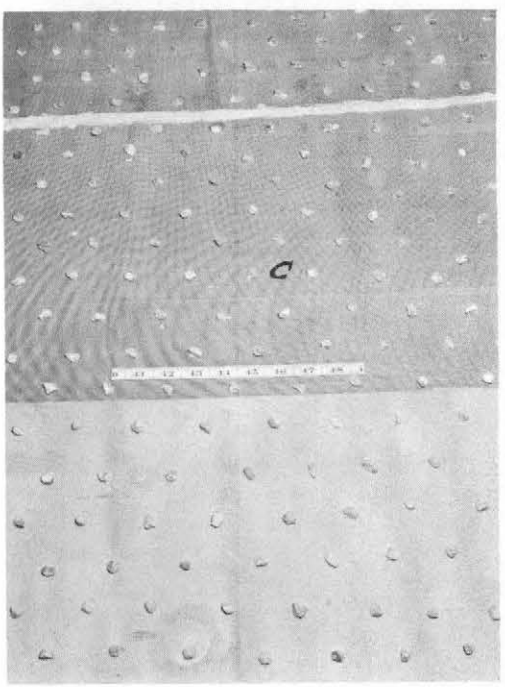

Fig. 7 Views of the Rough Surface

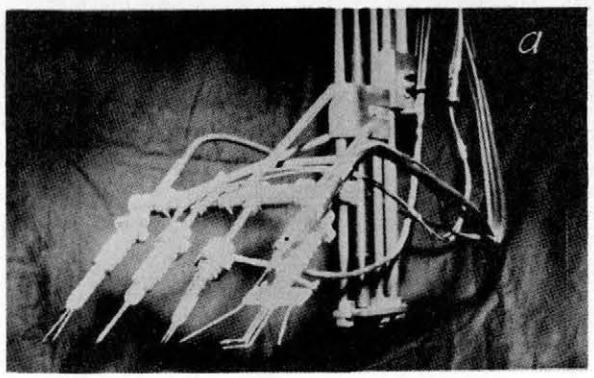

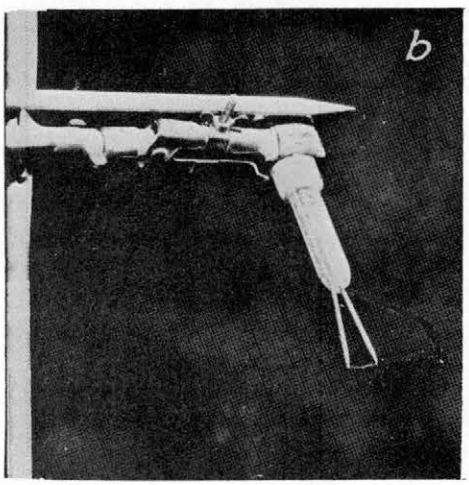

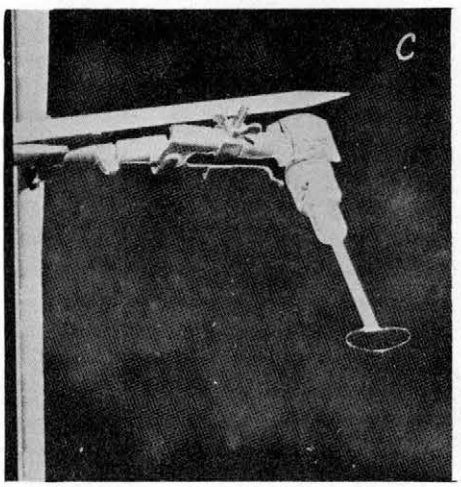

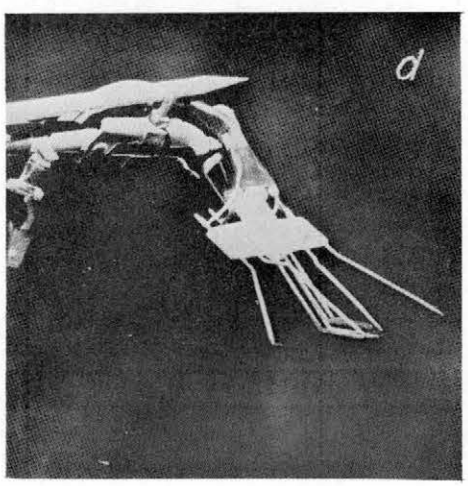

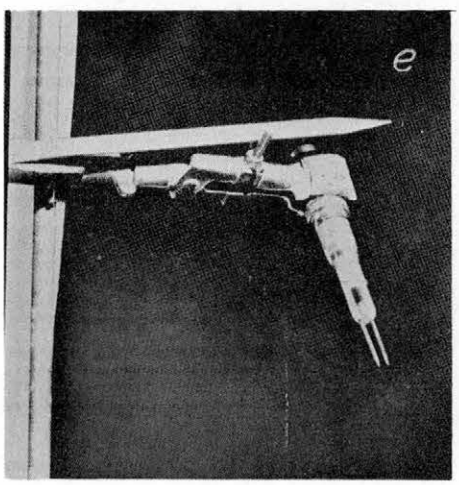

Fig. 8 Views of probes

a Probe assembly
b Mean velocity hot-wire probe
c Mean temperature thermocouple probe
d Turbulence intensities hot-wire probe
e Resistance thermometer probe

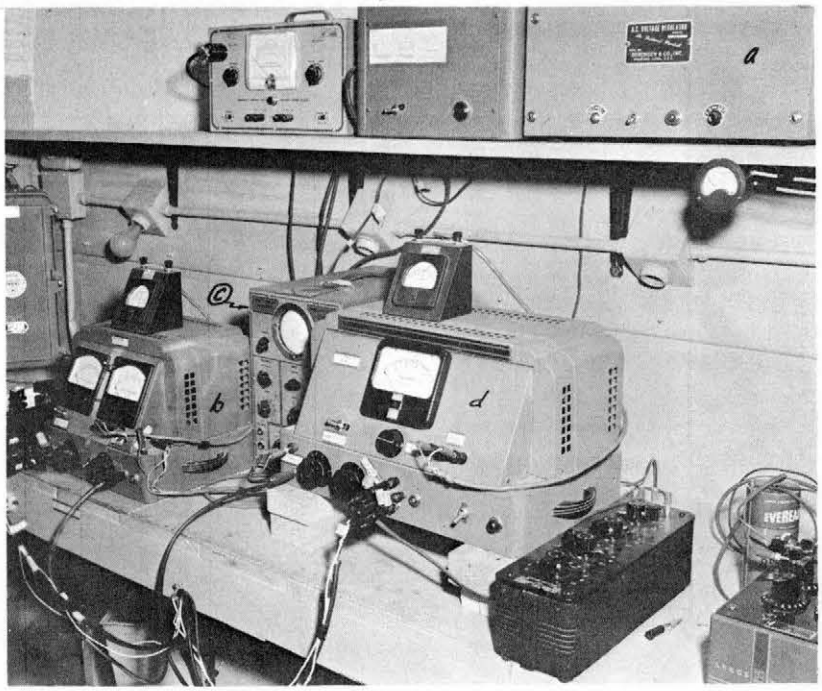

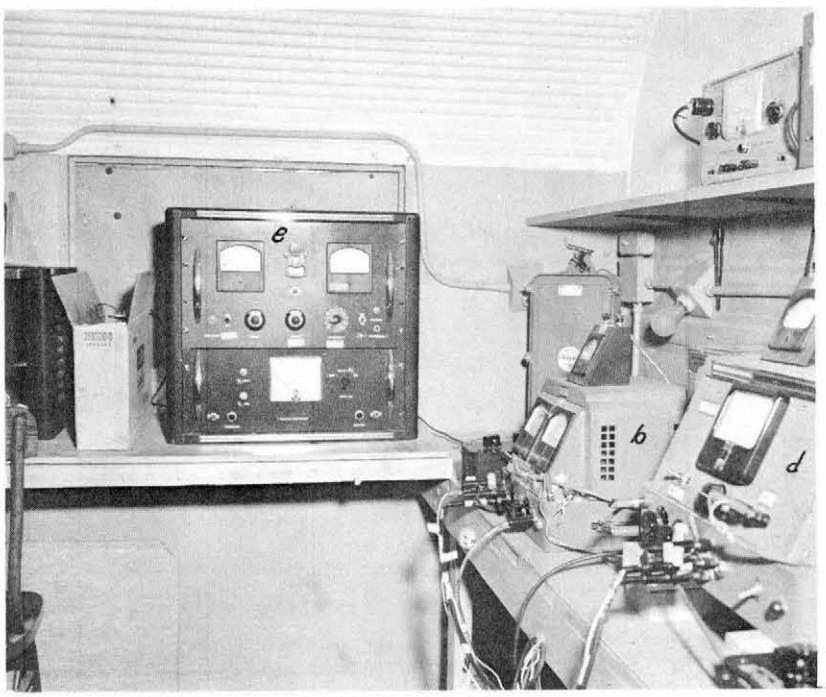

Fig. 9 Views of Instrument
b Hot-wire anemometer No. 1
d Hot-wire anemometer No. 2
e Resistance thermometer

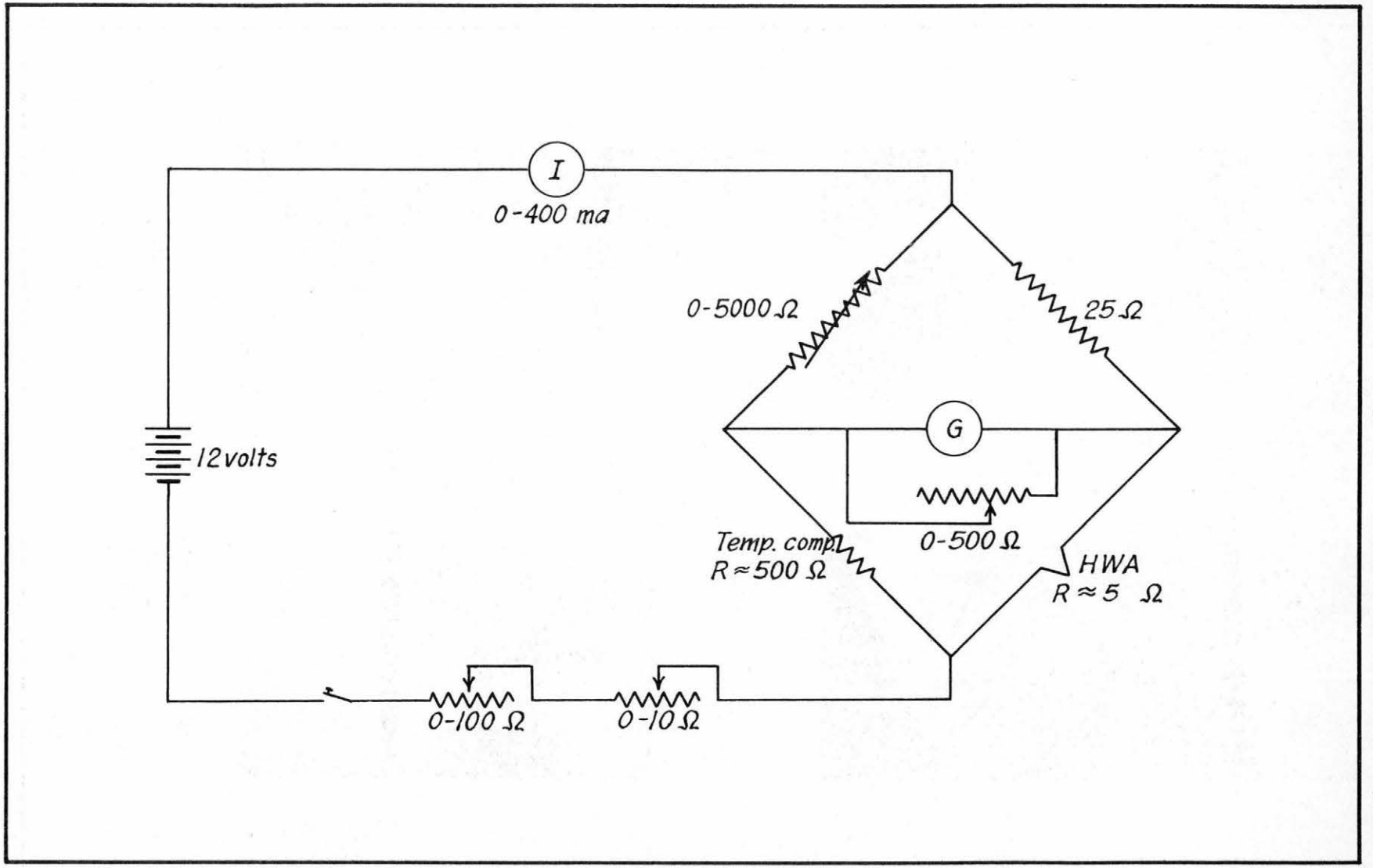

Fig. 10 Constant-temperature hot-wire anemometer for mean velocity

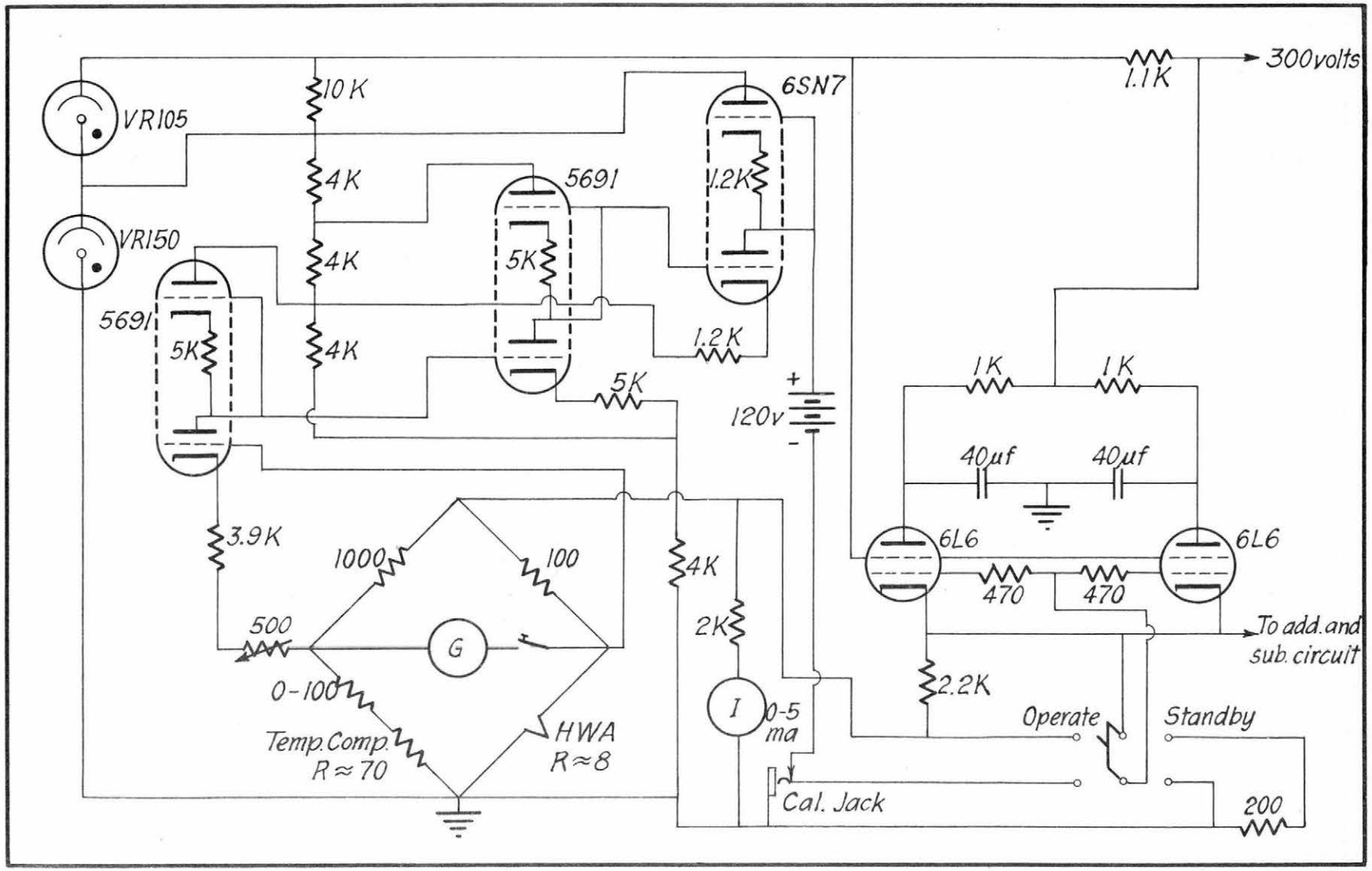

Fig. 11 Constant-temperature, tungsten hot-wire anemometer No. 1 (Current Control Circuit)

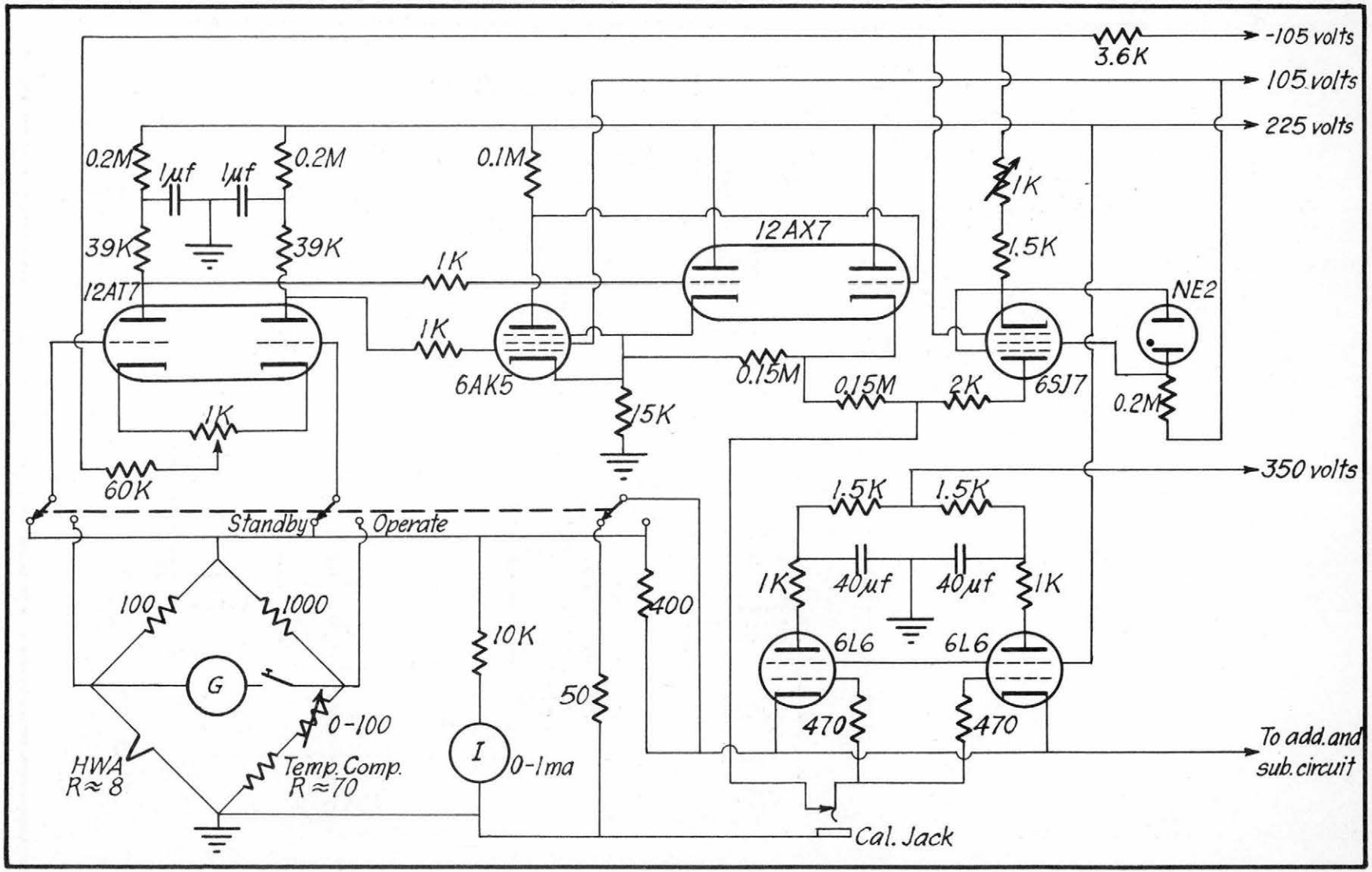

Fig. 12 Constant-temperature, tungsten hot-wire anemometer No. 2 (Current Control Circuit)

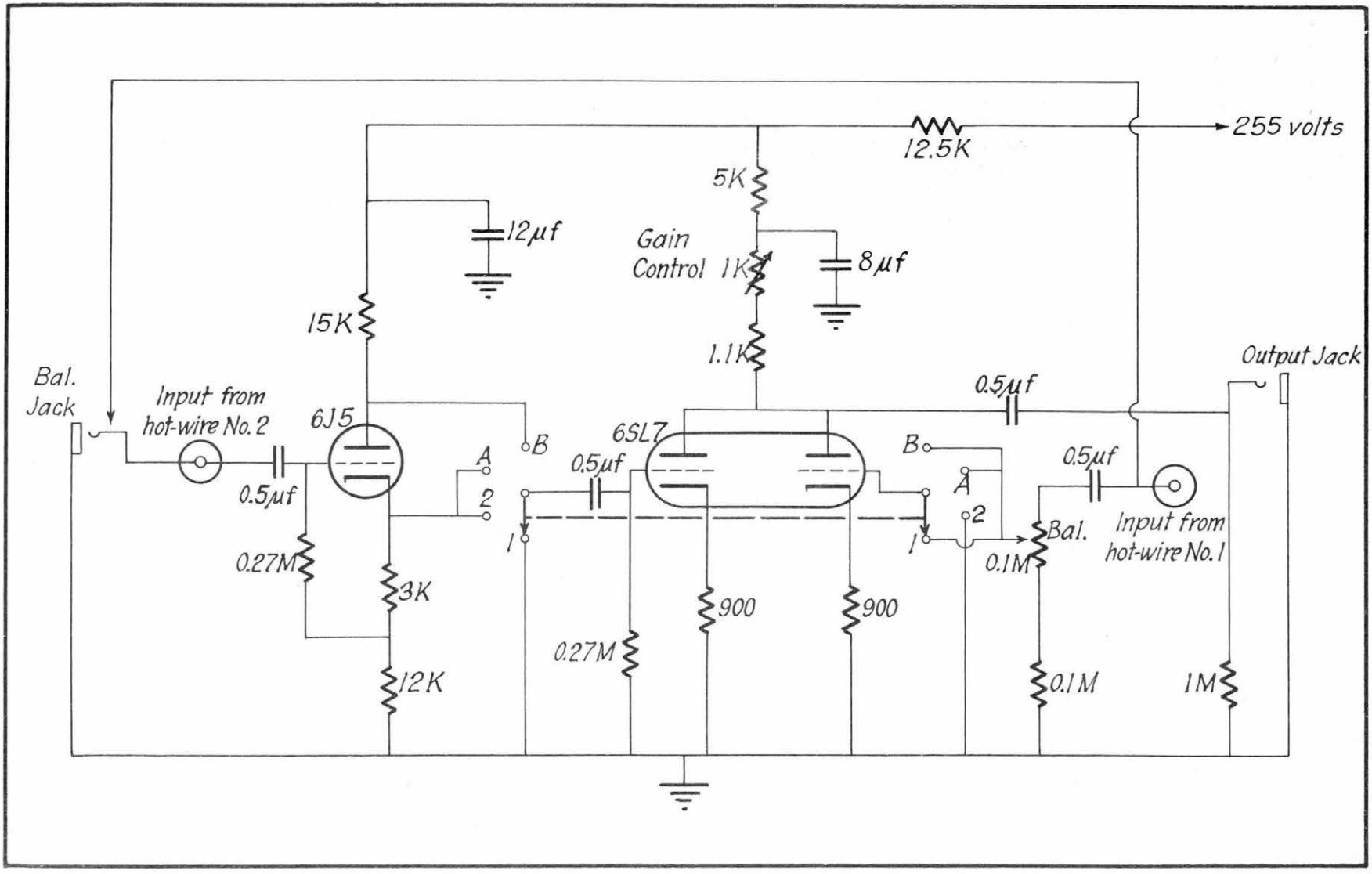

Fig. 13 Adding and subtracting circuit

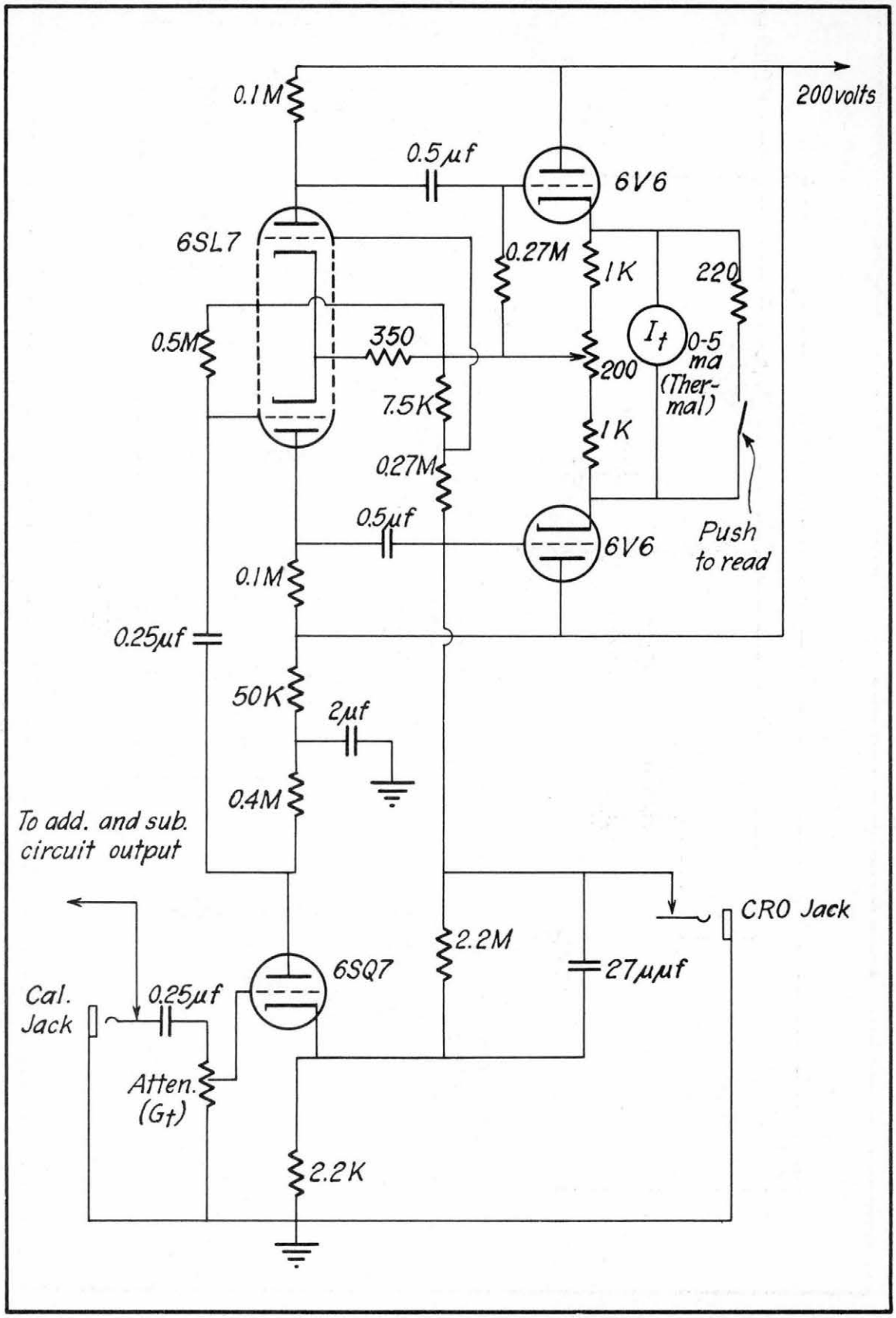

Fig. 14 Turbulence amplifier and RMS indicator circuit

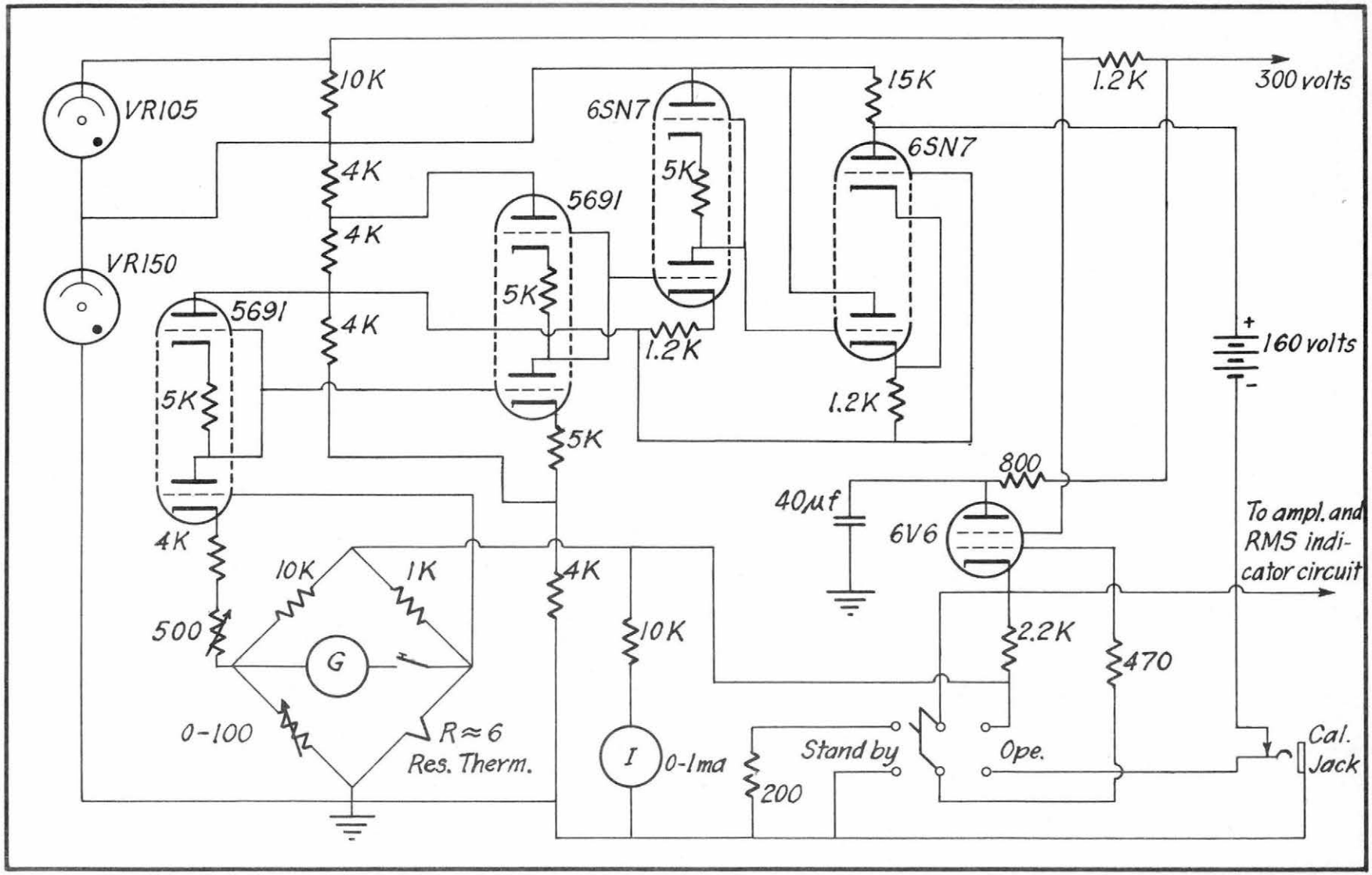

Fig. 15 Constant-temperature resistance thermometer (Current Control Circuit)

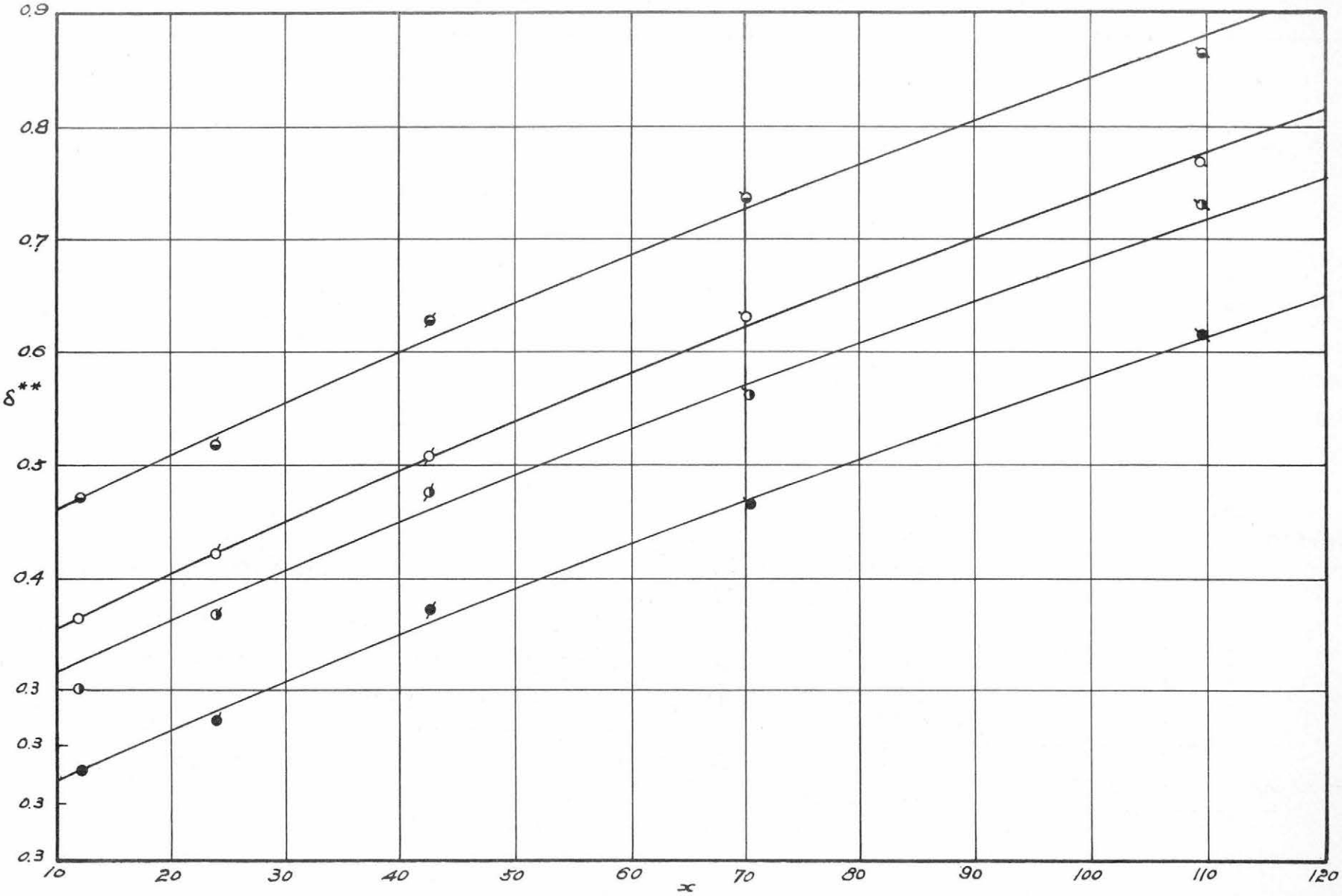

Fig. 16 Momentum thickness as a function of distance

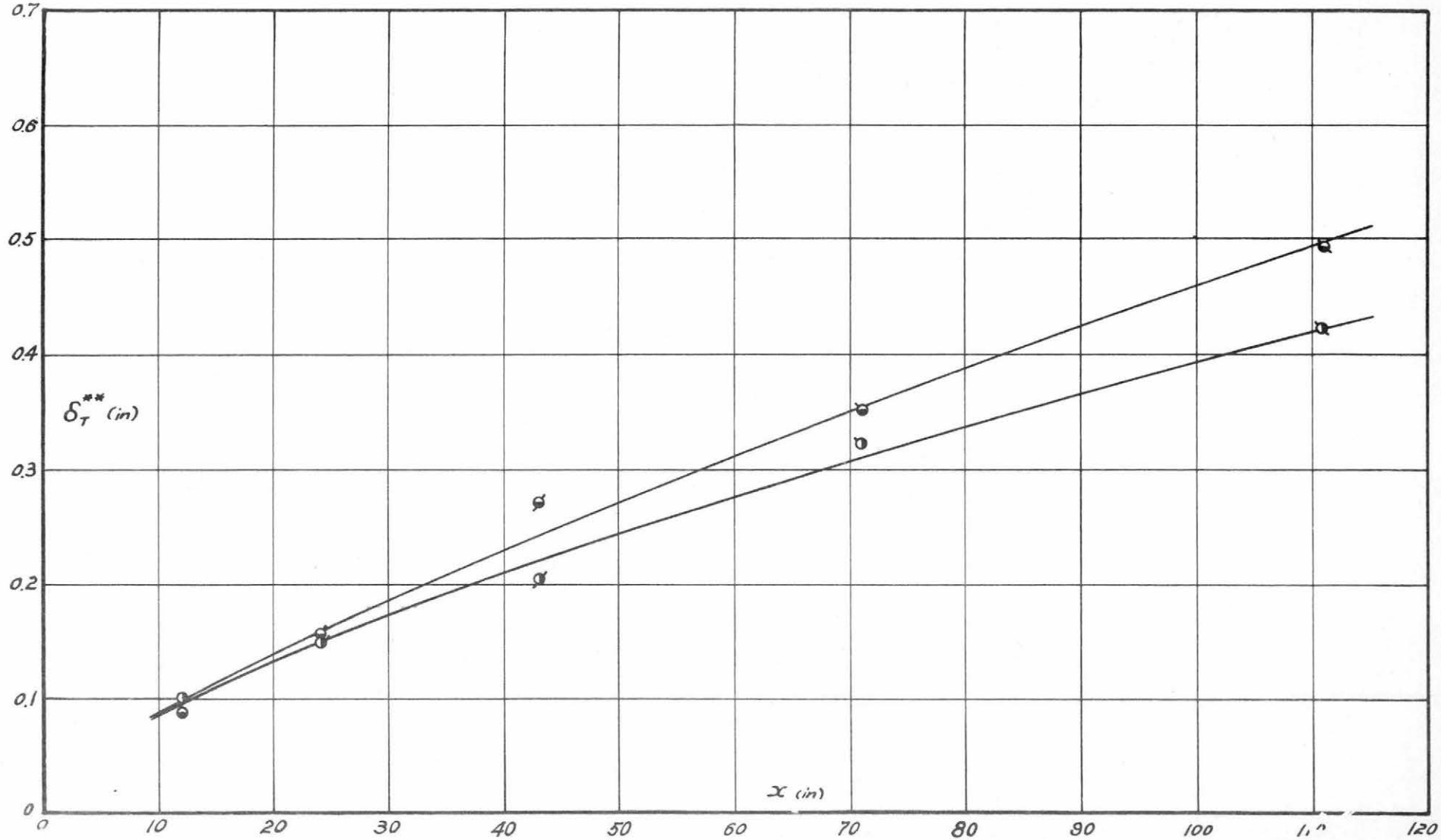

Fig. 17 Convective thickness as a function of distance.

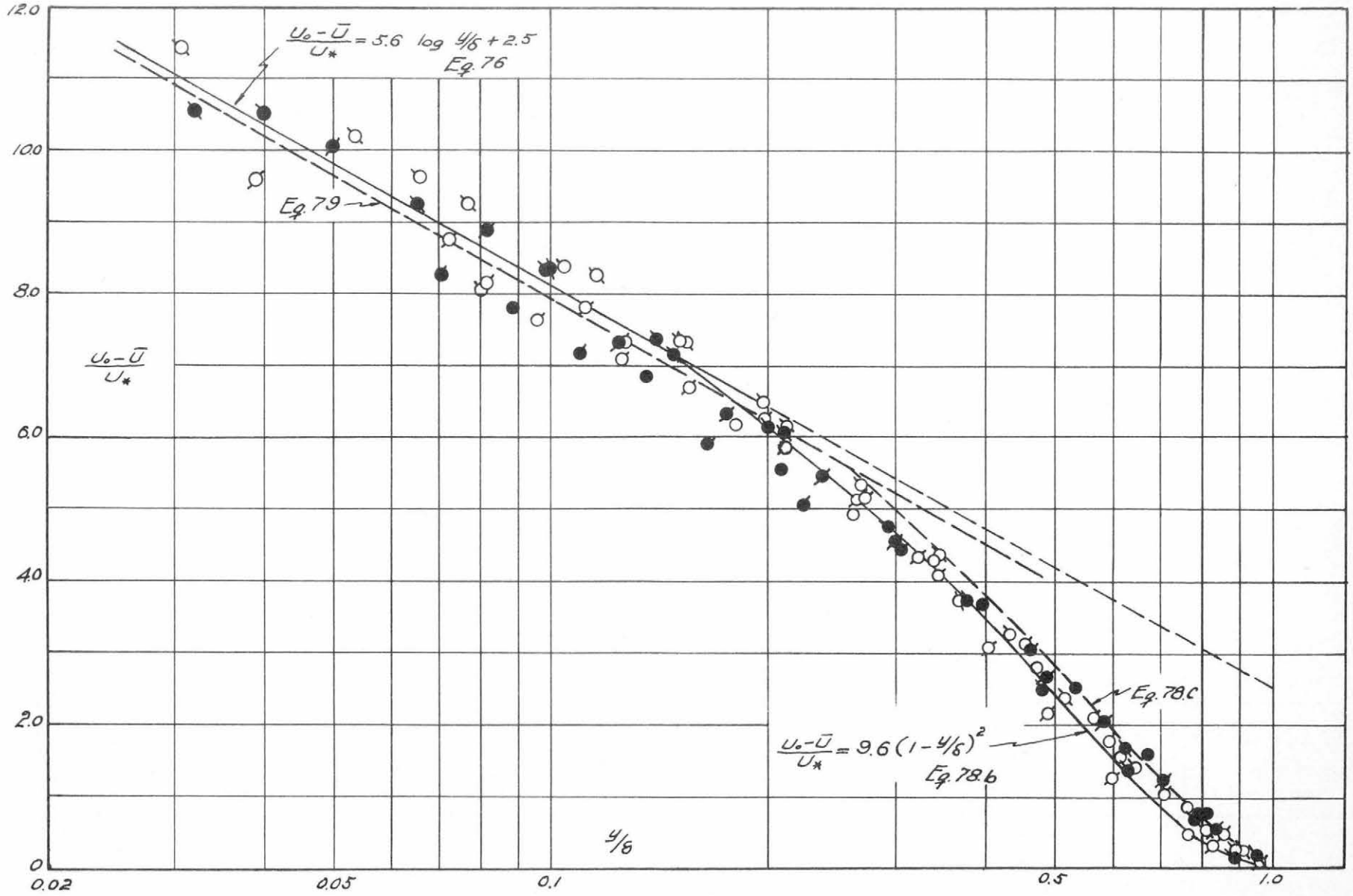

Fig. 18 Universal velocity profile for unheated surface

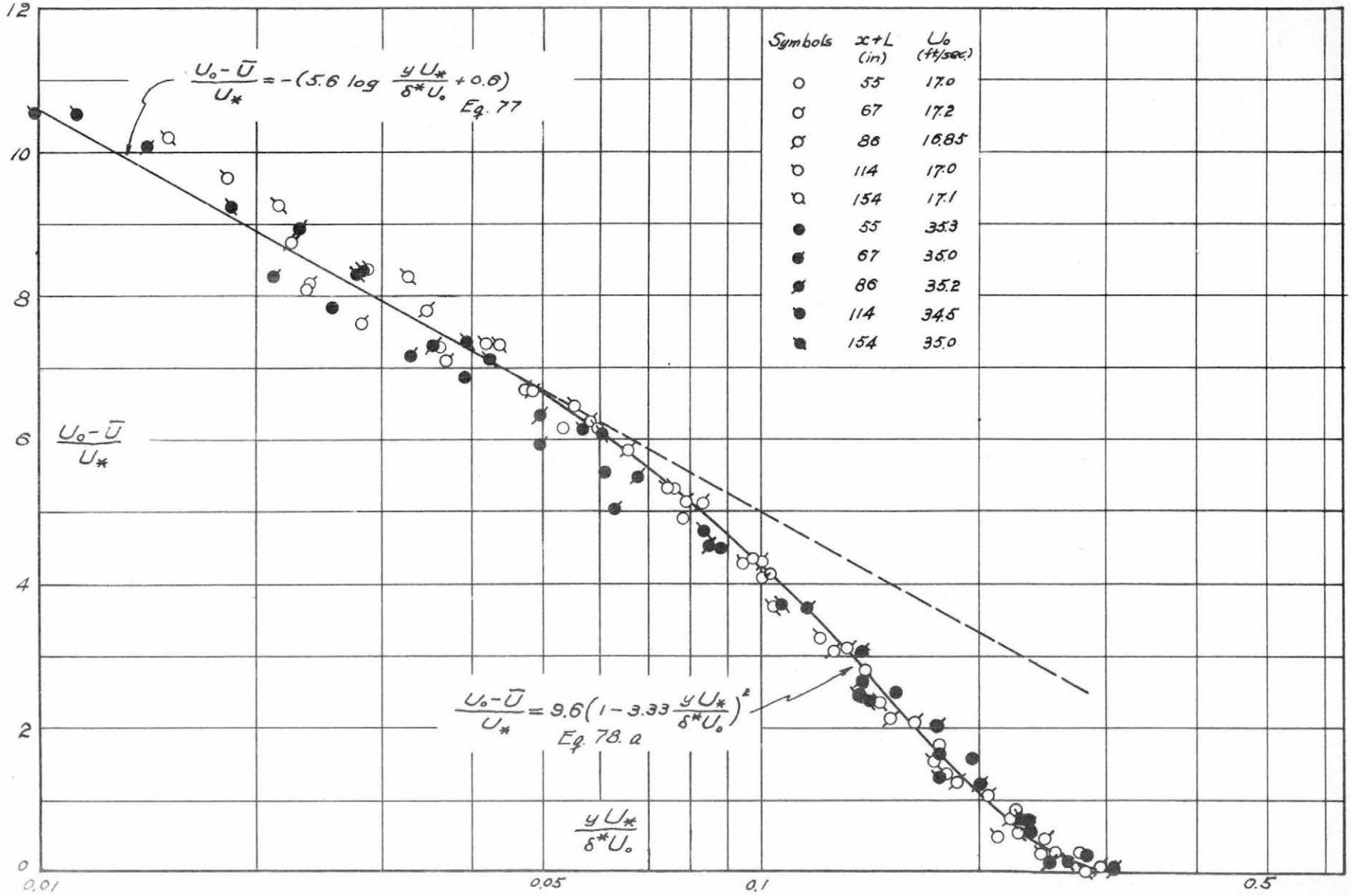

Fig. 19 Universal velocity profile for unheated surface

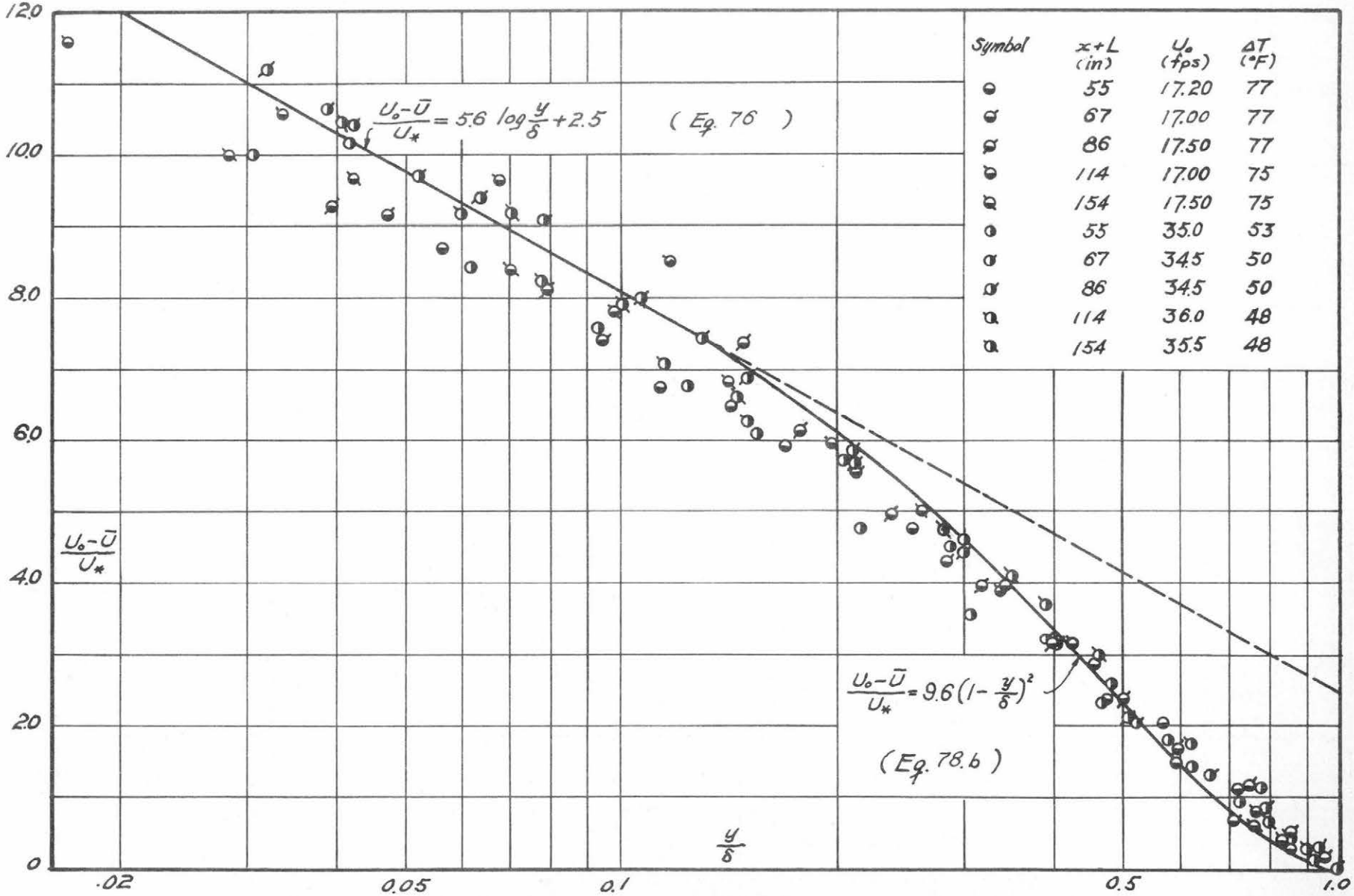

Fig. 20 Universal velocity profile for heated boundary.

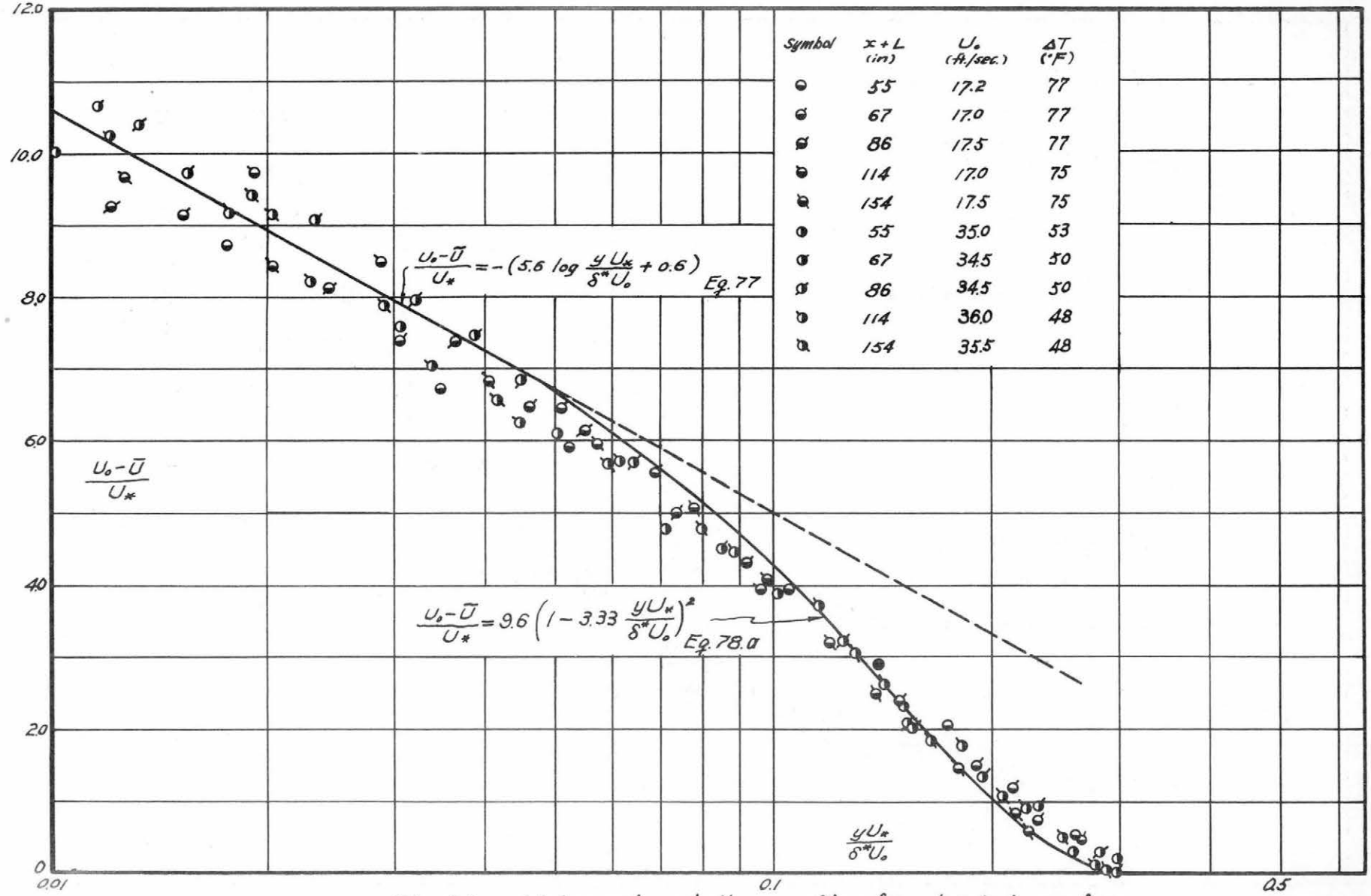

Fig. 21 Universal velocity profile for heated surface

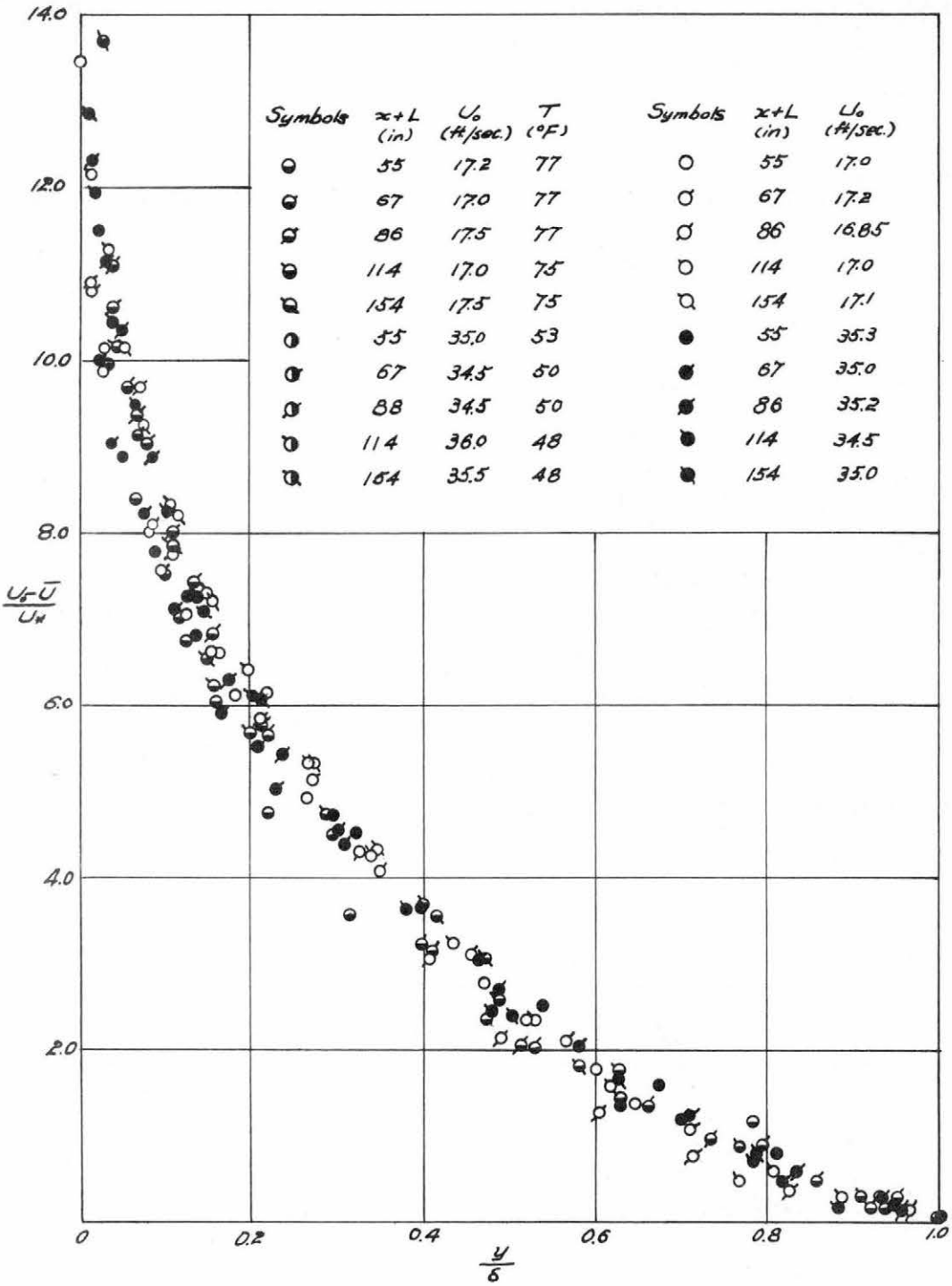

Fig. 22. Universal velocity profile for heated and unheated surfaces, linear plot

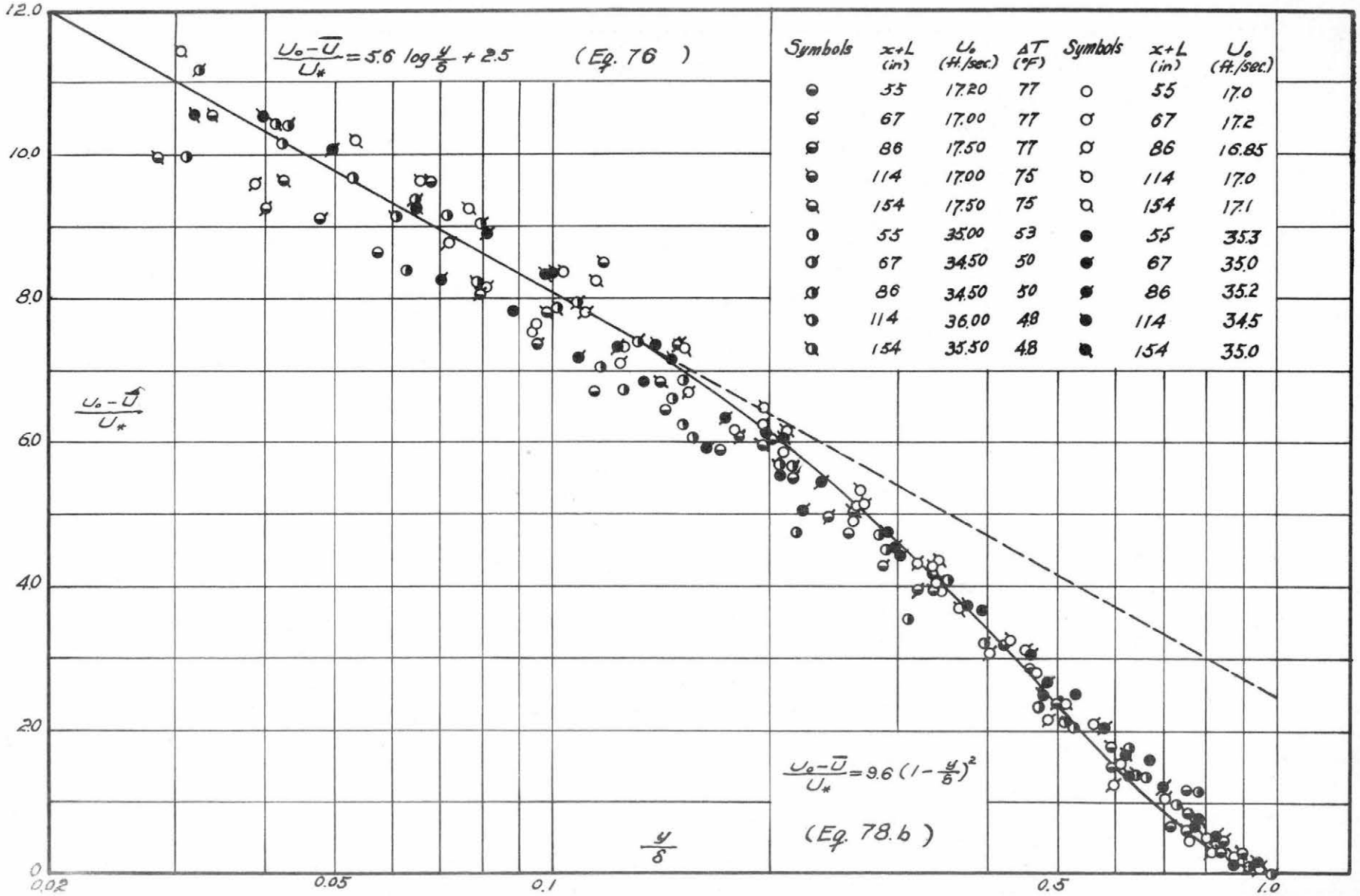

Fig. 23 Universal Velocity Profile for Heated and Unheated Surfaces.

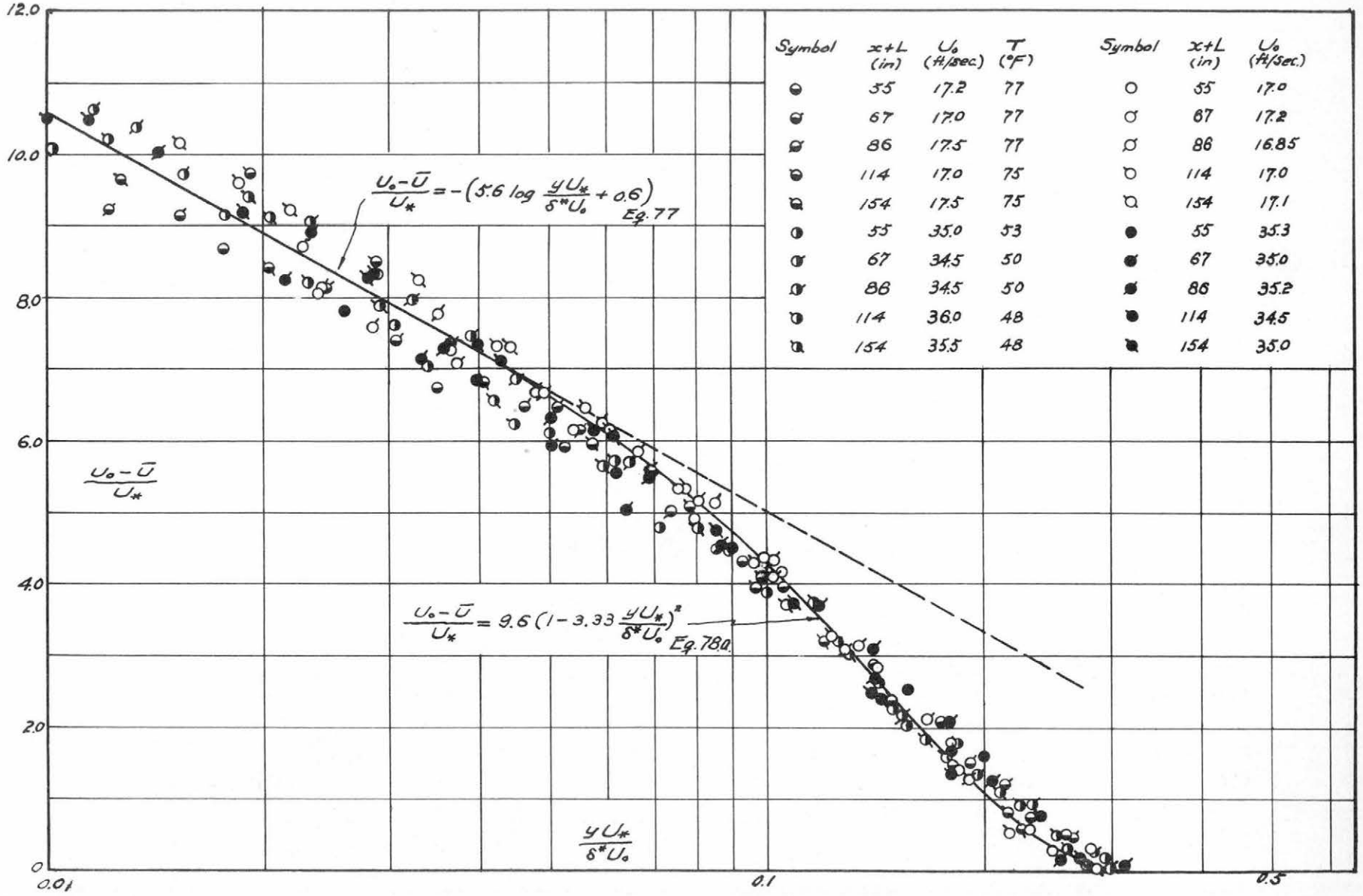

Fig. 24 Universal velocity profile for heated and unheated surfaces

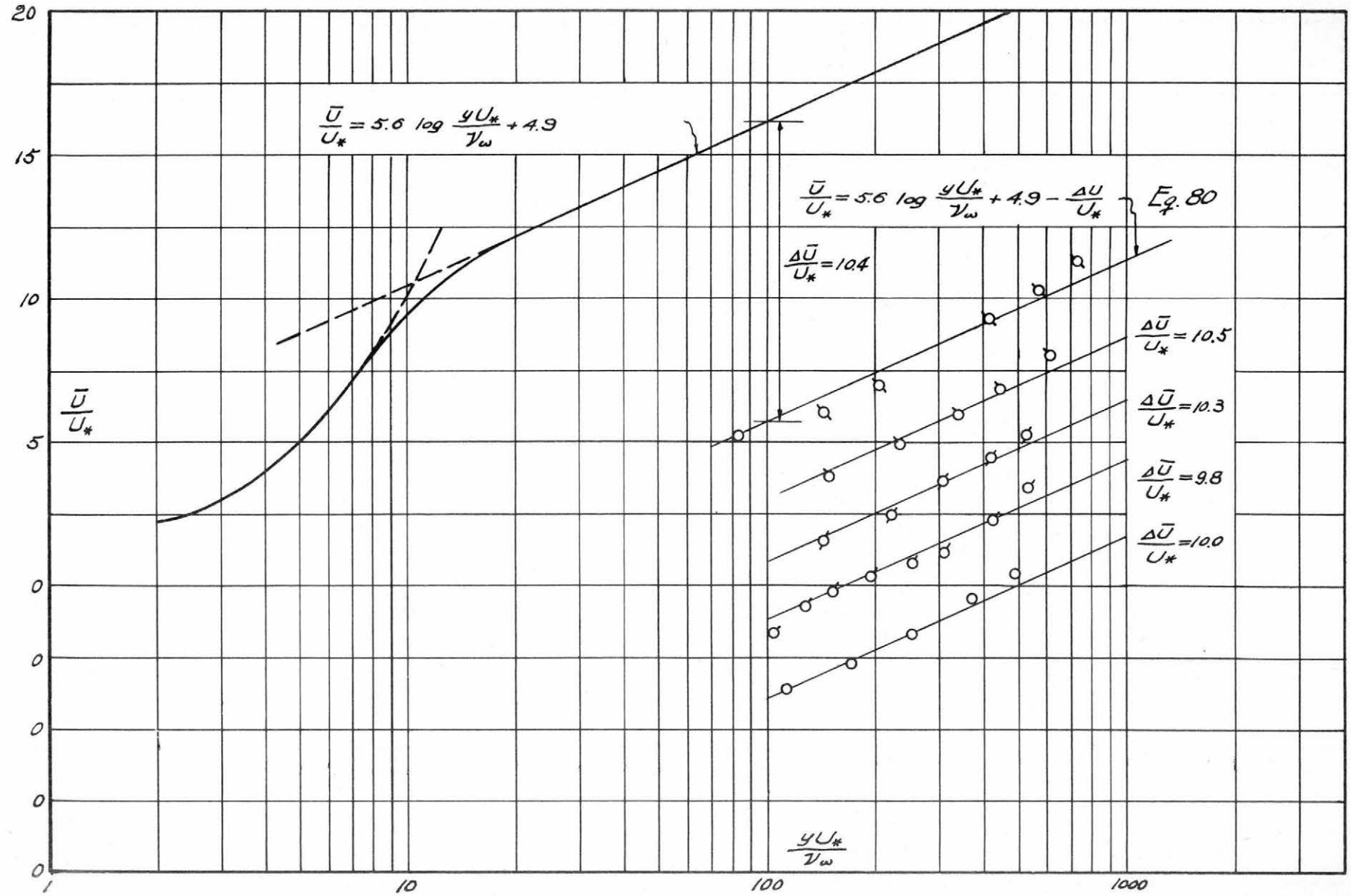

Fig. 25 Variation of $\frac{\Delta \bar{U}}{U_*}$ along the direction of flow for unheated surface ($U_o = 17$ fps)

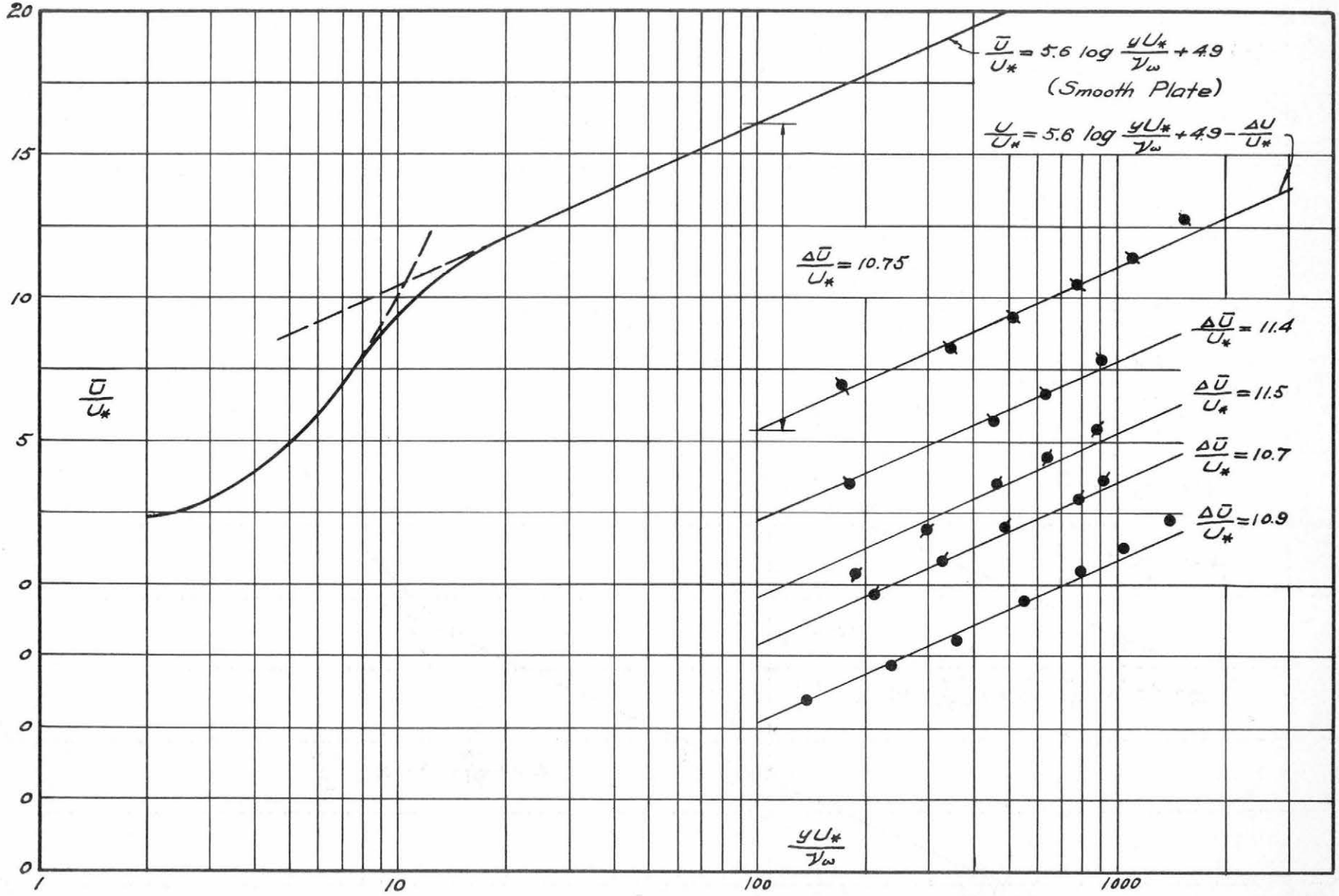

Fig. 26 Variation of $\frac{\Delta \bar{U}}{U_*}$ along the direction of flow for unheated surface ($U_o = 35$ fps)

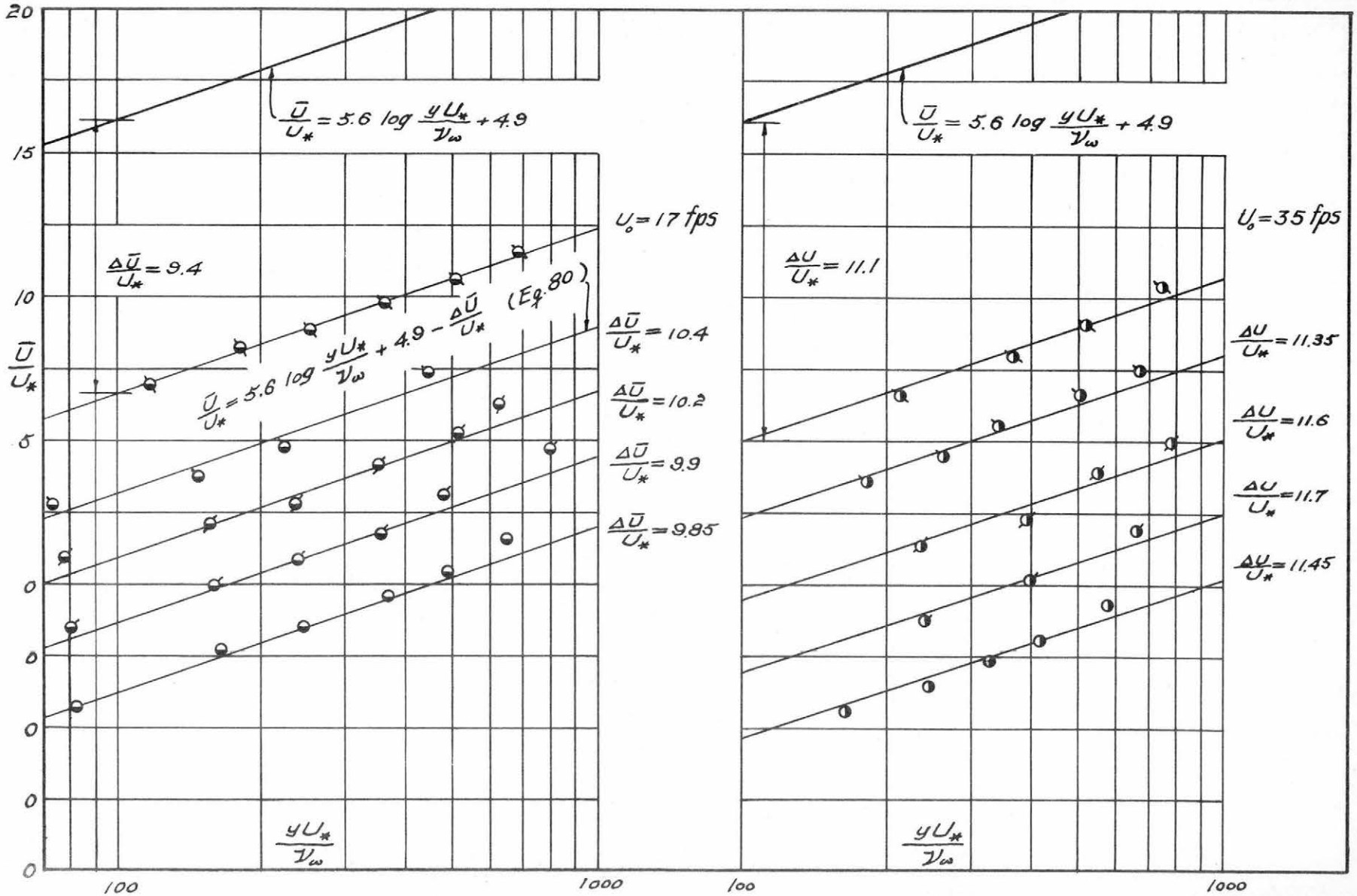

Fig. 27 Variation of $\frac{\Delta\bar{U}}{U_*}$ along direction of flow for heated surface.

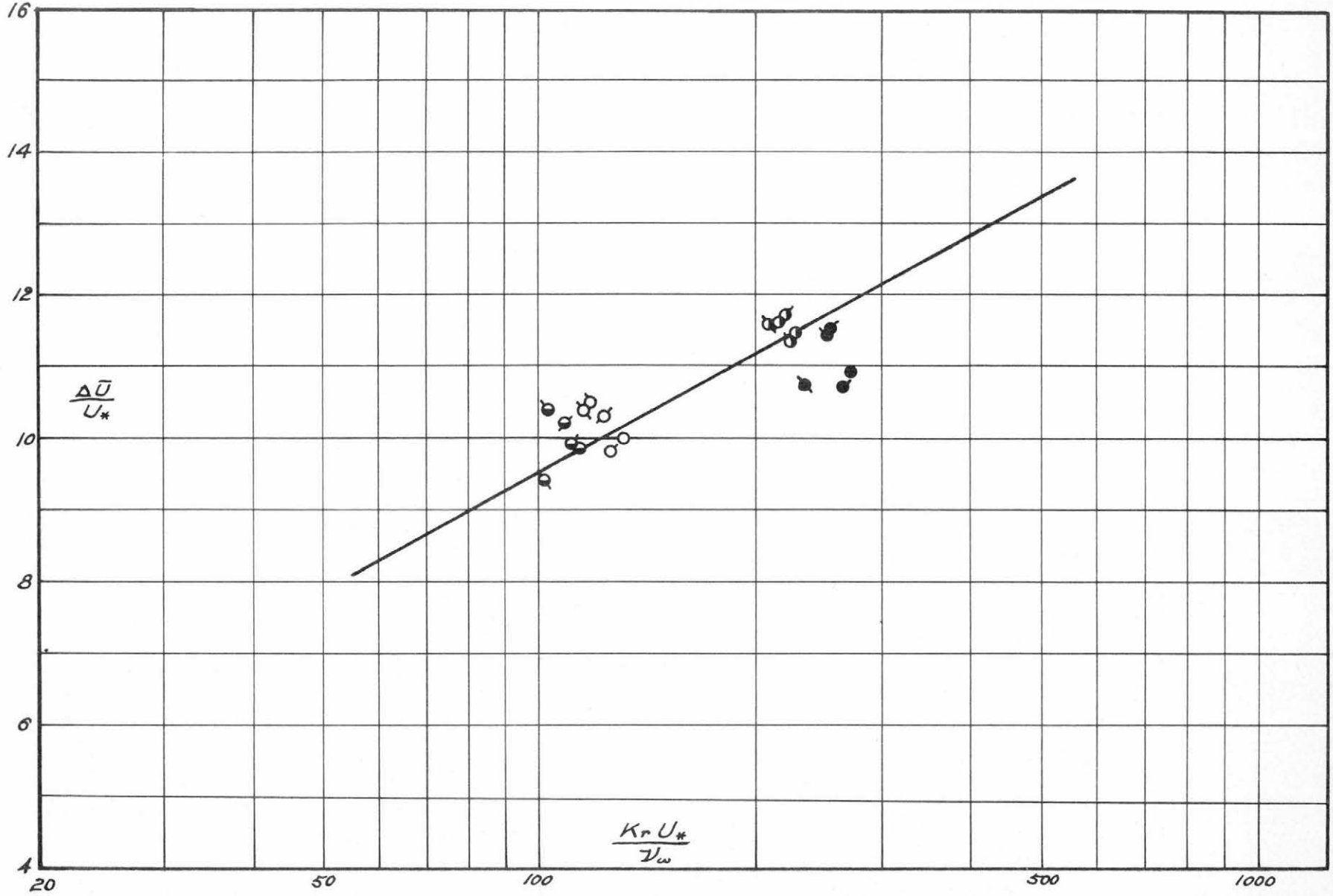

Fig. 28 Variation of $\frac{\Delta \bar{U}}{U_*}$ as function of $\frac{K_r U_*}{\nu_\omega}$

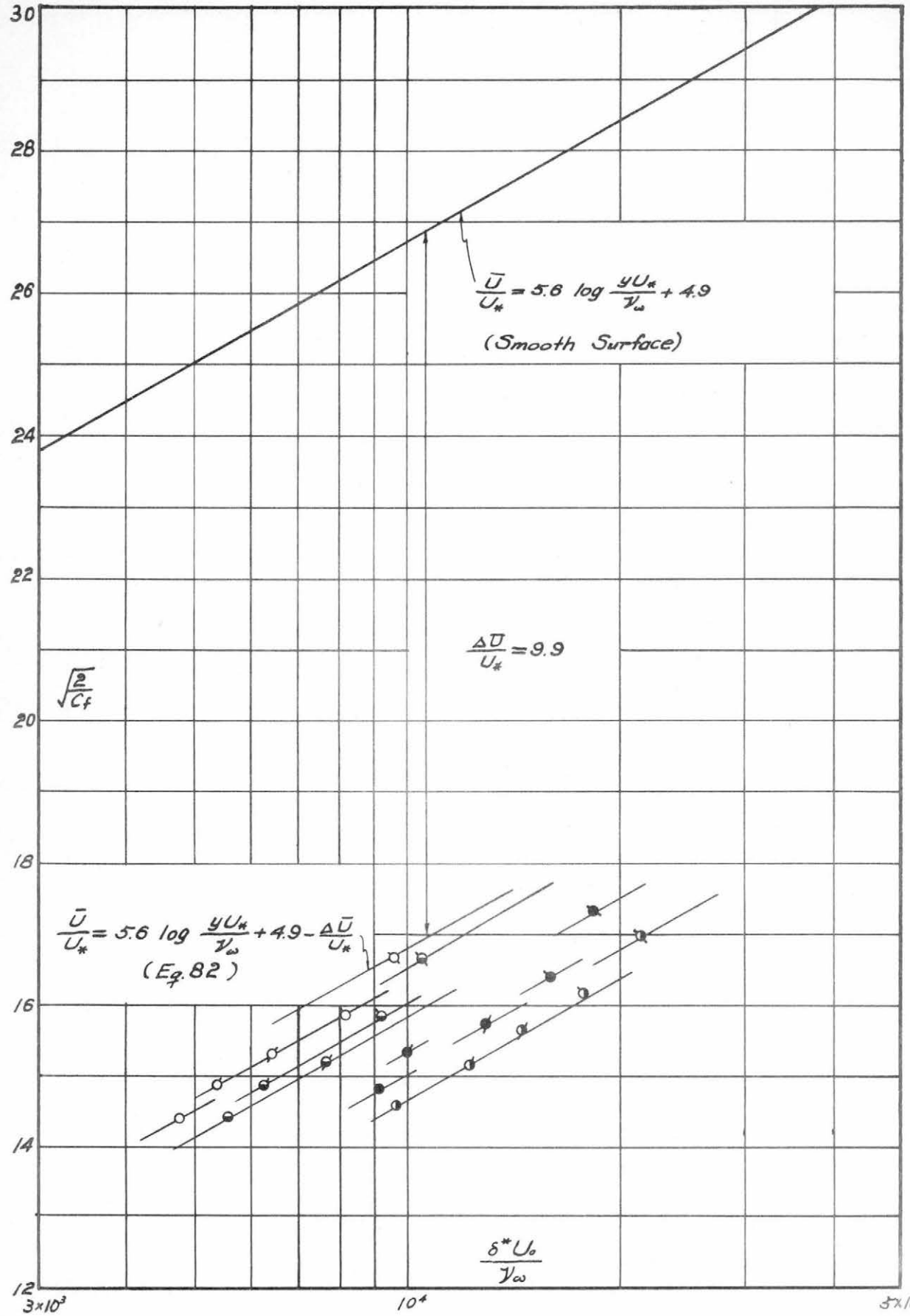

Fig. 29 Variation of $\sqrt{\frac{2}{C_f}}$ as a function of R_{δ^*} and $\frac{\Delta \bar{U}}{U_*}$

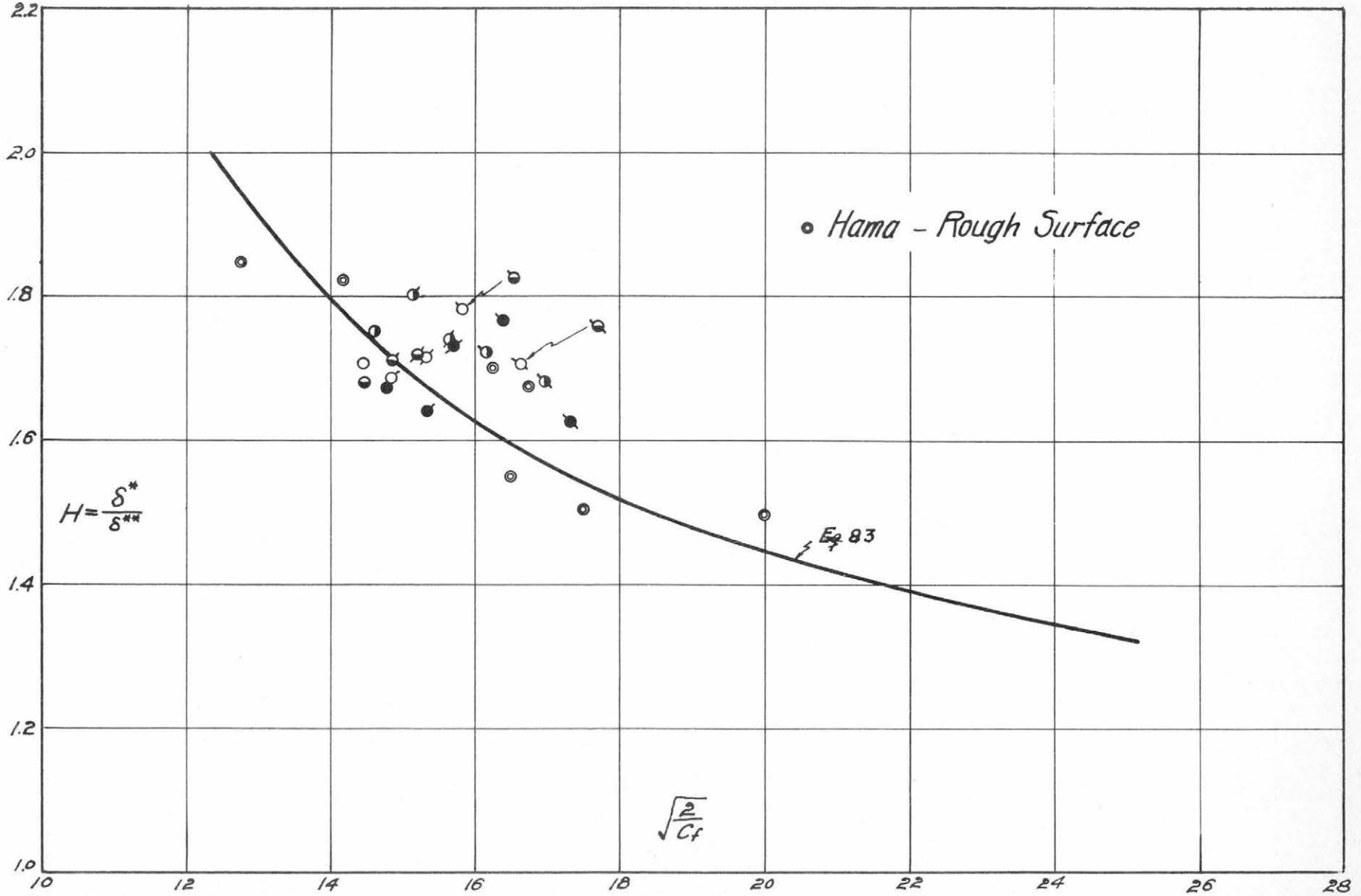

Fig. 30 Variation of Form Parameter As Function of C_f

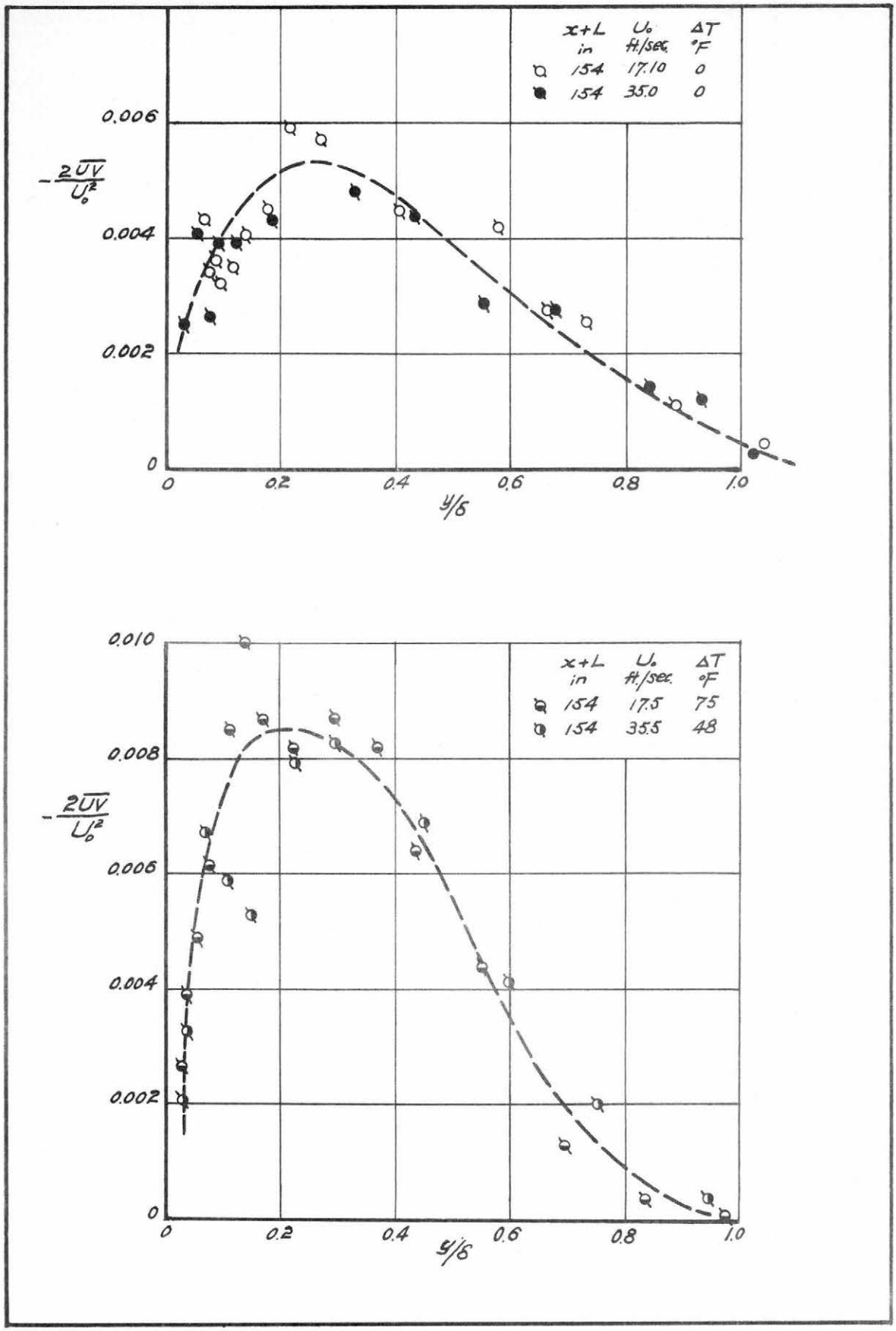

Fig. 31 Typical distribution of Reynolds stress in the boundary layer

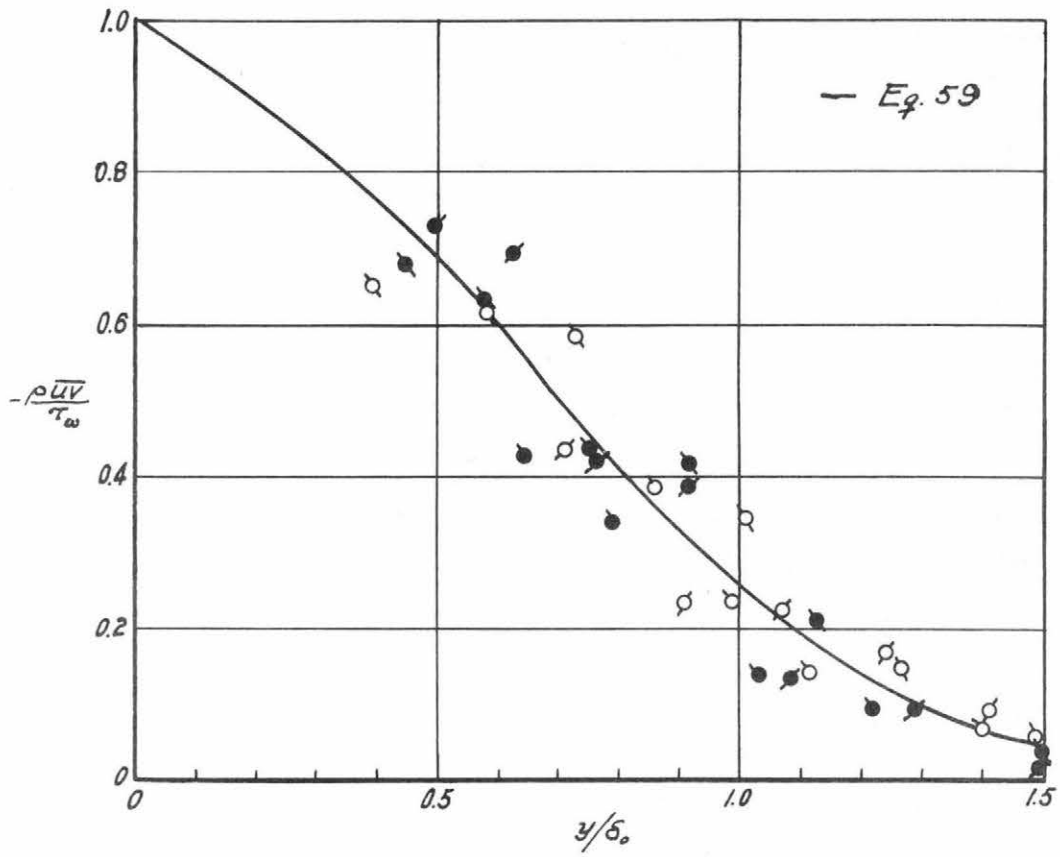

Fig. 32 Distribution of dimensionless Reynolds stress in the boundary layer (unheated)

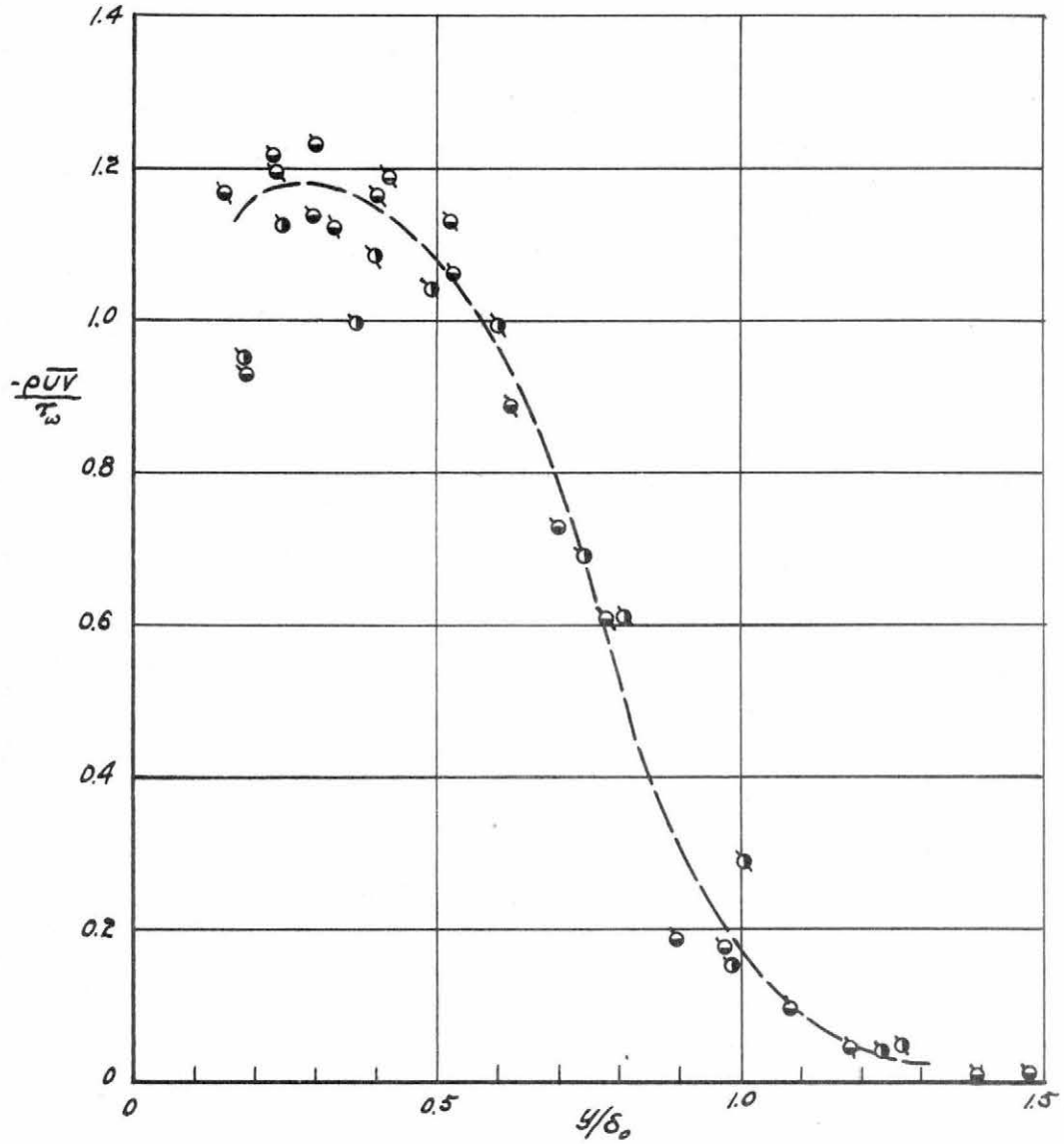

Fig. 33 Distribution of dimensionless Reynolds stress in the boundary layer (heated)

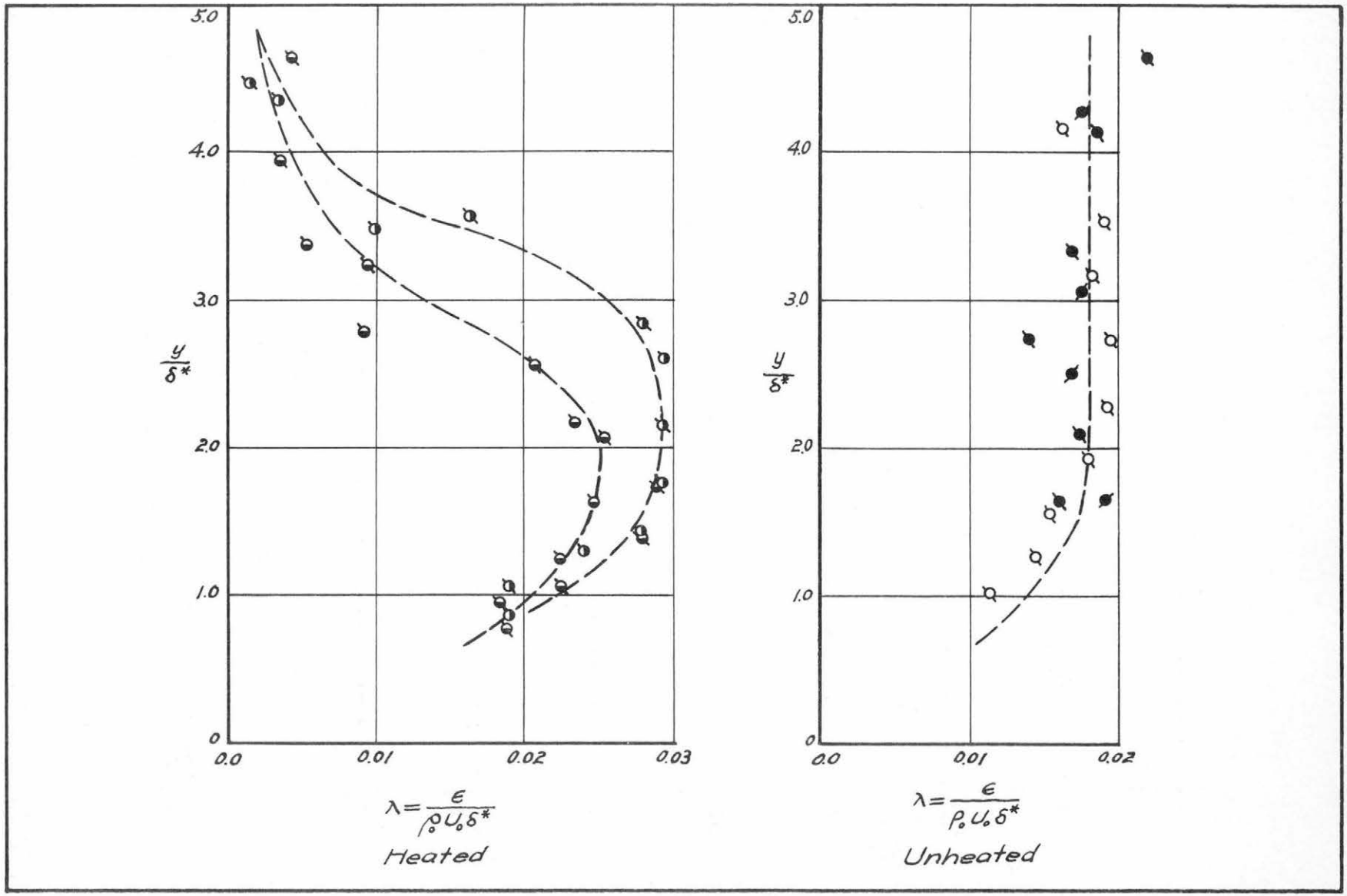

Fig. 34 Eddy viscosity as a function of distance from the surface

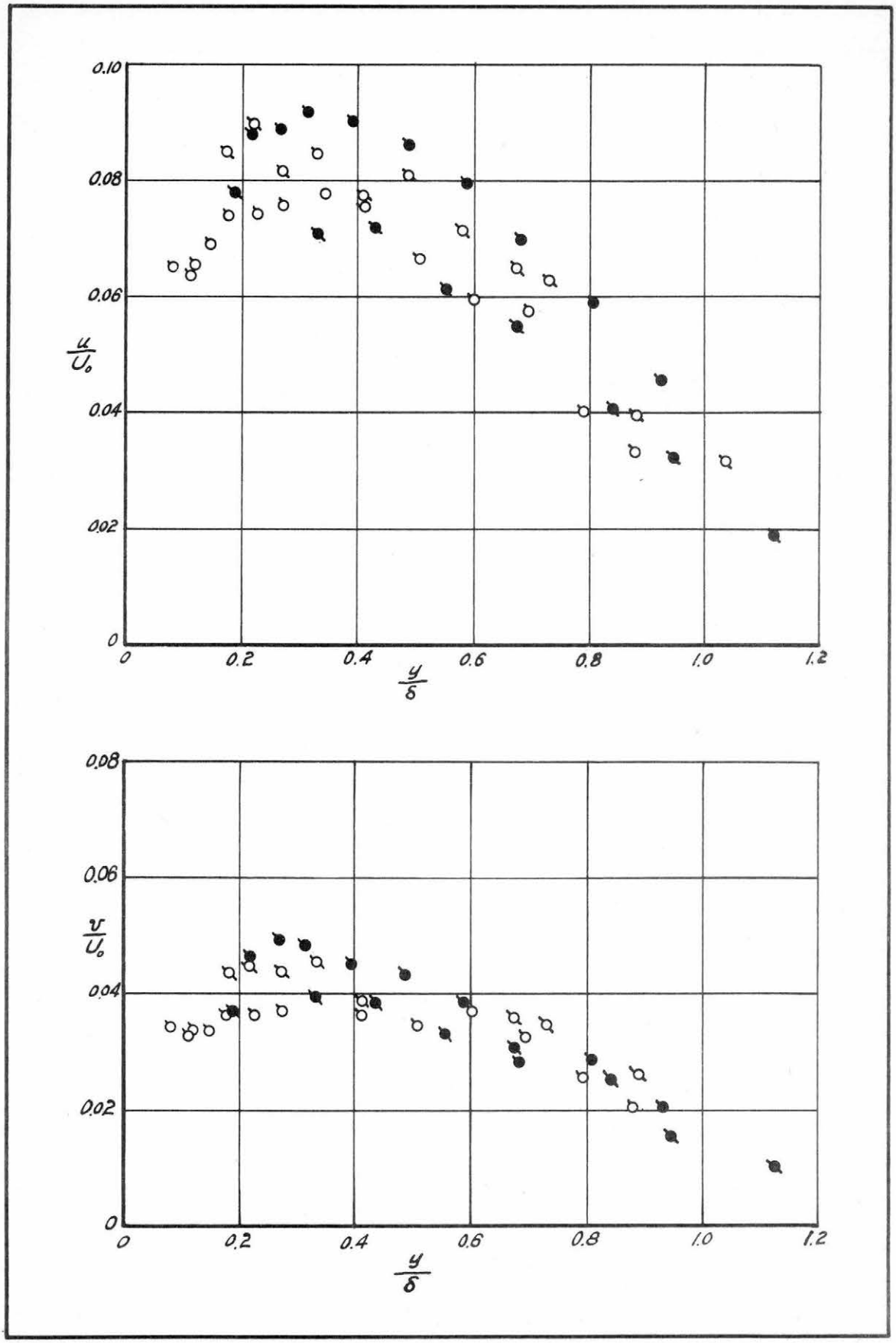

Fig. 35 Intensities of turbulence (u and v) in the boundary layer (unheated surface).

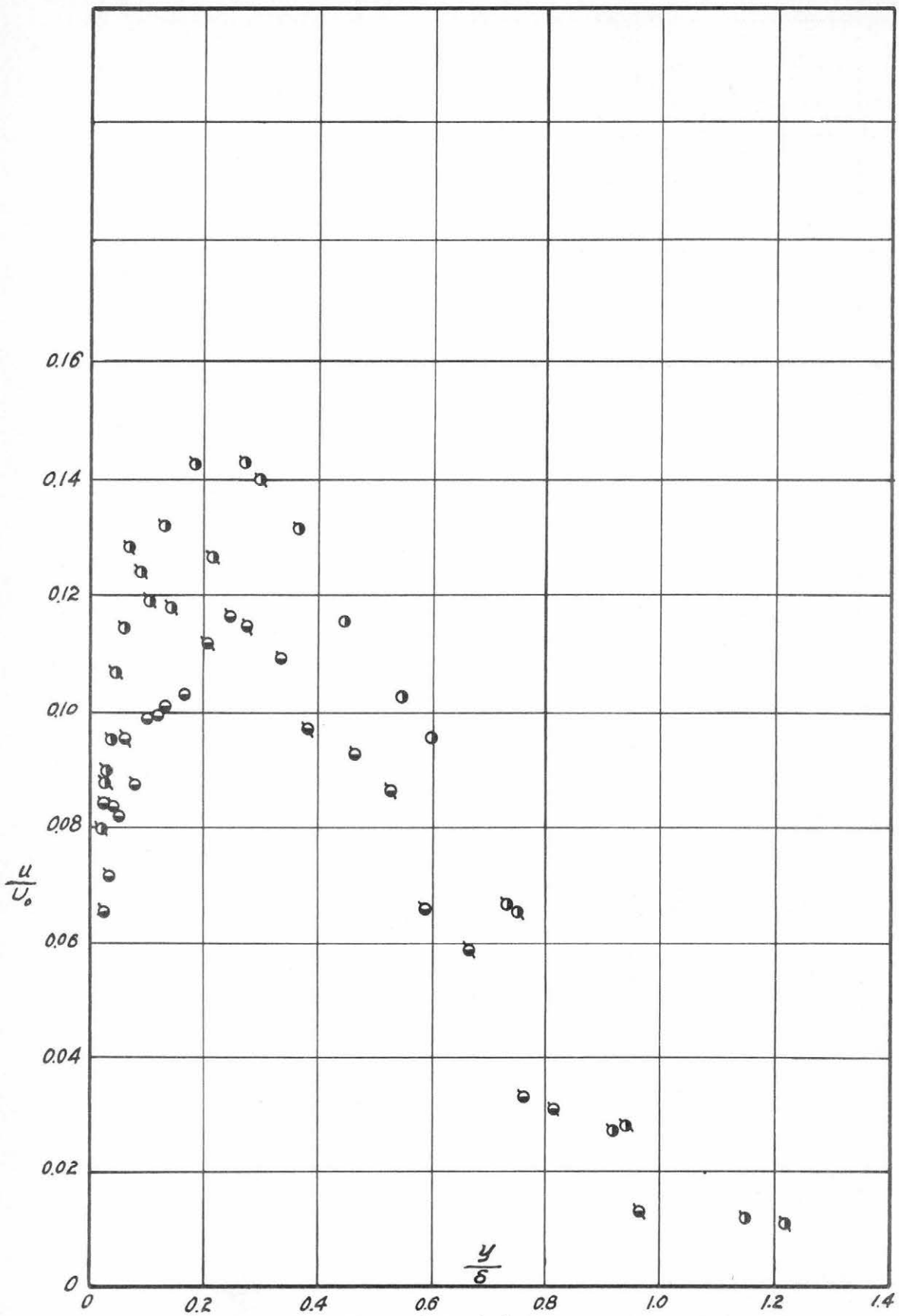

Fig. 36 Intensities of turbulence u in the boundary layer (heated surface).

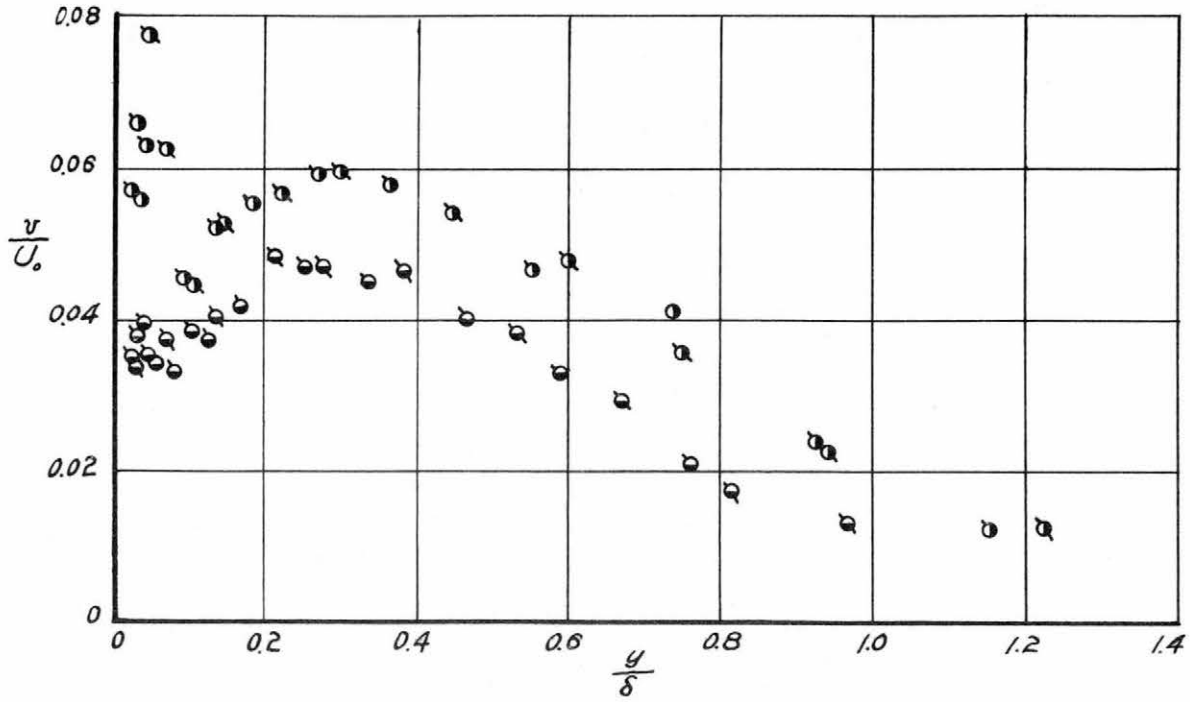

Fig. 37 Intensities of turbulence in the boundary layer.

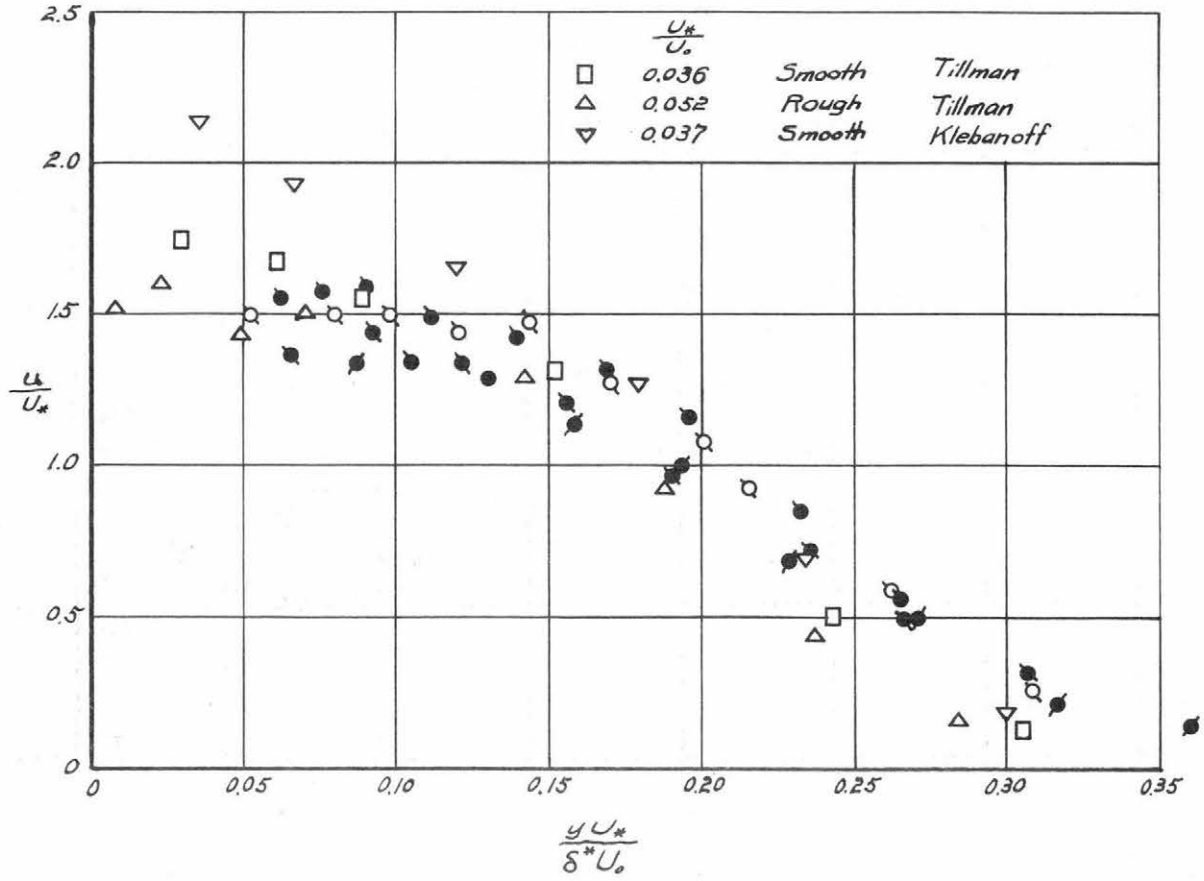

Fig. 38. Variation of the intensities of turbulence as a function of $\frac{y U_*}{\delta^* U_o}$ (unheated surface).

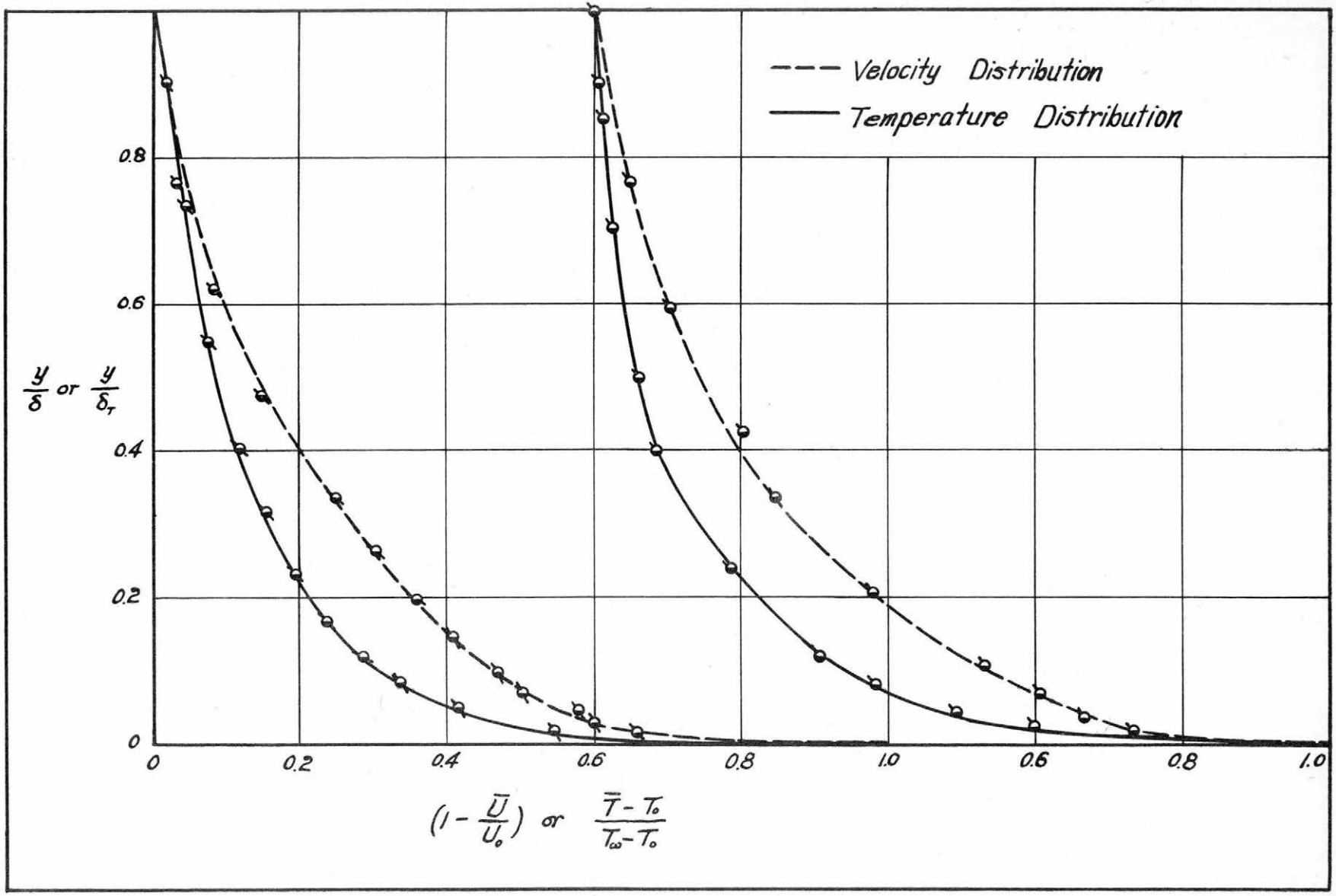

Fig. 39 Comparison of temperature and velocity profile in the momentum and thermal boundary layer ($x+L = 114$ in.)

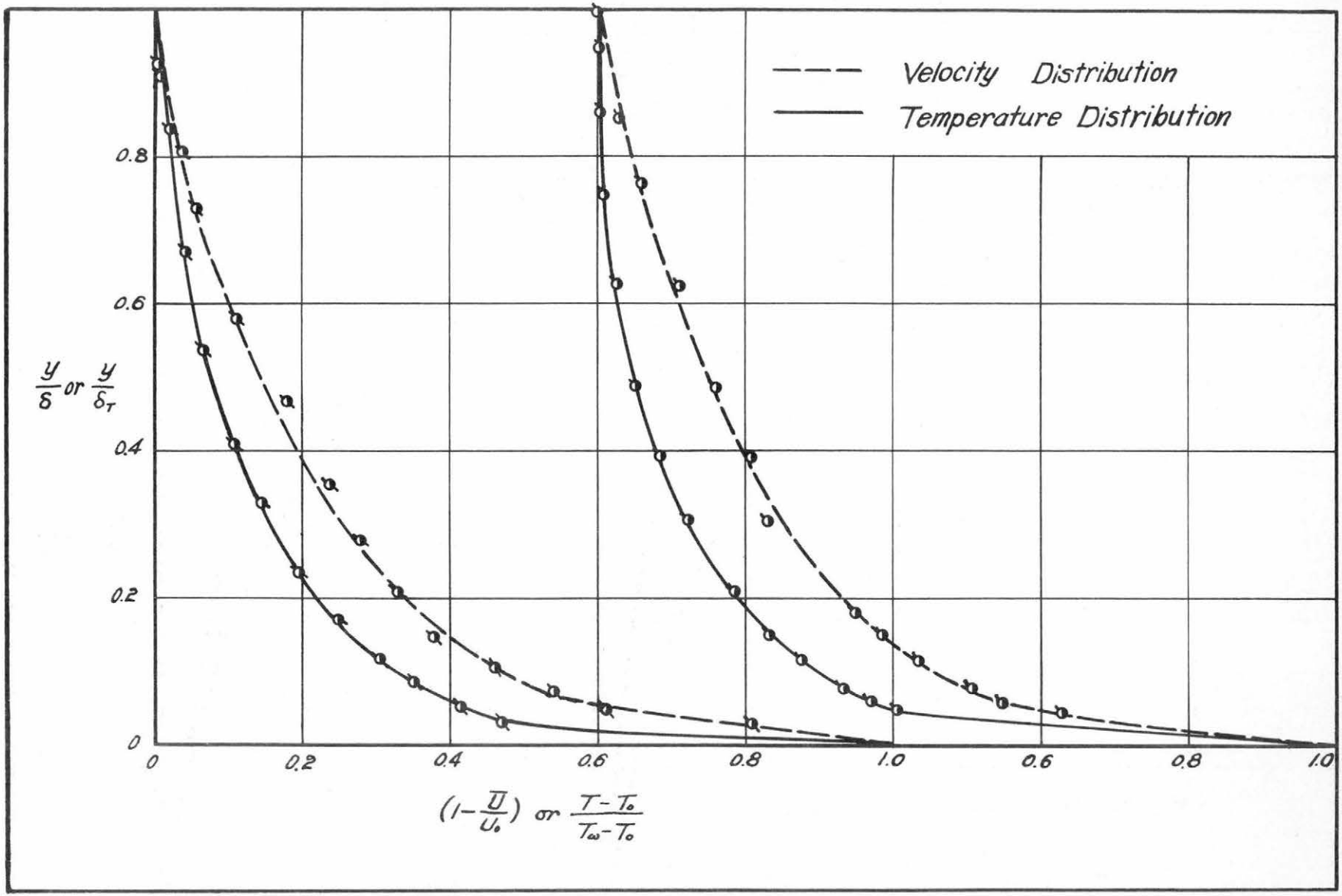

Fig. 40 Comparison of temperature and velocity profile in the momentum and thermal boundary layers ($x+L = 154$ in.)

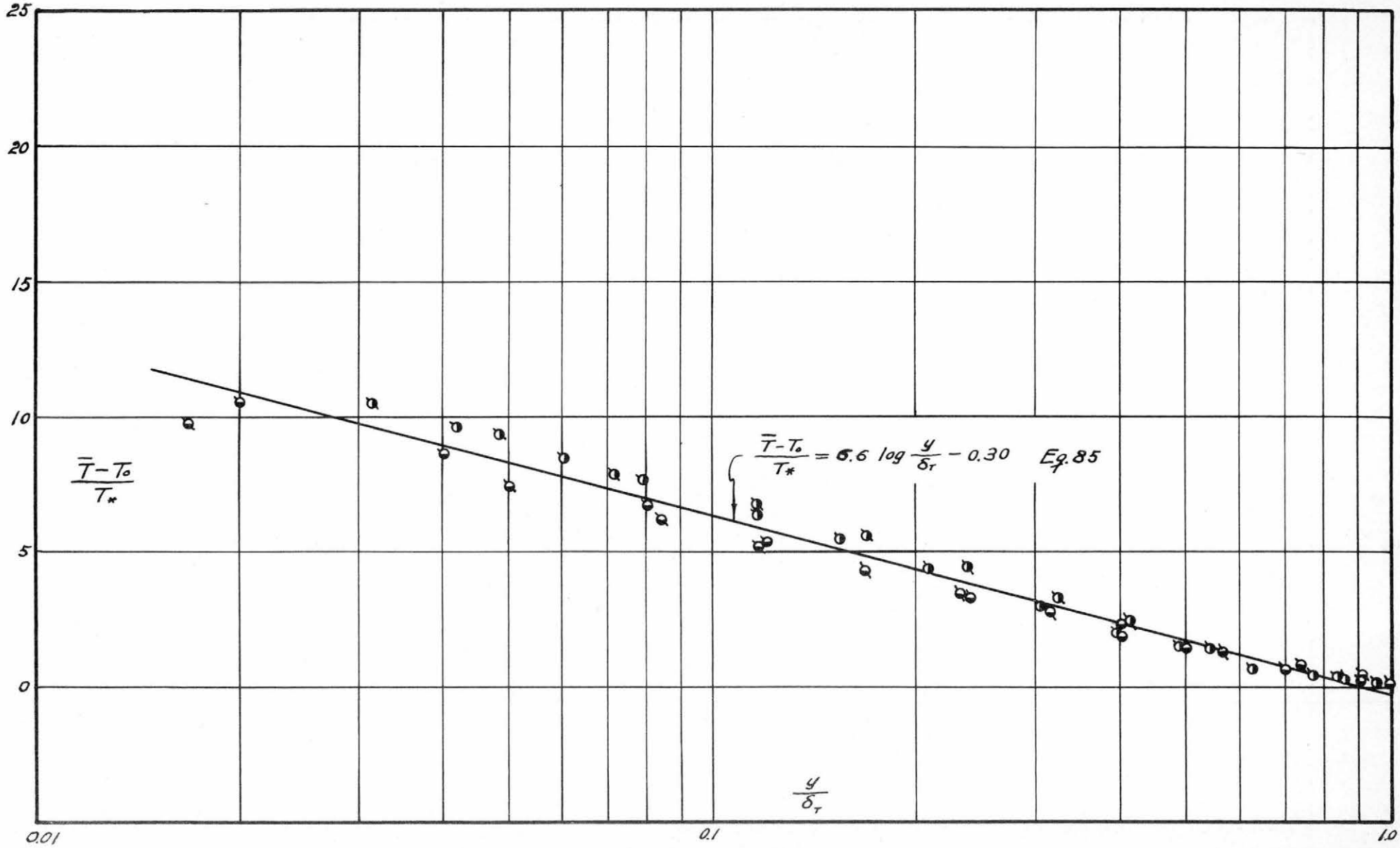

Fig. 41 Universal temperature profile.

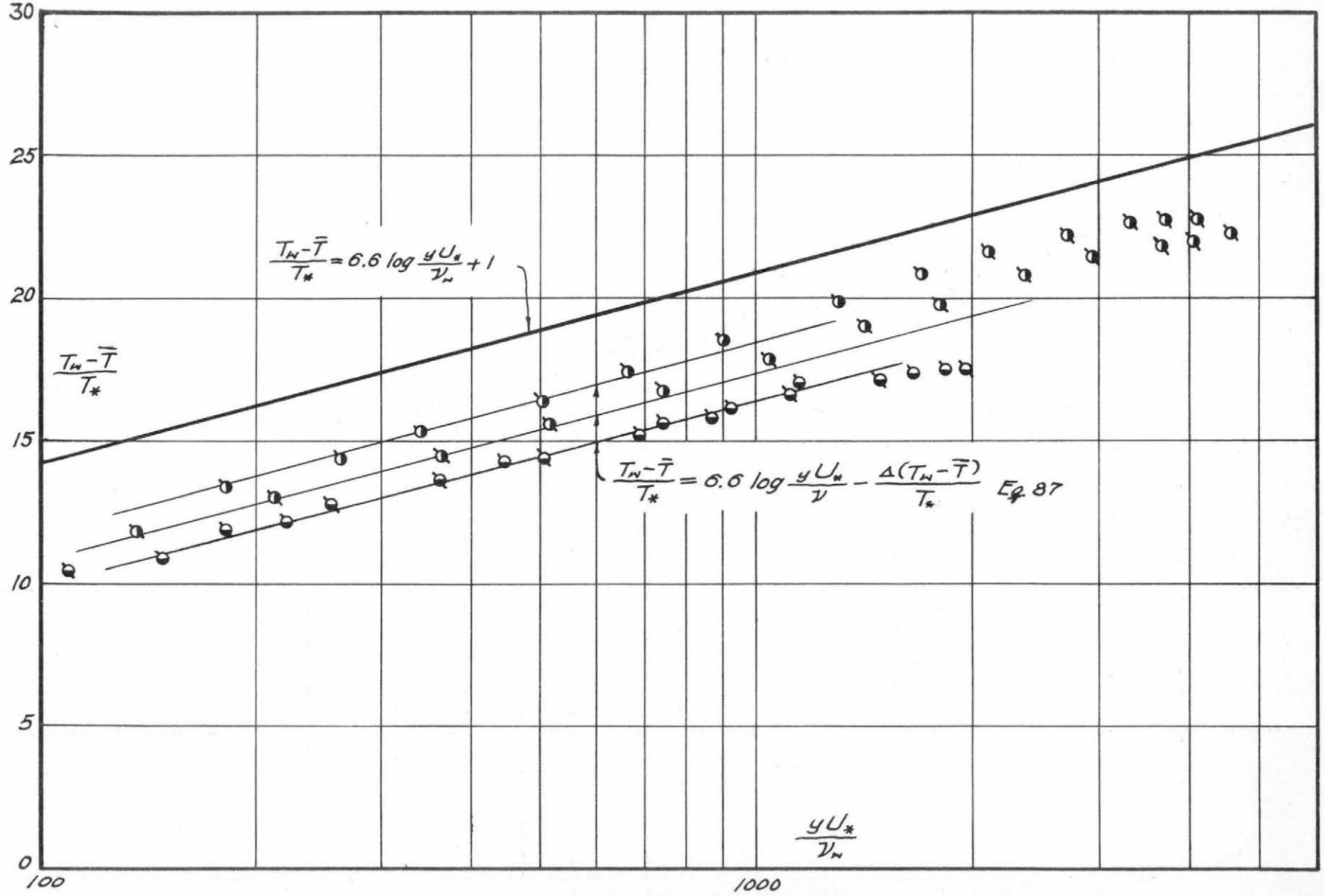

Fig. 42 Wall law of temperature profile.

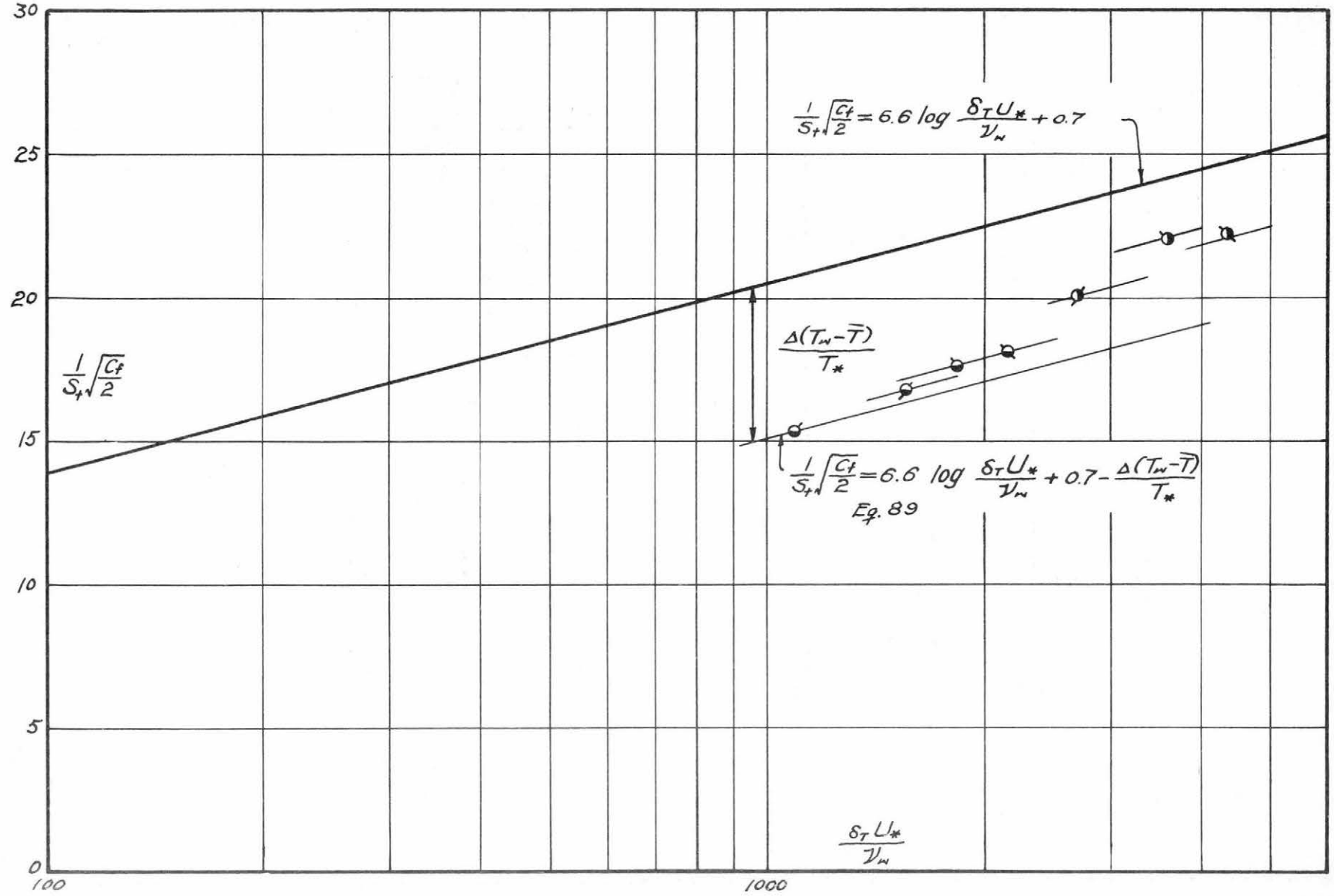

Fig. 43 Stanton number as function of Re_{δ_T}.

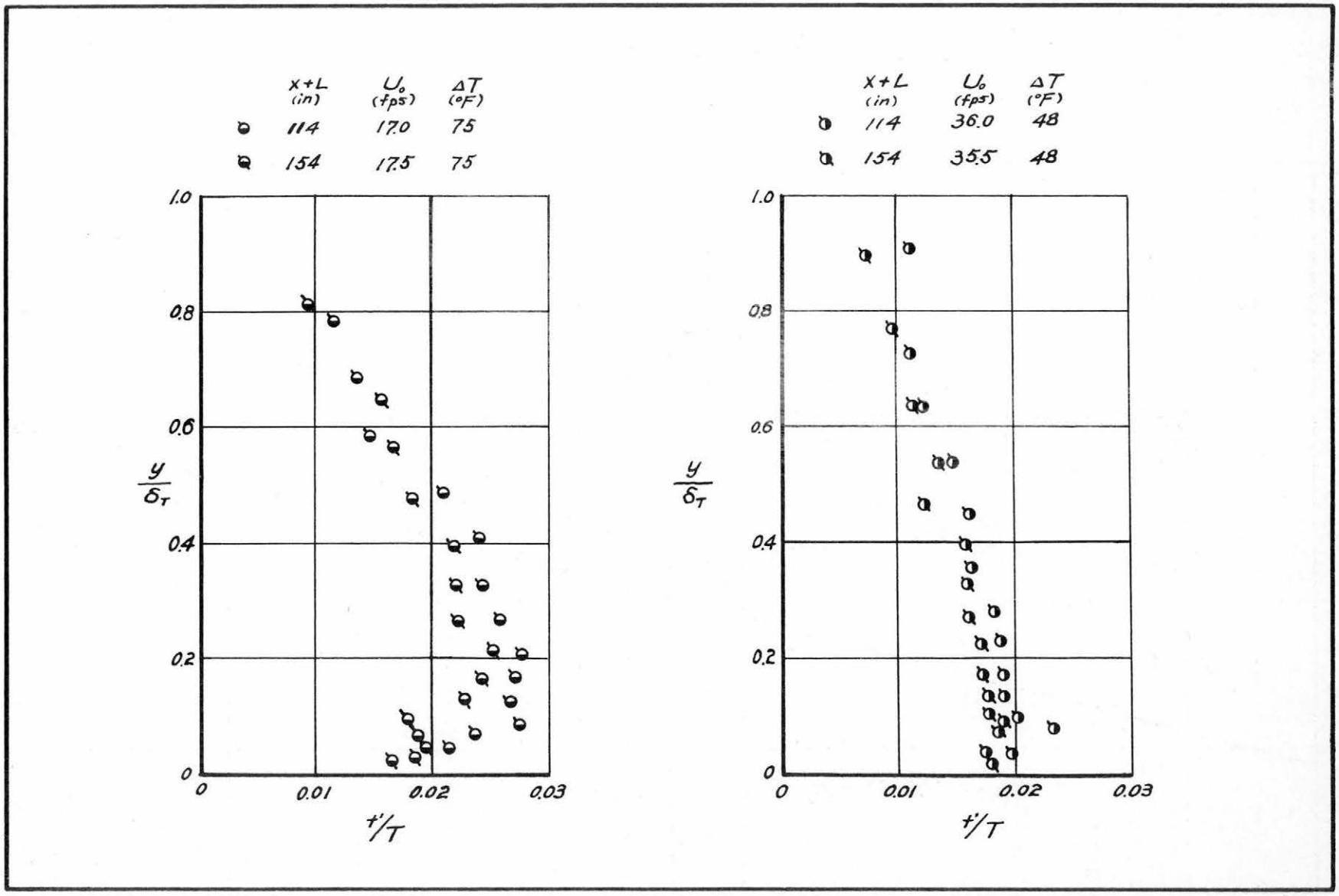

Fig. 44 Typical plot of intensities of temperature fluctuation in the thermal boundary layer.